Synthesis and Photophysical Characterization of an Artificial Photosynthetic Reaction Center Exhibiting Acid-Responsive Regulation of Charge Separation

by

Ian Pahk

A Dissertation Presented in Partial Fulfillment
of the Requirements for the Degree
Doctor of Philosophy

Approved April 2015 by the
Graduate Supervisory Committee:

Devens Gust, Chair
Ian Gould
Vladimiro Mujica

ARIZONA STATE UNIVERSITY

May 2015

ABSTRACT

Non-photochemical quenching (NPQ) is a photoprotective regulatory mechanism essential to the robustness of the photosynthetic apparatus of green plants. Energy flow within the low-light adapted reaction centers is dynamically optimized to match the continuously fluctuating light conditions found in nature. Activated by compartmentalized decreases in pH resulting from photosynthetic activity during periods of elevated photon flux, NPQ induces rapid thermal dissipation of excess excitation energy that would otherwise overwhelm the apparatus's ability to consume it. Consequently, the frequency of charge separation decreases and the formation of potentially deleterious, high-energy intermediates slows, thereby reducing the threat of photodamage by disallowing their accumulation. Herein is described the synthesis and photophysical analysis of a molecular triad that mimics the effects of NPQ on charge separation within the photosynthetic reaction centers. Steady-state absorption and emission, time-resolved fluorescence, and transient absorption spectroscopies were used to demonstrate reversible quenching of the first singlet excited state affecting the quantum yield of charge separation by approximately one order of magnitude. As in the natural system, the populations of unquenched and quenched states and, therefore, the overall yields of charge separation were found to be dependent upon acid concentration.

ACKNOWLEDGEMENTS

First and foremost, I would like to thank Professor Devens Gust for providing me with the distinguished privilege of learning from his enormous wealth of knowledge in spectroscopy, photochemistry, and photophysics and for giving me the freedom, both through funding and in practice, to develop as a synthetic chemist who obsesses over purity, yields, and crystalline products. I would also like to thank Professors Tom and Ana Moore, together with Devens, for providing a diverse, multi-disciplinary learning environment benefiting from their own expertise, as well as those of the combined (GMM) research group members. Thanks go to all of the GMM researchers with whom I interacted over the course of my graduate studies: Ant, Jeffrey, Bobby, Jesse, Matthieu, Manuel, Michael, John, Smitha, Kul, Ben, Chris, Dustin, Brad, Dalvin, Jaro, Katie, Chelsea, Marely, Raquel, Nino, Max, Lucie, and Graeme. In particular, I would like to thank Ant for her kind acceptance in sharing both an office and lab space with me, and my ever-expanding messes. Also, I want to thank her for bearing first hand witness to the enormous range of moods and emotions, both high and low, that I showed up to work with over the last five years. On a brighter note, the countless fits of delirious laughter in the lab and office are some of my best memories of graduate school that I will never remember the causes of. In similar regard, I would also like to thank Jeffrey for dealing with me in close quarters for the majority of my graduate career, and also, for providing a constant stream of daily entertainment in the lab.

Special thanks go to Yuichi Terazono, who laid virtually all of the groundwork from which my dissertation work was based. Yuichi is one of the finest synthetic chemists I have had the pleasure of working with and I am forever grateful for his unending willingness to provide me with synthetic advice and encouragement, in addition to teaching me everything he had learned about working with these molecules. Of particular note – he taught me how to synthesize, purify, and manipulate the sometimes-impossibly-finicky rhodamine dye that is the crux of the novelty of this work. On this note, I would like to acknowledge Kul Bhushan for discovering this dye, which suits the photophysical demands of this project so very well.

Special thanks go to Paul Liddell, who taught me so much about working with porphyrins and polyaromatic compounds and especially palladium coupling reactions thereof. Paul is, perhaps, the epitome of what a synthetic organic chemist should be, and I think that I will never gain the appreciation and understanding of organic molecules that he gives the impression of having had since the first day he stepped up to a bench. I would like to thank Paul for sharing his prolific experience and giving me synthetic advice, talking strategies and techniques, occasionally providing me with chemicals and distilled solvents, and for flame sealing pressure vessels so that my precious compounds would not wind up splattered all over the inside of my hood.

Special thanks go to Gerdenis Kodis, who taught me much of what I know about photophysics and who performed all of the time-resolved fluorescence and transient absorption experiments and data analysis and provided the mechanistic interpretations described later in this work. Gerdenis was always willing to reteach me the aspects of ultrafast non-linear spectroscopy and photophysical analyses that I forgot, over and over and over. I would also like to thank Gerdenis for always appeasing my requests for additional experiments and for walking me through his reasoning until I was fully convinced by his interpretations of the data.

Finally, I would like to thank my friends and family for the unending love and support they showed me during this period of my life. I am forever grateful that my mother and father have always supported me in choosing my own path in life. I would also like to express my gratitude for my sister, whom I don't see often, but who somehow seems to share all of my weirdest quirks. It is nice to know there is at least one other person who is weird, almost just like me. I would especially like to thank Josh, Eri, Io, Jeffe, Kayla, Brian, Jamie, Logan, Brian, and Jenna for always being there when I needed you to listen, to laugh, to tell me when I'm wrong, to remind me to just relax; I'm doing fine, to help me get away, and to help me find myself again and again (and again). You all mean the world to me and I am so grateful to have you as companions on this ride.

This work was funded by the Helios Solar Energy Research Center, which is supported by the Director, Office of Science, Office of Basic Energy Science of the U.S. Department of Energy under Contract No. DE-AC02-05CH11231; the Office of Basic Energy Sciences, Division of Chemical Sciences, Geosciences, and Energy Biosciences, Department of Energy under contract DE-FG02-03ER15393; and the Center for Bio-Inspired Solar Fuel Production, an Energy Frontier Research Center funded by the U.S. Department of Energy, Office of Science, Office of Basic Energy Sciences under Award Number DE-SC0001016.

TABLE OF CONTENTS

LIST OF TABLES

LIST OF FIGURES

LIST OF SCHEMES

Chapter 1

Non-Photochemical Quenching and Artificial Mimics Thereof

Charge separation is the primary light-driven reaction in photosynthesis. Solar energy is converted to electrochemical potential in the form of charge separated states within photosynthetic reaction centers. This provides driving force for water oxidation; the critical step toward phototrophic production of chemical fuels. The ability for the photosynthetic apparatus, a membrane-bound nanomolecular factory, to regulate the efficiency of energy conversion in response to solar energy flux is paramount to the survival of photosynthetic organisms. In parallel, developing responsive, self-regulating systems is important to address in the design of practical and robust nanomolecular devices.[1] In this regard, solar energy technologies based on organic molecular components are expected to require regulatory and photoprotective mechanisms in order to maximize their operating efficiencies and lifespans.[2, 3] Biomimicry is recognized as an important approach to the design of complex nanomolecular systems.[4, 5] Nature's answer to photoprotection and the regulation of photosynthetic activity at the molecular level is a mechanism known as non-photochemical quenching (NPQ), which has been the subject of rigorous investigations for over 40 years. While many of the quantifiable operating parameters of NPQ have been well characterized, our mechanistic understanding declines with- and is limited by- our ability to resolve and deconvolute complex spectroscopic information to a molecular level. This is a major obstacle in studying any natural system, as many mechanistic details change or simply vanish when moving from highly complex holistic samples to relatively simplified in vitro preparations.[6] Approaching this problem from the bottom up, the development of small-molecule functional analogs and, in a stepwise fashion building up a biomimetic environment around them, may help to advance our understanding of how individual inter- and intramolecular interactions influence the overall functioning of complex natural systems. Toward these ends, the research described in this dissertation involves the synthesis and photophysical characterization of a molecular triad that exhibits the responsive, self-regulation of charge separation that is a hallmark

of NPQ. A brief overview of photosynthesis and the necessity for photoprotection, the state of knowledge regarding NPQ, and the most relevant examples of its mimicry in model systems follows.

Photosynthesis is the biochemical process by which phototrophic organisms use solar energy to pay the thermodynamic cost of sustained life. A series of photon capture, energy transfer, charge separation, and energy conversion reactions ultimately produce the chemical equivalents needed to maintain non-equilibrium, reduced (living) states in an oxidizing environment. Chlorophyll, a porphyrin, serves as a primary photosynthetic pigment that fills dual roles as light absorbers and as electron donors. Photo-excitation of the P680 special chlorophyll pair within Photosystem II (PSII) generates its first excited singlet state, $^{1}P680$, which then readily undergoes one of the most significant charge separation reactions in photosynthesis; donation of an electron, via a series of electron transfer reactions, to a quinone (Q) thus generating $P680^{\bullet+}$, a powerful oxidizer. The oxidizing potential of $P680^{\bullet+}$ is transferred to the metal center of the oxygen-evolving complex (OEC) where it is used to split water by the following chemical equation:

$$2\ H_2O + 4\ h\nu \rightarrow O_2 + 4\ H^+ + 4\ e^-$$

Protons liberated by this reaction are selectively released into the lumen side of the photosynthetic membrane, thereby generating an electrochemical potential gradient. Reduced quinones, $Q^{\bullet-}$, shuttle electrons unidirectionally to Photosystem I (PSI) in a series of electron transfer steps across multiple intermediaries. The exchange of electrons between each species also drives protons across the photosynthetic membrane and into the lumen, further building the potential gradient. The electrons that PSI receives from this transport chain are reenergized by a light-based reaction so that they can be used in NADPH production. Simultaneously, ATP is produced by channeling protons back across the photosynthetic membrane thereby consuming

the potential stored in the gradient. The energy stored in both NADPH and ATP is utilized in the reduction of CO_2 to form carbohydrates, the final step in photosynthetic energy conversion.

Light harvesting antennae, namely light harvesting complex II (LHCII), are employed in the photosynthetic apparatus of plants to increase photon capture and funnel excitation energy into PSII. This has the net effect of increasing the frequency of early charge separation reactions and water oxidation in PSII. In this way, photosynthesis has evolved to be adaptive to intermittent periods of low light intensity. Conversely, periods of high-intensity irradiation lead to higher frequencies of photon capture and charge separation to the point of overwhelming the maximum turn over frequencies of slower downstream electron transfer reactions and generation of NADPH and ATP.[7] Consequently, the high-energy intermediates involved in these reactions accumulate and, if not efficiently consumed, can cause irreversible damage to- and permanent deactivation of- PSII.[8-10] Photo-damage to PSII is primarily associated with P680.[9] If the rate at which ^{1}P680 is oxidized far exceeds that at which electrons are donated back to $P680^{\bullet+}$ from the OEC, the resulting increase in the lifetime of $P680^{\bullet+}$ allows it to oxidize pigment molecules and amino acid residues within its immediate vicinity.[8, 9] Alternatively, if the reduced quinone pool is too large, signifying the inability for downstream reactions to keep pace with the light based reactions within PSII, the $P680^{\bullet+}$-$Q^{\bullet-}$ charge separated state can recombine leading to formation of the triplet, ^{3}P680.[8, 9] This triplet can interact with oxygen to form singlet oxygen, $^1O_2$, which will react with many components of the photosynthetic apparatus leading to pigment bleaching and, eventually, PSII deactivation.[8, 9]

Given the nature of interactions between organic pigments, light, and oxygen, the evolutionary emergence of oxygenic phototrophs stipulated a compulsory requirement for layering of multi-level regulatory and protective mechanisms to prevent the primary source of energy, the sun, from engendering their destruction. Non-photochemical quenching (NPQ) is a photoprotective regulatory mechanism that modulates the efficiency of energy transfer from LHCII to PSII in response to fluctuating light intensity. During periods of low photon flux, it is necessary for solar energy conversion to be performed with maximal efficiency in order to provide the

organism with enough energy and reducing capacity to maintain homeostasis. Therefore, the photosynthetic apparatus has adapted to fulfill this demand by dividing electron transport into a series of slower but highly energy efficient steps. Conversely, during periods of high photon flux, the initial photon capture and energy transfer steps of photosynthesis make available an excess of excitation energy to the reaction centers that downstream electron transport and chemical fuel producing reactions have no innate way of processing. As the release of protons into the thylakoid lumen continues to outpace the ability for ATP synthesis to utilize the potential stored in the proton gradient, the resulting decrease in lumen pH signals an over abundance of solar energy and proportional activation of NPQ.[6, 7, 11] Time-resolved fluorescence spectroscopy has shown that NPQ attenuates the excited state lifetime of LHCII chlorophylls, thereby reducing the quantum efficiency of energy transfer to PSII.[12-14] Consequently the frequency of charge separation in the reaction center also decreases (as does the charge separation efficiency relative to total photons captured by the apparatus), thereby bringing light-to-potential energy conversion into equilibrium with potential-to-chemical energy conversion.[15, 16] Exposure to low light conditions allows for consumption of the proton gradient, which is reciprocated by proportional deactivation of NPQ and return to elevated efficiencies of charge separation. In this way NPQ is dynamically responsive to fluctuations in light intensity.

NPQ activates one or more decay pathway(s) by which excess excitation energy collected by the antennae can be harmlessly dissipated as heat rather than being used to generate charge separated states.[15] While decreases in lumen pH have long been known to play a causative role in the activation of NPQ, the molecular nature of this responsiveness remains uncertain.[11, 17] As such, the complex and multi-layered feedback mechanisms that allow for highly adaptive and robust control over NPQ are not fully understood.[6] NPQ activation is thought to induce reorganization and aggregation of protein complexes along the photosynthetic membrane, for which several models have been proposed.[18, 19] In relation to these spatial and superstructural changes, factors including the pH-responsive cycling of xanthophyll carotenoids and protonation

of an auxiliary protein, PsbS, have been implicated as modulators of the rates of activation and relaxation of quenching as well as the pH threshold at which NPQ activation is initiated.[20-22]

The identities of the photophysical mechanism and molecular quencher responsible for the rapid thermal dissipation observed in NPQ have been subjects of debate for over 20 years.[6] Discernment of potential quenching mechanisms is restricted by the kinetic parameters set by the experimentally observed fluorescence lifetimes of LHCII chlorophyll; around 2 ns in the unquenched state and roughly 0.5 ns in the quenched state.[12] In the absense of interchromophore interactions, the first singlet excited state of chlorophyll is known to decay by fluorescence, internal conversion, and intersystem crossing; processes more rigorously defined in Chapter 3. The decay lifetimes associated with intersystem crossing are generally much longer than the observed quenched lifetime making involvement of this type of process unlikely. On the other hand changes in the local protein environment of a particular chlorophyll could conceivably transform it into a quenching species by increasing its rate of decay by internal conversion, thereby fulfilling this kinetic requirement.[6] Structural changes to the local environment of a chlorophyll could also bring another highly quenched pigment into sufficiently close proximity to allow for energy transfer and dissipation.[6] Ultrafast spectroscopic studies focusing on carotenoid and chlorophyll pigments in vivo and in vitro have yielded several prominent but disputed theories regarding the molecular identity of the quencher. Earlier time-resolved fluorescence work suggested formation of a chlorophyll-chlorophyll dimer within LHCII complexes as the primary NPQ quencher based on the similarly red-shifted emission characteristics of LHCII and those of known chlorophyll aggregates with short excited state lifetimes.[12, 19, 23] More recent transient absorption and computational studies assign the role of quencher to a xanthophyll carotenoid. Some implicate coherently coupled chromophores and quenchers over which an excited state wavefunction is distributed.[24, 25] Such coherent excited states are proposed to decay by charge transfer in which rapid charge separation and subsequent recombination yield the ground state with the release of heat.[26, 27] Others have suggested an incoherent energy transfer mechansim where the excited state discretely "hops" from one pigment to another until reaching a quencher

with an intrinsically short excited state lifetime.[28] One of the most recent reports revisited chlorophyll-chlorophyll charge transfer complexes (rather than chlorophyll-carotenoid) under a coherently coupled regime to explain the chromophore coupling and charge transfer characteristics that had been previously reported.[29] While each of these theories is supported by experimental and in some cases computational results, they are all also opposed by contradictory interpretations and lack the support of undisputable substantiating evidence in their favor. In short, the physical environment that surrounds the quenching process in NPQ is intricately complex, which makes detailed and biologically relevant studies difficult to perform. Alternatively, research has turned toward developing simplified model systems with the goal of adapting them to increasingly complex biomimetic local environments in order to identify specific operating parameters and interaction-based photophysical phenomenon that activate different quenching processes in a highly controllable manner.

In the last decade, the laboratories of Professors Devens Gust, Ana L. Moore, and Thomas A. Moore have reported several small molecules that model various aspects of NPQ. The earliest work in this area involved quenching of chromophore excited states through interactions with synthetic carotenoids.[30, 31] Prior to the work described in this dissertation, there were only two published examples of small molecules that demonstrate *self-regulating* quenching behavior. The first was an antenna-reaction center model that utilized a photonic switch to provide non-linear control over its charge separation efficiency in an inverse relationship with incident light intensity, a good analog to the overall behavior observed in NPQ.[32] In an effort to more closely mimic the response mechanisms of NPQ, an antenna model was designed around an acid-sensitive quenching switch that could shorten the excited state lifetime of the antenna chromophores upon its protonation at elevated acid concentrations.[33] What follows are reviews of these reports to provide context for the subject of this dissertation. The spectroscopic analyses of these systems rely heavily on theoretical approaches to charge separation in molecular donor-acceptor manifolds put forth by Rudolph A. Marcus, and through-space singlet-singlet energy transfer put forth by Theodor Förster.[34-36] Conceptual summaries of these theories as well as

theoretical descriptions of the optical spectroscopic techniques used in this research are provided in Chapter 3.

The first model system to demonstrate adaptive regulation over charge separation, shown in Figure 1.1, utilized a photochromic dihyroindolizine (DHI)/betaine (BT) switch, originally developed for molecular logic applications, to modulate the quantum yield of charge separated states formed relative to incident light intensity.[32, 37] Designed around established operating parameters for the photochrome, the reaction center was comprised of two bis(phenylethynyl)anthracene (BPEA) antenna moieties capable of singlet-singlet energy transfer to a porphyrin electron donor in essentially unity yield, thereby expanding the spectral cross section of light that could lead to formation of a charge separated state via electron transfer to the fullerene acceptor. The more stable spirocyclic DHI form of the switch does not interact with either the BPEA or porphyrin moieties, and is therefore photophysically passive in this capacity. DHI does, however, absorb blue light, which induces photoisomerization to its BT form, a good energy acceptor for the first singlet excited state of the porphyrin. Rapid energy transfer to BT thus effectively down-regulates the capacity for formation of the porphyrin-cation-fullerene-anion charge separated state, $P^{\bullet+}$-$C_{60}^{\bullet-}$. As the closed form is favored thermodynamically, it can be restored by thermal isomerization at ambient temperatures in the dark with a 37 s time constant. Isomerization could also be effected by irradiation with red light, albeit inefficiently. In this way, the photochromic switch is able to non-linearly transduce incident white light intensity as charge separation efficiency.

In the closed form, the reaction center exhibits charge separation by electron transfer to the fullerene with a 2 ns time constant. This gives a ‘low light’ charge separation efficiency of 82% with respect to the porphyrin excited state. Energy transfer to the open, BT form of the photochrome was found to have a time constant of 33 ps thereby reducing the charge separation efficiency to 1%, thus demonstrating its efficacy as a quenching switch. Simulations of its behavior under real operating conditions were generated first by monitoring absorption from the charge separated state over 15 cycles of light and dark periods to demonstrate reversibility and

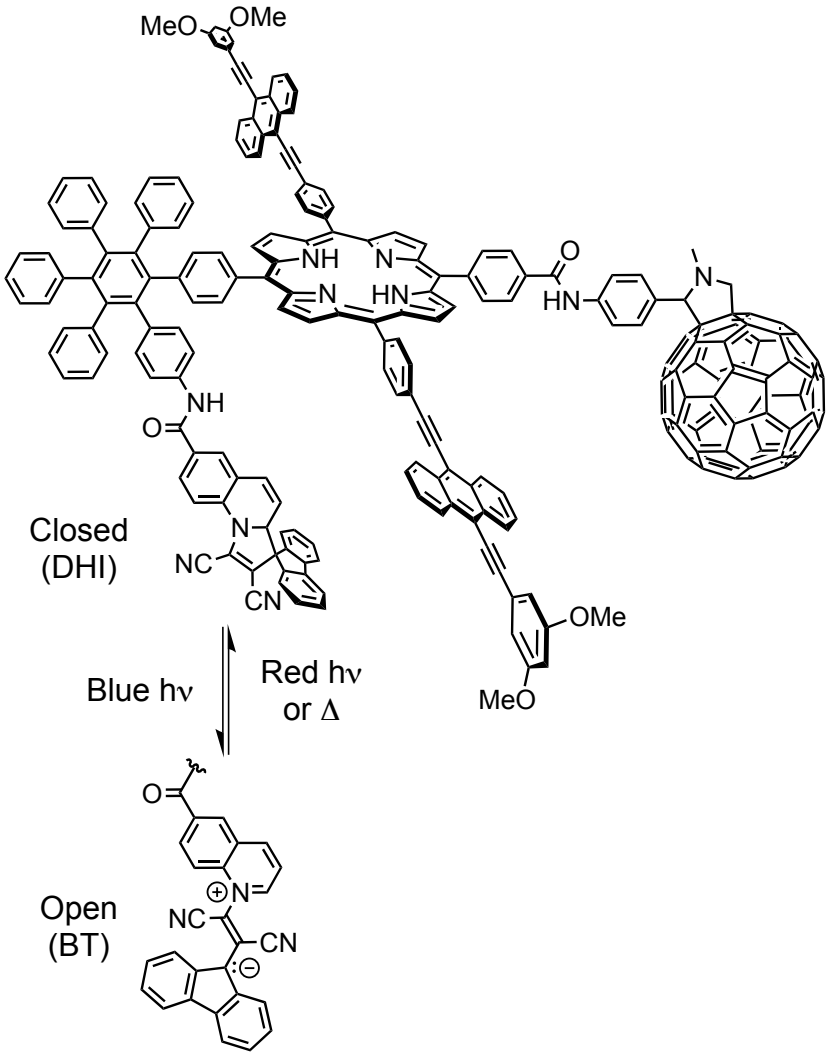

Figure 1.1 A photochromically controlled antenna-reaction center model. With the closed (DHI) form of the switch, excitation of the BPEA or porphyrin moieties readily leads to formation of the $P^{\bullet+}$-$C_{60}^{\bullet-}$ charge separated state. Photoisomerization to the open (BT) form leads to quenching of the porphyrin first singlet excited state via rapid energy transfer to BT.

robustness, and second by determination of charge separation efficiencies at varying intensities of white light to demonstrate its dynamic responsiveness. In the latter experiment the lowest charge separation efficiency of the total population of closed and open isomers was 37%, less than half of the maximum efficiency observed under 'low light' conditions. While this model system achieves its intended functionality, it is only responsive to the blue wavelengths of light absorbed by DHI rather than total light absorbed by the antenna-reaction center complex. The mechanism by which quenching is activated is not biomimetic in the sense that it does not rely on the relay of information regarding system performance via proton activity. This limitation of responsiveness to light absorbed specifically by the photochrome eliminates the capacity for self-regulation in response to a hypothetical downstream product of reaction center activity.

A multi-porphyrin antenna linked to a rhodamine dye, shown in Figure 1.2, is the first reported model system to exhibit acid-responsive regulation of its excited state lifetime in an analogous fashion to NPQ.[33] Development of this antenna stemmed from the discovery of a novel rhodamine dye that possesses photophysical properties in its protonated, open form that make it an excellent energy acceptor for the singlet excited states of zinc tetra-aryl porphyrins. This acid-responsive colorimetric behavior is a hallmark of rhodamine dyes making them useful as pH indicators. Titration of a solution of the model antenna with acetic acid was monitored by steady-state absorption and emission spectroscopies to observe the shift in equilibrium from the closed (colorless) form to the open (blue) form of the dye. The amplitude of a new absorption band at 656 nm, diagnostic for the open dye, was found to be directly influenced by the concentration of acid. The impact of this equilibrium shift was observed in the corresponding emission spectra, in which the porphyrin fluorescence intensity was reduced in proportion to the population of antennae that had been converted to the open dye form. Thus, it was demonstrated that this dye effectively models the pH-responsive excitation energy quenching that characterizes NPQ.

Photophysical analysis of the antenna provides a quantitative description of the efficiency of the dye as an excitation energy quencher. In its closed form, the dye imparts no effect on the

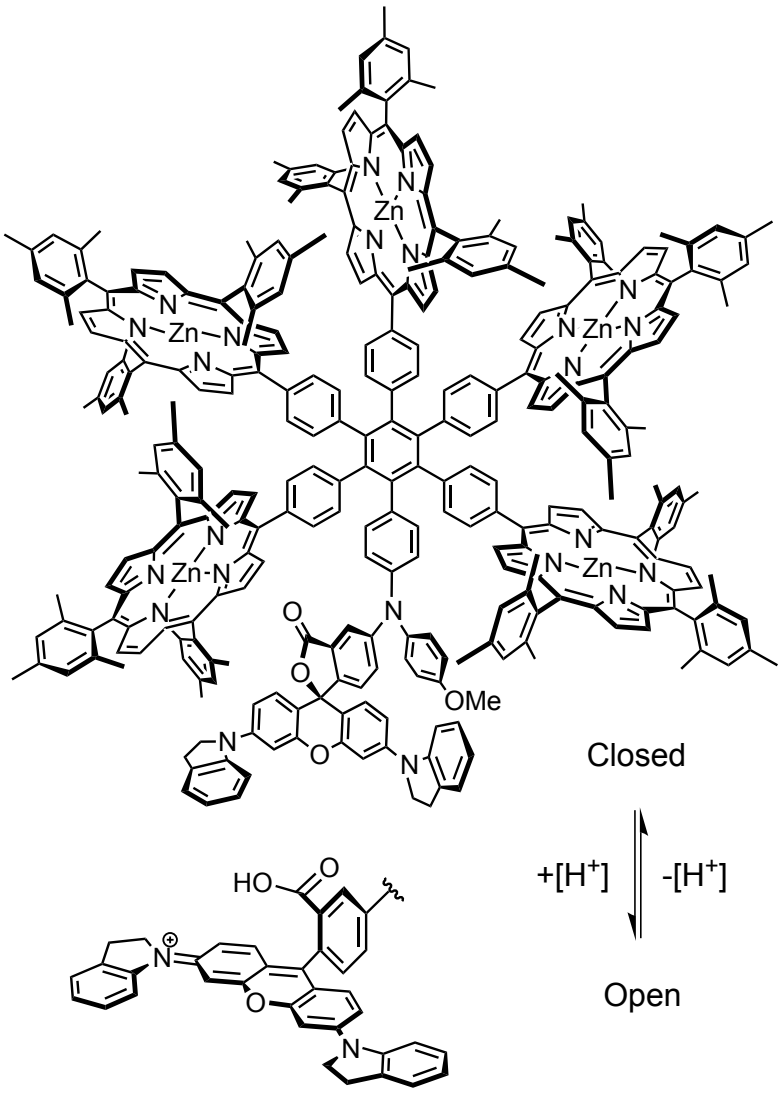

Figure 1.2 An acid-responsive multi-porphyrin antenna model. In the closed form, the dye imparts no effect on photophysical behavior of the antenna. The open, protonated dye acts as an energy sink for the first singlet excited states of the zinc porphyrins, decreasing their fluorescence lifetimes via rapid singlet-singlet energy transfer.

excited state lifetime of zinc porphyrins. Thus, in a neutral solution the antenna was found to possess a fluorescence decay lifetime of 2.1 ns, characteristic of a typical zinc porphyrin. Treatment with an excess of acetic acid resulted in new decay components with time constants of 10 ps and 39 ps. The Förster model for singlet-singlet energy transfer was used to calculate theoretical rates of energy transfer from the zinc porphyrins to the dye allowing for assignment of the 10 ps decay to energy transfer from the ortho-porphyrin and the 39 ps decay to energy transfer from the para-porphyrin. Exponential decay fitting could not separate a component for the meta-porphyrin, and so its decay is assumed to be mixed with those of the ortho- and para-moieties. Aside from ascribing the mechanism of excited state quenching to Förster-type energy transfer, the mechanism of energy dissipation by the dye was not investigated in detail. In contrast to more common rhodamine dyes (such as rhodamine 6G) that are used as fluorescence standards, no emission coud be detected from this novel dye by either steady-state or ultrafast fluorescence measurements. Transient absorption spectroscopy of the isolated dye gave a 5 ps excited state decay lifetime for its open form, which physically rationalizes the lack of detectable emission. In summary, this work showed the efficacy of the novel rhodamine dye as an energy sink for the excited states of zinc porphyrins. The kinetics analysis shows attenuation of the antenna's excited state lifetime by roughly two orders of magnitude, which suggests that the dye could also effectively inhibit electron transfer to an electron acceptor given that the necessary kinetic parameters are met.

Herein is described the synthesis and photophysical characterization of triad **1,** shown in Figure 1.3, a reaction center model comprised of a zinc porphyrin donor, a fullerene acceptor, and the aforementioned rhodamine dye quenching switch. In a neutral solution, excitation of the porphyrin leads to formation of a long-lived charge separated state via transfer of an electron to the fullerene. As in the reported antenna compound the protonated, open form of the dye rapidly quenches the porphyrin singlet excited state via singlet-singlet energy transfer. Consequently, the quantum yield of charge separation decreases dramatically. Steady-state absorption and emission, time-resolved fluorescence, and transient absorption spectroscopies were used to

evaluate the efficacy of energy transfer to the dye as a regulator of charge separation in addition to providing a more complete description of the energy quenching mechanism. Model compounds **2** and **3**, shown in Figure 1.4, were also prepared and spectroscopically characterized in parallel with **1** in order to isolate the decay kinetics of photophysical processes associated with the porphyrin, rhodamine, and fullerene in exclusion of one or both of the others.

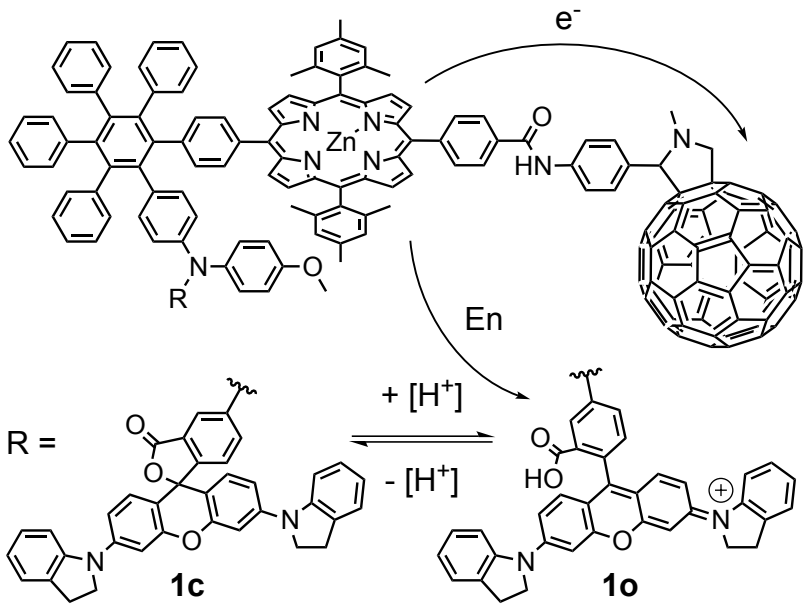

Figure 1.3 An acid-responsive reaction center model, triad **1**, that can be reversibly interconverted between its closed (**1c**) to its open (**1o**) forms by protonation/deprotonation of the rhodamine dye (D_C, D_O). Excitation of the porphyrin moiety of **1c** leads to transfer of an electron (e^-) to the fullerene to form a long-lived charge separated state, D_C-$P_{Zn}^{\bullet+}$-$C_{60}^{\bullet-}$. Conversion to **1o** allows for rapid singlet-singlet energy (En) transfer from $^1P_{Zn}$ to D_O thereby reducing the quantum yield of charge separation.

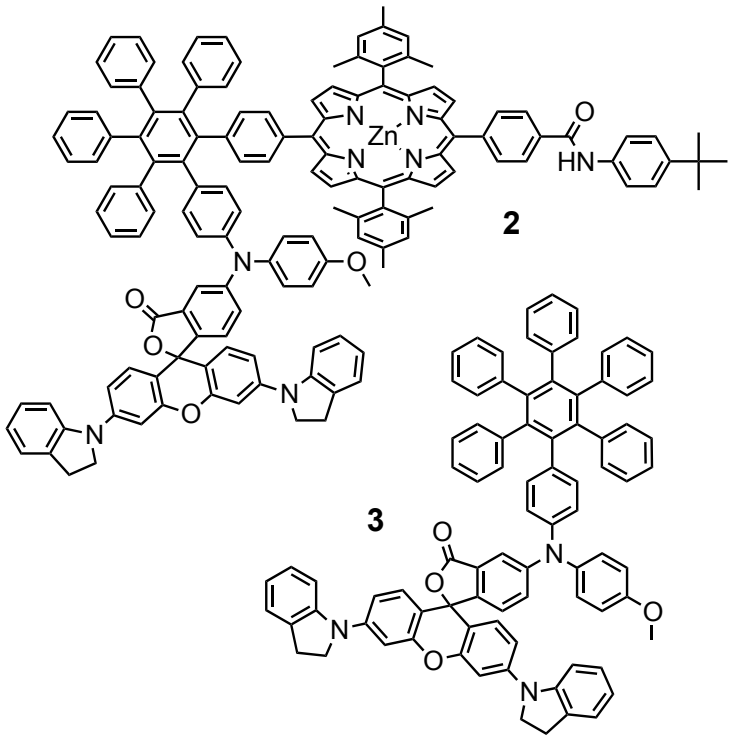

Figure 1.4 Model compounds dyad **2** and dye **3** were prepared to aid in the photophysical analysis of triad **1**. In acidic solutions, they also exist in open forms analogous to that of **1o**.

Chapter 2

Synthesis of an Acid-Responsive Reaction Center Model

Synthesis of triad **1** constituted the majority of time and funding put toward this body of work. This chapter details the most important efforts toward developing a reproducible synthetic pathway that yielded a sufficient quantity of **1** in at accetably high purity for use in photophysical investigations. The total synthesis of **1** involved twenty-four non-linear synthetic steps that were all carried out independently by the author. However, twelve of these reactions had been previously reported and are simply referenced in this dissertation. While most of the steps along unsucessful synthetic pathways discussed herein were novel, several previously reported reactions are also described as they are of strategic significance or were the sources of major synthetic challenges that warrant extended discussion. Experimental methods for all reasonably successful, novel reactions and any characteristic chemical identification data (^{1}H NMR, MALDI-TOF-MS, UV-Vis) that were obtained are provided in Appendix A.

Retrosynthetic analysis of **1** (Scheme 2.1) indicates the necessity to form an intermediate porphyrin-hexaphenylbenzene compound (**iii**) bearing both secondary amine and carboxylic acid functionalities for coupling the rhodamine and fullerene moieties, respectively. It was expected that these coupling reactions needed to be performed in this order to ensure that the reaction conditions would be compatible with the reactivities of all substituents present. The reaction used to attach the rhodamine dye, developed by Yuichi Terazono, involves the use of a palladium catalyst that could, potentially, react with the fullerene moiety and therefore needed to be carried out before the fullerene was introduced.[33] Solubility is a concern with carboxylic acid bearing porphyrins in non-polar organic solvents such as toluene, as is required for this reaction. Thus, it was assumed that an ester would need to be present (**iii**, R = alkyl) to overcome possible solubility issues that could have prevented the coupling reaction leading to **iv** from occurring. While benzoic acid-bearing porphyrins are usually condensed as their corresponding methyl esters (**ii**), the hydrolytic conditions required to obtain the acid involve either a large excess of

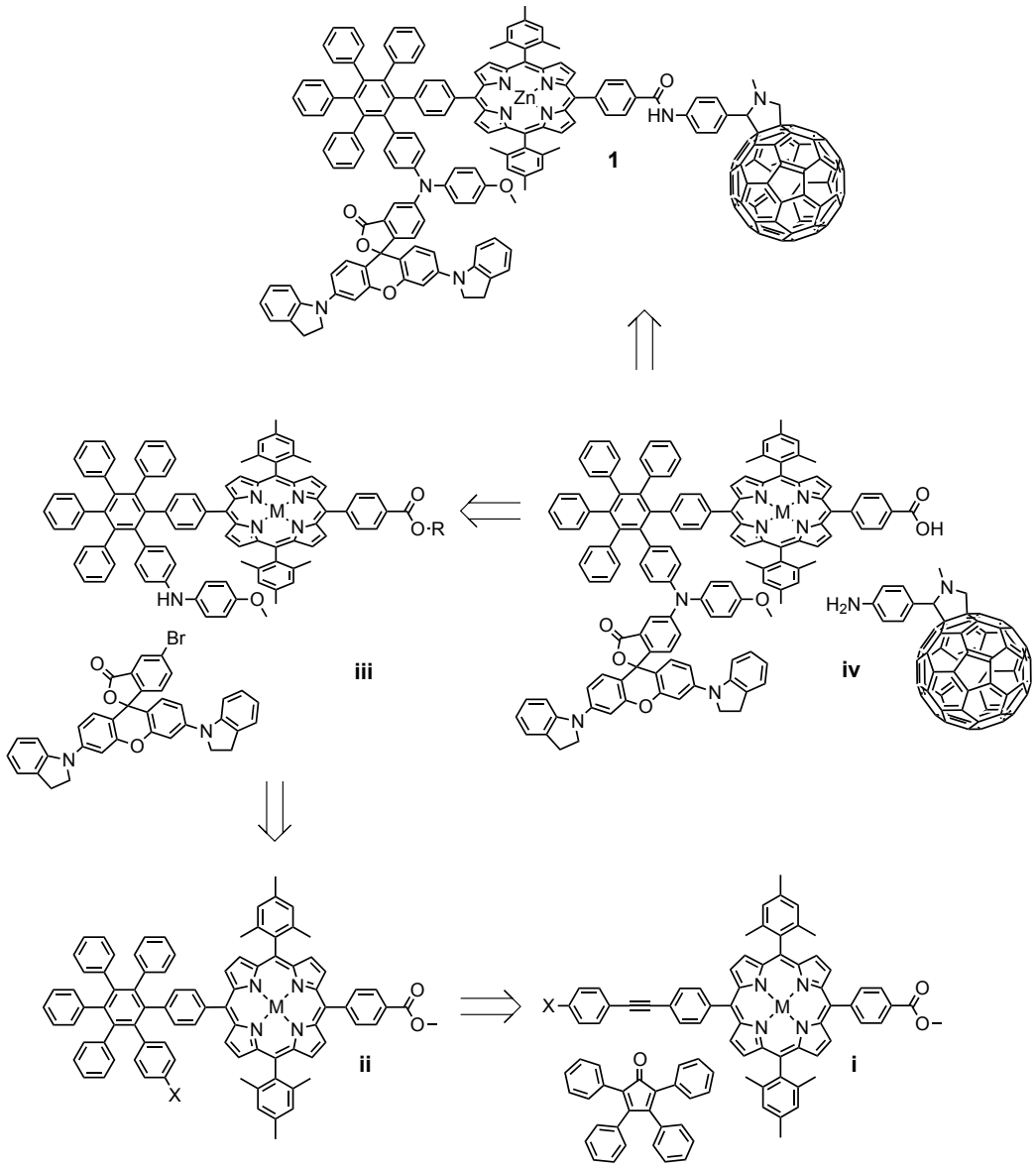

Scheme 2.1 Retrosynthetic analysis of triad **1**.

potassium hydroxide or heating in a mixture of hydrochloric and trifluoroacetic acids. Rhodamine dyes are known to decompose hydrolytically in the presence of hydroxide bases and so the former conditions would not be a viable option for the removal of this protecting group.[38] There was also concern that the indoline groups may be oxidized to more stable indoles with prolonged exposure to elevated temperatures in the presence of a strong acid, thereby eliminating the option of using the latter conditions. Therefore, an electron-rich 2,4,6-trimethylbenzyl ester (Scheme 2.2) was selected because it could be removed in the presence of a relatively mild acid, trifluoroacetic acid, at ambient temperature (Terazono, et al. unpublished). The most attractive and elegant method to obtain the porphyrin-hexphenylbenzene intermediate **ii** involves formation of the hexaphenylbenzene moiety via a thermally driven [2+4] Diels-Alder cycloaddition between a diphenylacetylene-bearing porphyrin and tetraphenylcyclopentadienone (**i**) followed by elimination of carbon monoxide. This methodology was the most obvious starting place given its reported efficacy toward obtaining intermediate **ii** and several structural analogs bearing unique substituents at the 2' phenyl ring relative to that connected to the porphyrin.[32, 33, 39]

With these constraints in mind, the synthetic pathway shown in Scheme 2.2 was proposed. Porphyrin **5**, bearing a diphenylacetylene moiety at the 20-meso position, was prepared by borontrifluoride diethyletherate catalyzed [2+2] condensation from mesityl dipyrromethane and the corresponding aldehydes.[39] The hexaphenylbenzene moiety was then formed by way of the Diels-Alder cycloaddition mentioned above to obtain **6**.[39] Treatment with zinc acetate afforded **7**, which was subsequently coupled with *p*-anisidine via a Buchwald-Hartwig palladium catalyzed aryl-amination reaction yielding the secondary amine **8**. Hydrolysis with potassium hydroxide gave the carboxylic acid, **9**, which was then treated with a carbodiimide coupling reagent, 1-ethyl-3-(3-dimethylaminopropyl)carbodiimide hydrochloride (EDCI), in the presence of 4-dimethylaminopyridine (DMAP) and 2,4,6-trimethylbenzyl alcohol to afford the desired ester, **10**. Following established protocols for the rhodamine dye, **11**, the protected dyad **12** was obtained.[33] Deprotection of the ester with trifluoroacetic acid was carried out, however an inseparable mixture of products was formed.

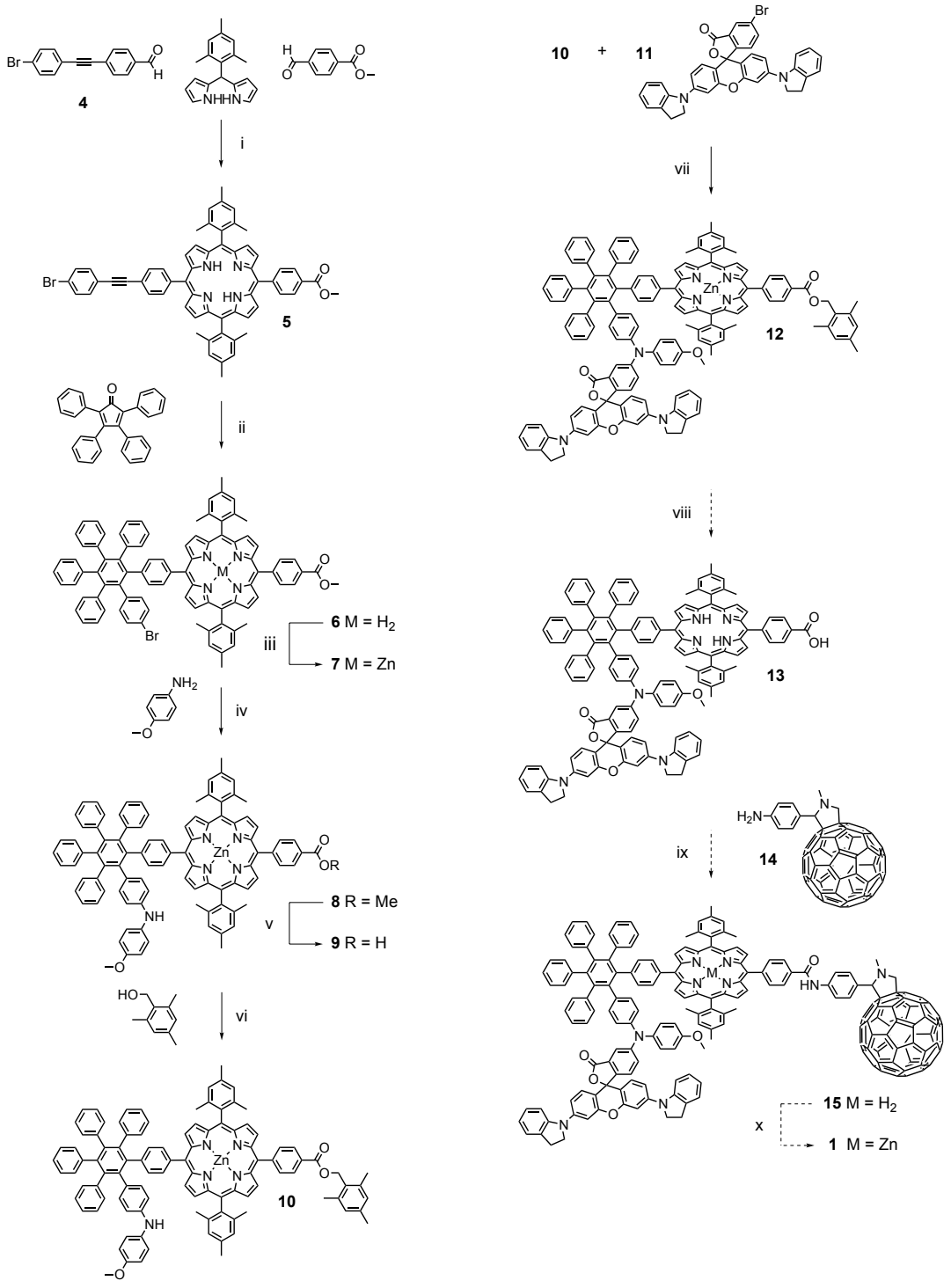

Scheme 2.2 A proposed synthetic pathway to **1**: i a) BF_3OEt_2/EtOH, $CHCl_3$, RT b) DDQ, RT; ii) Ph_2O, reflux; iii) $Zn(OAc)_2{\cdot}2H_2O$/MeOH, $CHCl_3$, RT; iv) $Pd(OAc)_2$, Cs_2CO_3, $P(^tBu)_3$, toluene, reflux; v) KOH (aq), MeOH/THF, RT; vi) EDCI, DMAP, CH_2Cl_2, RT; vii) $Pd(OAc)_2$, Cs_2CO_3, $P(^tBu)_3$, toluene, reflux; viii) TFA/CH_2Cl_2 ix) EDCI, DMAP, CH_2Cl_2; x) $Zn(OAc)_2{\cdot}2H_2O$/MeOH, $CHCl_3$.

The stabilized benzylic carbocation intermediate produced in this reaction has a long lifetime that allowed it to react with the desired product, **13**, to form single and double adducts of the 2,4,6-trimethylbenzyl group (133 amu). These adducts were detected by MALDI TOF-MS which showed that, in addition to the expected molecular ion peak at *m/z* = 1853, peaks at *m/z* = 1985 and 2118 were present in relatively high intensities. These compounds ran as a single spot by thin layer chromatography in all solvent systems that were screened. Resolution of the mixture was attempted numerous times by flash chromatography and preparative thin layer chromatography to no avail. A major issue with chromatographing compounds containing this rhodamine dye is that, in the presence of the silica gel stationary phase, the dye is in equilibrium between its closed (colorless) and open (blue) forms. This has the plainly visible effect of severe band broadening during column chromatography. Other stationary phases including basic and neutral alumina were found to be similarly ineffective. The newly formed carboxylic acid of **13** was also suspected of hindering chromatographic resolution, and so treatment with EDCI and DMAP in the presence of anilinofullerene **14** was carried out in hopes of fascilitating separation of the desired product from this mixture. Unfortunately, the desired product still could not be separated and the batch of material was abandoned. Further literature research on this type of deprotection reaction revealed that cation scavengers such as triethylsilane and 1,3,5-trimethoxybenzene can be added in excess to prevent this type of side reaction from occurring.[32]

Repetition of the porphyrin condensation yielded the expected statistical mixture of trans-A_2BC (**5**), trans-A_2B_2, and trans-A_2C_2 porphyrins shown in Figure 2.1. Following chromatographic separation, the mass spectrum of the band containing **5** showed an additional peak at *m/z* = 799 which was attributed to the A_3B porphyrin shown in Figure 2.1. Repeated chromatographic purification yielded a fraction free of this impurity. However, the ^{1}H NMR spectrum still indicated the presence of a porphyrin impurity based on observation of minor signals that apparently arose from a distinct mesityl group. At this point the mass spectrum only contained the expected molecular ion peak at *m/z* = 936, so it is assumed that the cis-A_2BC geometric isomer of **5** (Figure 2.1) may have been formed. This and the A_3B porphyrin are

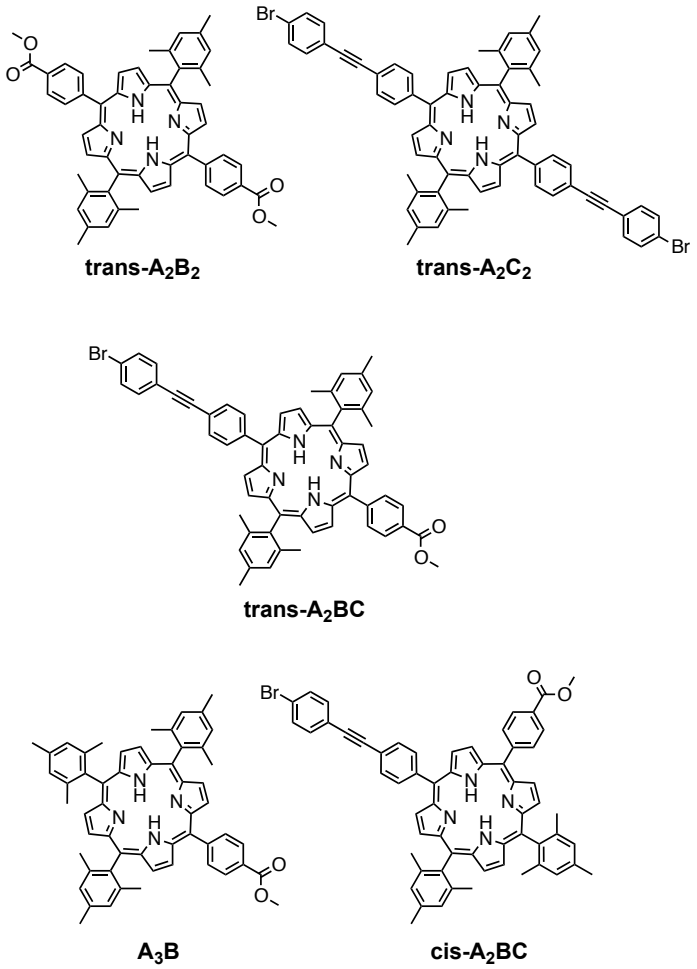

Figure 2.1 Proposed products of the porphyrin condensation shown in Scheme 2.2 (reaction i) including the expected trans-A_2BC (**5**), trans-A_2B_2, and trans-A_2C_2 porphyrins as well as the A_3B and cis-A_2BC porphyrins that could result from scrambling.

potential products of scrambling side-reactions, which are discussed in greater detail below. As no chromatographic or recrystallization technique was found that could resolve this mixture, effort was put into achieving resolution of the material via synthetic modifications. Conversion from the free base to the zinc-coordinating tetrapyrrole is often used to aid in resolution of otherwise inseparable porphyrin mixtures. In this case, there was no change noted. The mixture was also carried through several subsequent steps of the synthetic pathway outlined in Scheme 2.2 without success.

The group of Jonathan S. Lindsey has published extensively on porphyrin synthesis methodologies with several reports dedicated to the mechanism of scrambling and methods of reducing its occurrence.[40, 41] Essentially, dipyrromethanes and porphyrin condensation intermediates can undergo acid-catalyzed fragmentation to yield pyrrolic and azafulvene compounds. These species are then able to recombine to form products of unwanted compositions and geometries. Scrambling occurs in varying degrees depending upon the acid catalyst, its concentration, and the structures and concentrations of the reactants. Reducing the concentration of the acid catalyst has been shown to reduce scrambling.[40] Additionally, catalysis with trifluoroacetic acid in dichloromethane (CH_2Cl_2) was reported as a 'no scrambling' method for porphyrin condensations.[40] Reaction conditions were screened using varying concentrations of different acid catalysts in combination with varying concentrations of reactants, also to no end. Subsequently, the porphyrin condensation reactions shown in Scheme 2.3 were carried out. The amine-functionalized aldehyde **17** was formed by way of a Sonogashira coupling reaction of acetylene **16** with 4-iodobenzaldehyde. A portion of this material was converted to the trifluoroacetamide **18** by treatment with trifluoroacetic anhydride. Again, all variations of the porphyrin condensation reaction conditions oulined above resulted in inseparable scrambled mixtures.

These failed attempts to produce isomerically pure batches of porphyrins **5**, **19**, and **20** necessitated the need for a new strategic approach to the synthesis of a workable porphyrin-hexaphenylbenzene compound. Several structurally analogous antenna and reaction

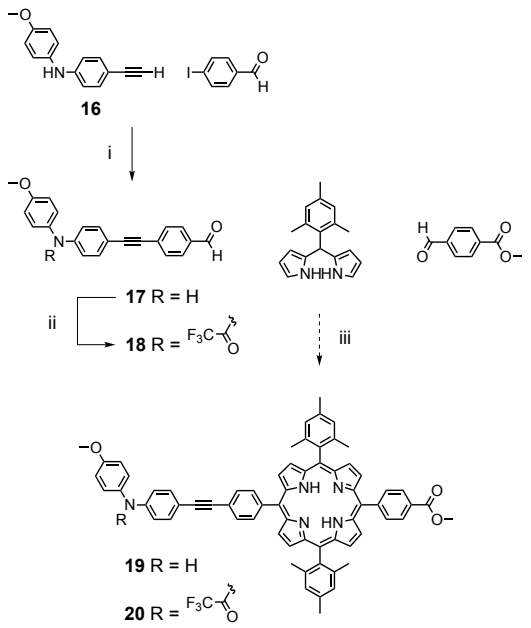

Scheme 2.3 Functionalization of aldehydes and alternative porphyrin condensations: i) $PdCl_2(PPh_3)_2$, CuI, THF/Et_3N, RT; ii) TFAA, pyridine, CH_2Cl_2 0 °C to RT; iii) a) BF_3OEt_2/EtOH, $CHCl_3$, RT b) DDQ, RT or a)TFA/CH_2Cl_2, RT b) DDQ, RT.

center model compounds had previously been prepared following different synthetic methodologies. In one report, a cobalt-templated [2+2+2] cycloaddition of three diphenylacetylene compounds was used to produce a porphyrin-substituted hexaphenylbenzene.[33] However, this method would not be selective for non-symmetrical substitution at the desired 2' position relative to that of the porphyrin as in the structure of triad **1**. The yield of the desired compound would therefore be drastically reduced due to the statistical mixture of potentially inseparable geometric isomers that would form. Another report used an aldehyde-substituted hexaphenylbenzene as a reactant in a porphyrin condensation reaction.[32] While this method would solve the issue of geometric selectivity, the yield was unacceptably low for the purpose of this project.[32] In contrast, Suzuki coupling reactions between meso-bromoporphyrins and aromatic boronate esters have been reported in excellent yields.[42-44] This strategy was pursued to form the requisite hexaphenylbenzene-porphyrin intermediate via a novel hexaphenylbenzene boronate ester.

The synthetic efforts toward obtaining the desired hexaphenylbenzene boronate ester **28** are outlined in Scheme 2.5. Initial attempts to synthesize this non-symmetrical disubstituted hexaphenylbenzene involved substitution of dibromo-hexaphenylbenzene **21** with *p*-anisidine using a Buchwald-Hartwig reaction. A complex mixture of products was obtained, and while it did appear to contain the desired compound **22**, the yield was unacceptably low. The presence of two bromine atoms allowed for catalysis to continue beyond the first substitution to yield the di-substituted and various cross-coupled products. Elimination of this issue required that the hexaphenylbenzene be formed by a [2+4] cycloaddition involving a non-symmetrically substituted diphenylacetylene. To this end, diphenylacetylene **23** was readily formed via a Sonogashira palladium coupling of acetylene **16** and 4-bromo-iodobenzene. Due to the high temperature of the forthcoming Diels-Alder cycloaddition reaction, 260 °C, and the propensity for diphenylamines to undergo oxidative degradation, formation of a thermally and oxidatively resilient amide was desired.[45, 46] The use of a trifluoroacetamide was an attractive option as it could be hydrolyzed using a hydroxide base at ambient temperature, conditions that would simultaneously hydrolyze a methylbenzoate porphyrin substituent (as was successfully used for conversion of **8** to **9**).

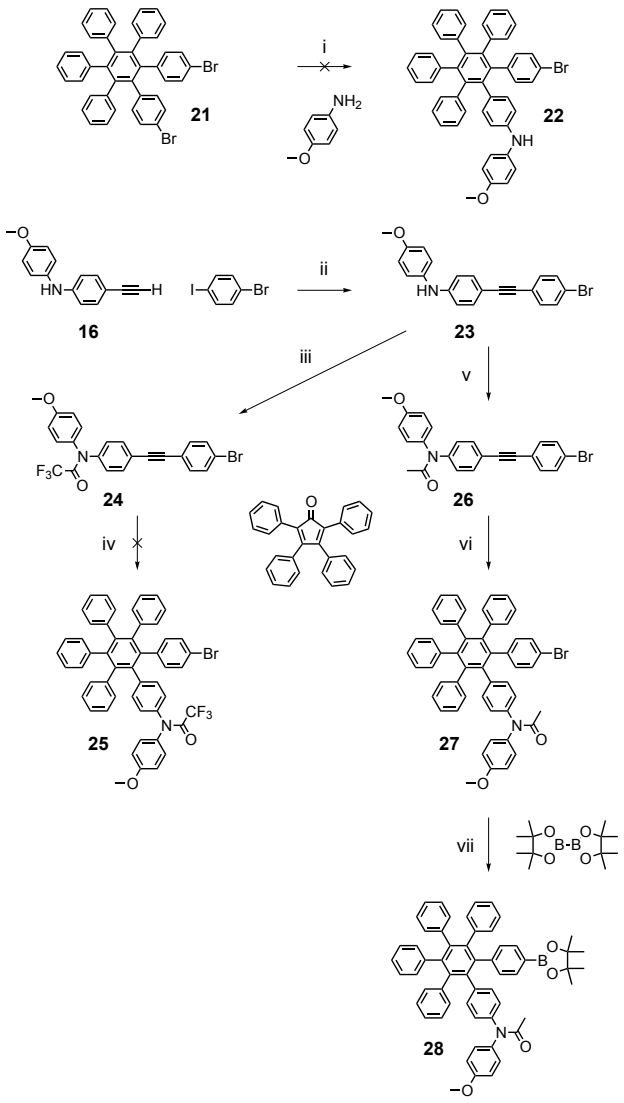

Scheme 2.4 Synthetic approaches to the non-symmetrical hexaphenylbenzene:
i) $Pd(OAc)_2$, Cs_2CO_3, $P(^tBu)_3$, toluene, reflux; ii) $PdCl_2(PPh_3)_2$, CuI, THF/Et_3N, RT; iii) TFAA, pyridine, CH_2Cl_2 0 °C to RT; iv) Ph_2O, reflux; v) acetyl chloride, pyridine, CH_2Cl_2 0 °C to RT; vi) Ph_2O, reflux; vii) $Pd(dppf)Cl_2 \bullet CH_2Cl_2$, KOAc, 1,4-dioxane, 100 °C.

However, trifluoroacetamides are also known to only possess moderate stability toward thermal decomposition above 150 °C.[47] Treatment of **23** with trifluoroacetic anhydride afforded the protected acetylene **24**. Formation of **25** by cycloaddition with tetraphenylcyclopentadieneone was accompanied by heavy, unresolvable decomposition as noted in the ^{1}H NMR spectrum of the product-containing fraction isolated by column chromatography. Clearly, a more thermally stable protecting group was required. Thus, acetamide **26** was prepared by treatment of **23** with acetyl chloride. The non-symmetrical hexaphenylbenzene **27** was then formed without decomposition by the cycloaddtion reaction. Final purification of this intermediate by recrystallization from refluxing toluene yielded a 1:1 complex of **27** with toluene, as noted by ^{1}H NMR after forcefull attempts to remove solvent residues under strong vacuum at elevated temperatures. Synthesis of the desired boronate ester **28** was completed by way of a palladium catalyzed coupling reaction of **27** with bis(pinacolato)diboron. During chromatographic purification, significant decomposition of the boronate ester to the boronic acid was noted if the rate of elution was too low.

With boronate ester **28** and bromoporphyrin **30** (prepared by zincation of the free base **29**[48]) in hand, the sequential assembly of triad **1** (Scheme 2.5) was begun. First, optimal conditions for the critical Suzuki coupling reaction to yield the desired porphyrin-hexaphenylbenzene **31** were investigated. Suzuki reactions are often carried out in coordinating organic solvents and, in particular, tetrahydrofuran (THF) has been used very successfully with porphyrin reactants.[42-44, 49] Initial trials using THF demonstrated that **31** could, in fact, be produced by this method. However, replacement of the meso-bromine atom with hydrogen was by far the favored reaction under these conditions suggesting that the intermediate palladium-porphyrin complex underwent protic elimination before it could react with the hexaphenylbenzene boronate ester. Given the likliehood that steric hinderance may have affected the reactivity of one or both compounds, it was hypothesized that a higher reaction temperature could improve the kinetic favorability of the desired coupling reaction versus elimination. Indeed, the same reaction, when allowed to proceed in refluxing toluene for three days, gave **31** in yields of 65-74%. Global deprotection of the ester and acetamide groups was

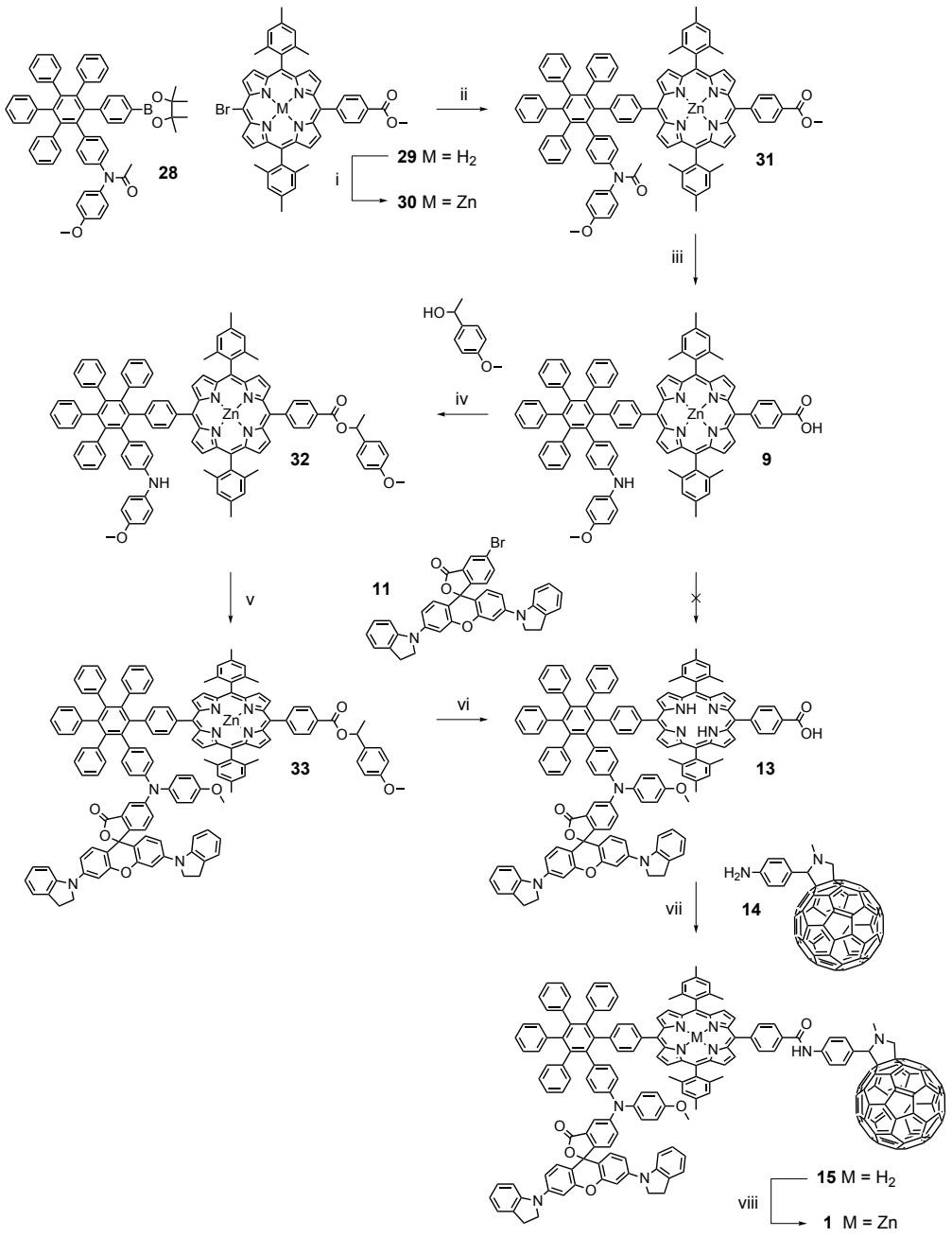

Scheme 2.5 The final synthetic pathway followed to obtain **1**: i) $Zn(OAc)_2 \cdot 2H_2O$/MeOH, $CHCl_3$, RT; ii) $Pd(PPh_3)_4$, K_3PO_4, toluene, reflux; iii) KOH/MeOH, THF, 75 °C; iv) EDCI, DMAP, CH_2Cl_2, RT; v) $Pd(OAc)_2$, Cs_2CO_3, $P(^tBu)_3$, toluene, reflux; vi) TFA/CH_2Cl_2, RT; vii) EDCI, DMAP, CH_2Cl_2, RT; viii) $Zn(OAc)_2 \cdot 2H_2O$/MeOH, CH_2Cl_2, RT.

attempted under both basic and acidic conditions. Alkaline hydrolysis was carried out by addition of saturated methanolic potassium hydroxide to a THF solution of **31** followed by reflux for 12 days. The mass spectrum showed complete conversion to the carboxylic and secondary amine as indicated by a single peak with *m/z* = 1384 corresponding to the mass of **9**. Daily analysis of the reaction progress had shown complete hydrolysis of the methyl ester and minimal hydrolysis of the acetamide within the first day, indicating that the acetamide is overwhelmingly stable to this type of hydrolytic cleavage. In an attempt to achieve the desired reaction in less time, a sample of **31** was dissolved in a 2:1 mixture of concentrated hydrochloric and trifluoroacetic acids and held at 80 °C in a sealed vessel. After several days, analysis of the reaction mixture indicated that virtually no hydrolysis of the acetamide had occurred. Reiteration of the alkaline hydrolysis procedures in sealed pressure vessels and heating at 75 °C for 11-14 days gave **9** in yields of 91-99%.

Porphyrin **9** marks the intersection of the synthetic shown in Scheme 2.5 and the originally proposed pathway in Scheme 2.2. In an effort to completely circumvent the previous catastrophic deprotection reaction, a palladium catalyzed coupling of carboxylic acid-bearing **9** and rhodamine **11** was carried out in toluene. Following overnight reflux, TLC analysis of the reaction mixture did not show obvious formation of the desired product, **13**. However, the mass spectrum of this mixture revealed trace levels of a species with *m/z* = 1853 matching the molecular weight of **13**. Notwithstanding this positive result, the mixture was predominantly composed of unreacted porphyrin **9** and dehalogenated rhodamine **11**. Shortly after reaching reflux temperature, it was noted that a suspension of fine particulate appeared to have formed. Given the results of the reaction, this fine particulate was suspected to be an insoluble cesium carboxylate salt of **9**. In efforts to improve the solubility the reaction was attempted in coordinating organic solvents, THF and 1,4-dioxane. Surprisingly, no traces of **13** were detected following these reactions. These results suggested the necessity of a protecting group to eliminate formation of the carboxylate salt. Synthesis of the photonically controlled antenna-reaction center complex reviewed in Chapter 1 involved esterification of a porphyrin intermediate with 4-methoxy-α-methylbenzyl

alcohol, which was later removed by treatment with trifluoroacetic acid in the presence of a huge excess of a cation scavenger. Coupling of carbodiimide-activated **9** with this alcohol proceeded smoothly to give **32**. As was observed during chromatographic purification of boronate ester **28**, benzyl ester **32** was converted back to the carboxylic acid, **9**, if the material was not eluted quickly enough. Porphyrin **32** was coupled with rhodamine **11** using established Buchwald-Hartwig aryl amination conditions to give dyad **33**.[33] Treatment of **33** with trifluoroacetic acid in a 50 mg/mL solution of 1,3,5-trimethoxybenzene in dichloromethane cleanly afforded the free base dyad **13** bearing a carboxylic acid moiety. From dyad **13**, triad **15** was obtained via a well-known amide forming reaction with anilinofullerene **14**.[32, 39] Trace quantities of methanol from chromatographic purification of **13** were found to intercept the carbodiimide-activated acid leading to formation of the corresponding methyl ester as a minor byproduct. Unfortunately, this impurity was found to be impossible to separate from triad **15** by column chromatography and so preventing its formation by removal of trace methanol from **13** was pursued. The most effective method was found to be repeated dissolution in chloroform followed by distillation of the chloroform-methanol azeotrope. In spite of these efforts, the methyl ester was still formed in approximately 4% yield. Separation of this impurity could only be achieved by repeated preparative thin-layer chromatographic purification. Finally, the pure free base triad **15** was treated with zinc acetate to afford the target compound, triad **1**, in essentially quantitative yield.

Diverging from the synthetic pathway to **1**, the model compound dyad **2** was synthesized from the carboxylic acid-bearing hexaphenylbenzene-porphyrin **9** as shown in Scheme 2.6. The *tert*-butylanilide **34** was readily obtained by way of carbodiimide-activatation of **9** in the presence of 4-*tert*-butylaniline. This was followed by a Buchwald-Hartwig aryl-amination with rhodamine **11** to give the desired model dyad **2** in modest yield. Model dye **3** was generously provided by Yuichi Terazono.[33]

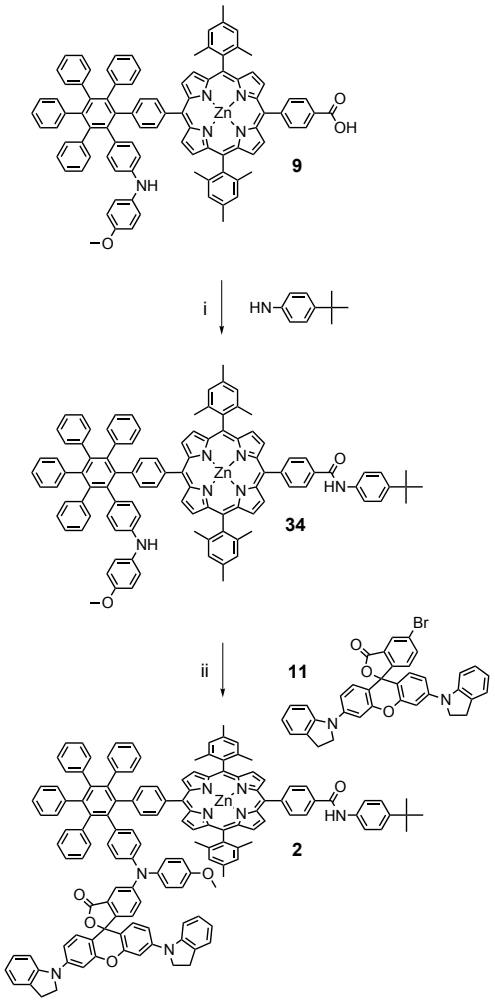

Scheme 2.6 The synthetic pathway followed to obtain 2: i) EDCI, DMAP, CH_2Cl_2, RT; ii) $Pd(OAc)_2$, Cs_2CO_3, $P(^tBu)_3$, toluene, reflux.

Chapter 3

Photophysical and Kinetics Analyses

Photophysical characterization of reaction center and antenna models focuses on the fate of photo-generated excited states of individual chromophores as they return to the ground state through various decay pathways. In the absence of interchromophore interactions, the mechanisms of excited state decay can generally be summarized as internal conversion, intersystem crossing, and fluorescence. Internal conversion (IC) refers to non-radiative vibrational decay to the ground state accompanied by the release of heat. Intersystem crossing (ISC) is a spin-forbidden transition signaling conversion between singlet and triplet states. Fluorescence involves emission of a photon whose wavelength is representative of the energy of the excited state to ground state transition from which it arises. In covalently linked multi-chromophore systems, additional singlet excited state decay pathways are activated and generally include electron and energy transfer processes.

As has been observed and characterized in many porphyrin donor – fullerene acceptor systems, the subject of this research, triad **1**, was designed to undergo photoinduced electron transfer to generate a long-lived (nanoseconds) porphyrin radical cation - fullerene radical anion charge separated state, $P_{Zn}^{\bullet+}$-$C_{60}^{\bullet-}$, under neutral conditions. The long lifetime arises from the ability of fullerenes to stabilize a single negative charge by distribution of the electron density over the entire carbon framework, thus making them attractive electron acceptors for reaction center models.[50, 51] The charge separated state lifetimes are sufficiently long (nano- to microseconds) to hypothetically allow for electron transfer to a secondary acceptor in analogy to the photosynthetic electron transport chain. However, in the absence of a secondary acceptor, the charge separated state recombines to form the neutral ground state, P_{Zn}-C_{60} accompanied by release of heat.

Marcus theory summarizes the significant contributions to the field of electron transfer kinetics and thermodynamics put forth by Rudolph A. Marcus.[34] The Marcus interpretation of excited state electron transfer for P_{Zn}-C_{60}, shown in Figure 3.1, treats the ground, excited, and

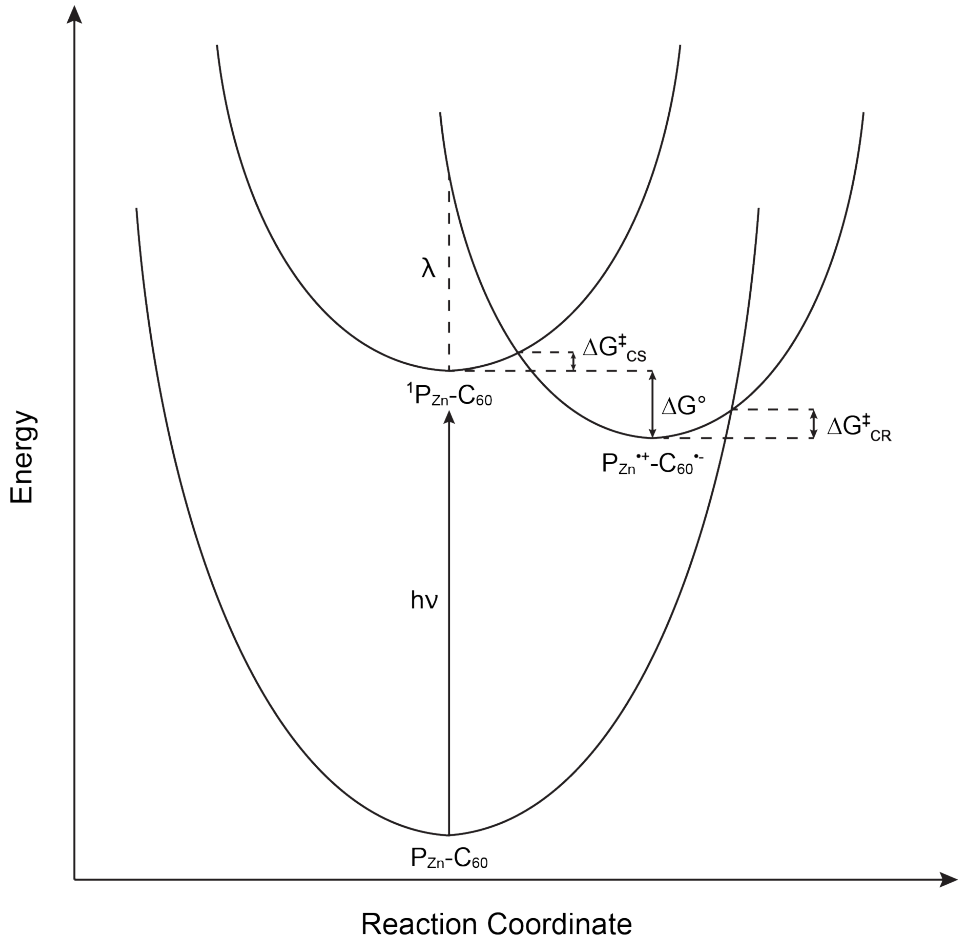

Figure 3.1 A schematic Marcus theory description of photoinduced electron transfer.

charge separated states as parabolic potential energy wells. Each well is representative of the combined P_{Zn} and C_{60} free energies along with contributions from solvation. First, absorption of a photon promotes an electron from the ground state to an excited state; in this case the lowest energy singlet excited state is shown. This vertical transition implies that no nuclear motion takes place. Transfer of an electron from $^1P_{Zn}$ to C_{60} to form $P_{Zn}^{\bullet+}$-$C_{60}^{\bullet-}$ is then thermodynamically allowed from this energized state. Electron transfer occurs along the horizontal reaction coordinate and takes the lowest energy path along which the potential energy surfaces of the initial and final states intersect. The rate of electron transfer (charge separation) can thus be defined using the following equations:

$$k_{CS} = v\, exp(-\Delta G^{\ddagger}_{CS}/RT) \quad (3.1)$$

$$\Delta G^{\ddagger}_{CS} = \frac{\lambda}{4}(1 + \Delta G°/\lambda)^2 \quad (3.2)$$

The term v includes the electronic coupling between the donor and acceptor, λ refers to the total reorganization energy associated with donor-acceptor and solvent nuclear rearrangements, $\Delta G^{\ddagger}_{CS}$ is the activation energy, and ΔG° represents the thermodynamic driving force for the reaction. Through these equations, changes in electron transfer rates in relation to solvent polarity can be rationalized. Polar solvents are able to stabilize $P_{Zn}^{\bullet+}$-$C_{60}^{\bullet-}$ state more so than non-polar solvents, represented by a negative vertical shift its potential well. Therefore, the driving force increases and the activation energy decreases resulting in rate enhancement. For the case shown, it is also worth noting that the activation energy of charge recombination, $\Delta G^{\ddagger}_{CR}$, is relatively large giving rise to the long lifetime of $P_{Zn}^{\bullet+}$-$C_{60}^{\bullet-}$.

As was found in previous studies involving the rhodamine dye moiety of compounds **1**, **2** and **3**, the ability of its open form to quench the excited states of covalently linked zinc porphyrins is attributed to rapid energy transfer and subsequent decay to the ground state.[33] A theoretical model for the decay of singlet excited states by through-space singlet-singlet energy transfer was

developed by Theodor Förster and has since become hugely influential in fields ranging from chemical physics to biophysical dynamics.[35, 36] The Förster resonance energy transfer (FRET) model describes transfer of excited state energy via donor-acceptor dipole-dipole interactions. Essentially, the strength of this interaction depends on resonant coupling between the donor and acceptor transition dipoles. The transition of the donor excited state decay must energetically overlap with the transition of the acceptor excited state formation to some degree; the better the overlap, the stronger the interaction. Förster's theory treats this as a Coulombic interaction between the oscillating transition dipoles of a single donor electron and a single acceptor electron. Oscillations of the donor electron induce oscillations in the acceptor electron by through-spce electrostatic interactions allowing for the passage of energy from one electron to the other. Thus, the relative orientations of the dipoles and the distance between them also influence the strength of the interaction. This model allows for prediction of energy transfer rates based on experimentally measurable properties using the following equation:

$$k_{FRET} = \frac{9000\, ln10\, \kappa^2\, k_r}{128\, \pi^5\, N_A\, n^4\, R_{DA}^6}\, J \qquad (3.3)$$

In this equation, κ^2 is the dipole-orientation factor, k_r is the radiative rate constant of the donor (calculated from the fluorescence decay lifetime and the fluorescence quantum yield), N_A is Avogadro's number, *n* is the refractive index of the solvent, R_{DA} is the donor-acceptor center-to-center separation distance, and *J* is the overlap integral related to the strength of donor-acceptor interactions.

Steady-state spectroscopies provide useful information regarding photophysical processes that can be detected at the equilibrium state of a system. Absorption measurements allow for observation of transitions from the ground state (S_0) to excited states (S_1, S_2, etc.) induced by photo-excitation via incremental exposure to a portion of the UV-visible-and near IR light spectrum. Each absorption band that is recorded, indicating that photons of particular

wavelengths were absorbed by the sample rather than passing through to the detector, refers to a particular transition of a particular species within the sample, barring the complete energetic overlap of transitions from different species. Emission measurements give information regarding transitions beginning from the first singlet excited state (S_1) or triplet (T_1) state leading to the ground state (S_0). A sample is continuously excited at a wavelength corresponding to a particular electronic transition and the photons emitted from the formed excited state are captured by a photon measuring device. Transitions detected by steady-state methods are often useful as diagnostic indicators of sample composition and can be used to calculate the relative energy levels of emissive excited state species.

Time-resolved fluorescence and transient absorption spectroscopies are used to obtain kinetic information regarding the excited state lifetimes of unique chemical species and the rates by which they decay. Sufficiently emissive excited states may be monitored by decay of their fluorescence at a particular wavelength. The decay profiles obtained by this type of measurement can then be fit by a multi-exponential decay model. Multiple decay components represent chemically unique species that share a common S_1 to S_0 transition energy (emission wavelength). Each component is fit by a decay time constant that represents the S_1 lifetime of that species. The inverse of this lifetime is the sum total of the rate constants of all decay processes available to that species. In order to detect very short-lived and/or non-emissive transient species and to deconvolute the decay kinetics of species whose emissions overlap signficantly, transient absorption spectroscopy is used. In contrast to the aforementioned optical techniques, transient absorption is readily able to record transitions from S_1 to S_n, S_1 to T_1, T_1 to S_0, S_1 to S_0, etc. The technique used to study triad **1** and model compounds **2** and **3** is known as pump-probe transient absorption spectroscopy. First, a population of excited states is generated by an intense, monochromatic 'pump' pulse. Then, following a specified time delay, a broad-spectrum 'probe' pulse is passed through the sample and the absorption spectrum is captured. Each spectrum captured is recorded as the difference in absorption collected before and after the pump pulse. This alternation of pump and probe pulses is repeated to obtain a series of difference absorption

spectra at varying time delays. For this work, the time delays separating these light pulses were varied from hundreds of femtoseconds to tens of nanoseconds. Taken together, this series of difference spectra at varying time delays can be globally fit to produce a set of decay associated spectra (DAS) that describe the formations and decays of individual transient species including singlet and triplet excited states and charge separated states. As a whole, the global fitting results describe photophysical processes such as fluorescence, energy transfer, charge separation, charge recombination, and intersystem crossing. The information obtained through these spectroscopic techniques allows for determination of rate constants and mechanisms for the formations and decays of individual transient chemical species.

Spectroscopic analyses of **1**, **2** and **3** were carried out in order to compile kinetic and mechanistic descriptions of the major photophysical processes that follow photo-excitation of **1** via its primary chromophore, a zinc porphyrin (P_{Zn}). The steady-state experiments and the kinetics interpretation from the total system perspective described in this chapter were predominantly the work of the author. The time-resolved fluorescence and transient absorption experiments, data analyses, and mechanistic interpretations were performed by Gerdenis Kodis.

Steady-State Absorption and Emission

The acetic acid (AcOH) mediated conversion of **1c** to **1o** in dichloromethane (CH_2Cl_2) was monitored using steady-state absorption and emission spectroscopies. The absorption spectrum of **1c** shown in Figure 3.2A (solid, black) is composed of maxima typical of a zinc porphyrin (P_{Zn}) at 422 nm (Soret) and 549 and 589 nm (Q-bands). Absorption bands attributed to the closed rhodamine dye (D_C) at 311 and 330 nm and the fullerene (C_{60}) at 706 nm were also observed but are not shown.[33] Addition of AcOH produced a broad absorbance band at ca.
650 nm accompanied by slightly increased absorbance across the visible range. These optical features are characteristic of the open dye (D_O) and indicate formation of **1o**.[33] Following acidification, the sample was neutralized with aqueous Na_2CO_3, filtered through a pad of silica,

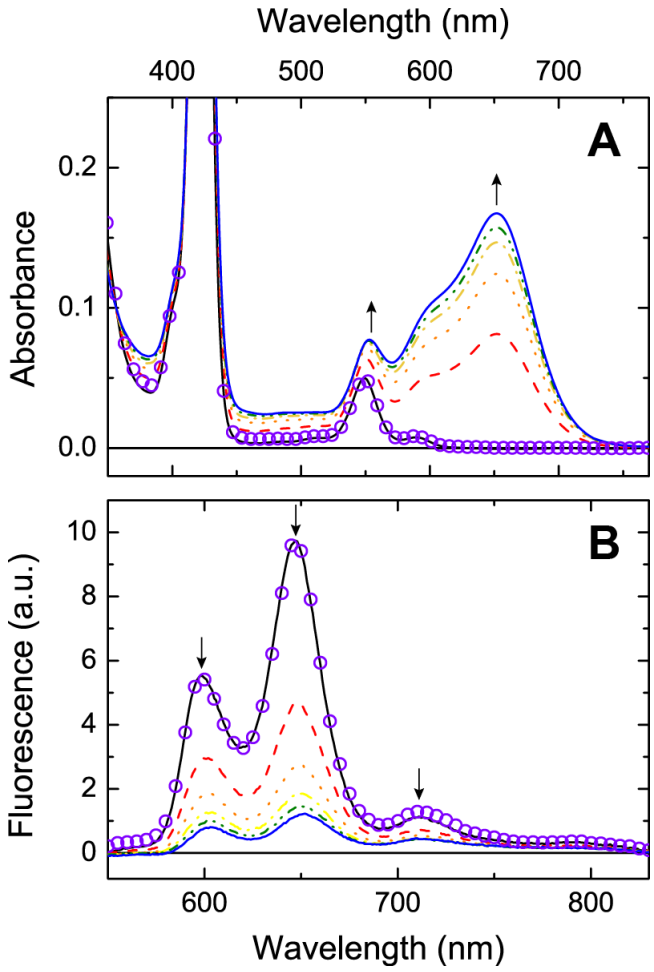

Figure 3.2 Absorption (**A**) and emission (**B**) spectra were collected as **1** was titrated with AcOH: 0 M (solid, black), 0.43 M (dash), 0.83 M (dot), 1.2 M (dot-dash), 1.6 M (dot-dash-dot), and 2.3 M (solid, blue). Neutralization with Na_2CO_3 (aq) resulted in the spectra shown as circles. Spectra have been corrected for volume changes. **A** The maxima at 422, 559, and 591 nm are characteristic of P_{Zn}. Increasing intensity of the feature at 652 nm, diagnostic for D_O, signifies formation of **1o**. **B** Emission spectra (λ_{ex} = 550 nm) show decreasing intensity of $^1P_{Zn}$ fluorescence at 598 and 647 nm concomitant with formation of **1o**. Maxima at 711 and 793 nm arise from $^1C_{60}$.

evaporated to dryness under a stream of argon, and redissolved in CH_2Cl_2. The resulting absorption spectrum (open circles) very closely matches the pre-titration spectrum of **1c**, thus indicating reversible interconversion between **1c** and **1o**. The emission spectrum collected for **1c** (λ_{ex} = 550 nm) shown in Figure 3.2B (solid, black) features maxima at 605 and 652 nm characteristic of fluorescence from the zinc porphyrin singlet excited state ($^1P_{Zn}$) and at 711 and 793 nm, which are attributed to fluorescence from the fullerene singlet excited state ($^1C_{60}$). Protonation of the dye with AcOH led to a significant reduction in porphyrin emission intensity indicating that Do strongly quenches $^1P_{Zn}$. Following neutralization, the emission spectrum (open circles) closely resembles that of **1c** further demonstrating reversible interconversion between **1c** and **1o** by protonation/deprotonation of the dye. The slight increase of $^1C_{60}$ emission intensity at 700-800 nm relative to that of $^1P_{Zn}$ at 600-650 nm can be explained by increased quenching of $^1P_{Zn}$ by charge separation due to rate enhancement in the presence of trace water or methanol from the work-up procedure.[34] This effect is noted in kinetics anlysis discussion vide infra. However, this may also/instead indicate that minor decomposition occurred during the experiment.

Time-Resolved Fluorescence

Fluorescence decays (λ_{ex} = 550 nm, λ_{obs} = 650 nm) for **1** and **2** in CH_2Cl_2 with 0 M, 1.6 M, and 4.5 M AcOH were recorded using the time correlated single photon counting technique and the data were fit by multi-exponential decay curves, shown in Figure 3.3, to obtain decay lifetimes for photophysically unique species (Table 3.1). The decays for **1c** and **2c** (0 M AcOH) gave τ_1 = 183 ps and 1.97 ns, respectively. The lifetime of **2c** is in good agreement with those reported for similar compounds suggesting that it decays via typical pathways.[33] The excited state lifetime of **1c** is an order of magnitude shorter than that of **2c**, a result of one or more quenching processes attributed to interactions between $^1P_{Zn}$ and C_{60}. The 183 ps lifetime of **1c** is expected to include the kinetics from charge separation to form the $P_{Zn}^{\bullet+}$-$C_{60}^{\bullet-}$ charge separated state and

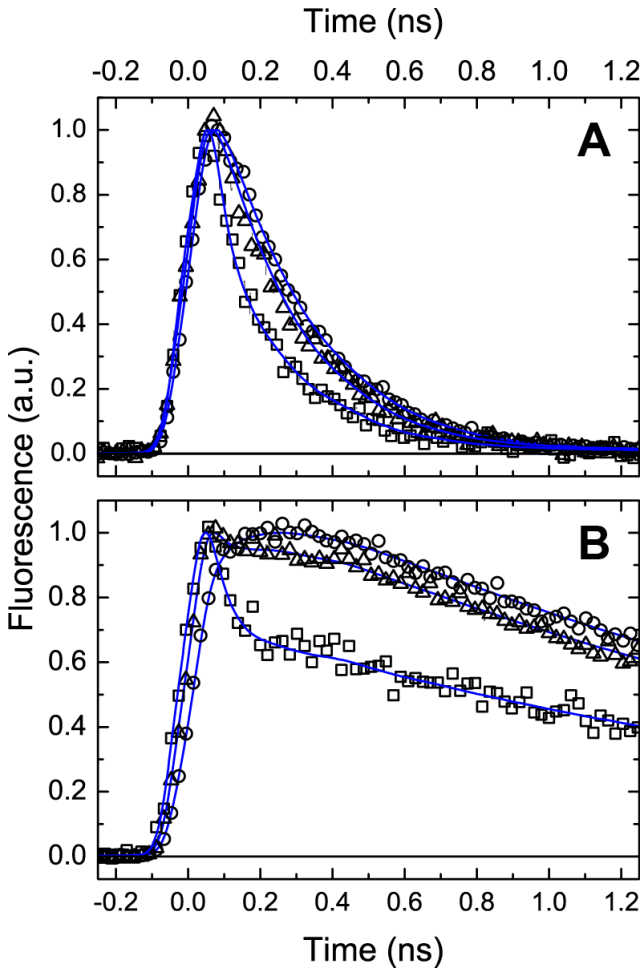

Figure 3.3 Time-resolved fluorescence decays collected at 650 nm for of **1** and **2** in CH_2Cl_2 (**A** and **B**, respectively) (λ_{ex} = 420 nm) and their exponential decay fit lines with [AcOH] = 0 M (circles), 1.6 M (triangles), and 4.5 M (squares).

Table 3.1 Time-resolved fluorescence exponential decay fitting results.

	[AcOH]	τ_1 (ps)	τ_2 (ps)	χ^2
1	0 M	183 (100%)	-	~1.1
	1.6 M	178 (33%)	17 (67%)	~1.1
	4.5 M	160 (15%)	17 (85%)	~1.1
2	0 M	1970 (100%)	-	~1.1
	1.6 M	1960 (32%)	19 (68%)	~1.1
	4.5 M	1970 (13%)	19 (87%)	~1.1

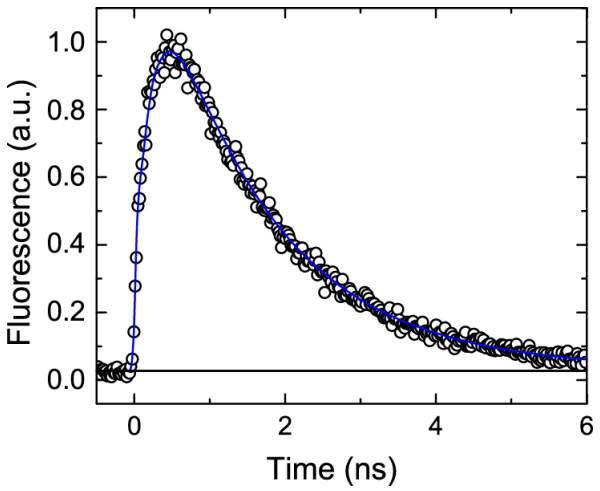

Figure 3.4 Time-resolved fluorescence decay profile collected at 800 nm **1** in toluene (λ_{ex} = 550 nm) and the exponential decay fit line. The fit is composed of a rise component with τ = 255 ps, and decay components with τ = 1.34 ns (90%) and 2.18 ns (10%). The rise time is attributed to formation of $^1C_{60}$ from decay of $^1P_{Zn}$. The 1.34 ns component is characteristic of $^1C_{60}$ decay and the 2.18 ns component is associated with impurities resulting from sample degradation.

also, possibly, energy transfer to form $^1C_{60}$.[39, 52-56] The fitting results obtained for **1** and **2** in the presence of AcOH were each composed of two decay components indicating that the samples contained mixtures of their closed and open forms, the relative populations of which are reflected by their associated pre-exponential factors (tabulated as percentages). In each case the longer τ_1 lifetimes are attributed to fluorescence decay arising from the closed forms, as they are similar to the τ_1 lifetimes observed in the absence of AcOH. The τ_1 lifetimes for **1c** are noted to decrease with increasing AcOH, a result of enhanced rates of charge separation in higher polarity solutions.[34] The shorter components, τ_2 = 17 ps and 19 ps, are assigned to decay of $^1P_{Zn}$ for **1o** and **2o**, respectively. The significant decreases in these lifetimes relative to the τ_1 lifetimes are attributed to the presence of a $^1P_{Zn}$ to D_O singlet-singlet energy transfer decay pathway for **1o** and **2o**. These lifetimes are also in good agreement with those previously reported for analogous compounds exhibiting this specific energy transfer mechanism.[33]

The fluorescence decay of **1c** in toluene was collected to investigate the possibility of singlet-singlet energy transfer from $^1P_{Zn}$ to C_{60}. The decay profile (λ_{ex} = 550 nm, λ_{obs} = 800 nm) was best fit by a multi-exponential decay, shown in Figure 3.4, giving a τ = 255 ps rise component and decay components with τ = 1.34 ns (90%) and 2.18 ns (10%). The dominant 1.34 ns component is attributed to decay of $^1C_{60}$, which coincides with the fluorescence ascribed to $^1C_{60}$ in the steady-state emission spectrum of **1c**. This lifetime is also in strong agreement with reported $^1C_{60}$ lifetimes.[52-54, 56] While some portion of $^1C_{60}$ is likely formed by direct excitation of C_{60} at 550 nm, the much greater OD_{550} of P_{Zn} relative to that of C_{60} suggests that some portion of the $^1C_{60}$ population likely evolved as a result of $^1P_{Zn}$ decay. The rise component is attributed to such a process, for which the mechanism is discussed vide infra.[52-54] The minor 2.18 ns component is similar to the decay lifetime of $^1P_{Zn}$ for **2c** in CH_2Cl_2 and so is attributed to decay of 'free'-$^1P_{Zn}$ produced by sample decomposition through which some C_{60} was completely cleaved from- or otherwise rendered an ineffective $^1P_{Zn}$ electron and energy acceptor in the degraded compound.

Transient Absorption

Pump-probe transient absorption spectroscopy was used to identify and characterize the kinetics of charge separation, singlet-singlet energy transfer, and other excited state decay processes associated with **1**, **2**, and **3**. Charge separation was induced in **1c** by excitation of P_{Zn} (λ_{ex} = 550 nm) in CH_2Cl_2 and the difference absorption spectra across several spectral windows were collected over 3 ns intervals to monitor decay of $^1P_{Zn}$ and formation of the resulting charge separated state. Global fitting of these data produced DAS showing formation of long-lived $P_{Zn}^{\bullet+}$ and $C_{60}^{\bullet-}$ species evolving from decay of $^1P_{Zn}$. The DAS in Figure 3.5A have two components showing stimulated emission (SE) from $^1P_{Zn}$ decay (dash) at 650 nm with τ = 190 ps leading to induced absorption (IA) from formation of $P_{Zn}^{\bullet+}$ (solid) at 660 nm that did not decay on the timescale of this experiment.[39, 53, 54] The DAS in Figure 3.5B show formation of a non-decaying IA at 1000 nm with τ = 190 ps indicative of formation of a long-lived $C_{60}^{\bullet-}$.[39, 53, 54] The fitted lifetimes of formation for $P_{Zn}^{\bullet+}$ and $C_{60}^{\bullet-}$ agree with the fluorescence decay lifetimes determined for **1c**. The kinetics of formation of $^1C_{60}$ via energy transfer from $^1P_{Zn}$ may also be a component of these lifetimes. A longer timescale experiment was performed with a deoxygenated sample of **1c** in CH_2Cl_2 (λ_{ex} = 560 nm) to observe decay of the charge separated state by recombination and to detect for other long-lived species. The DAS in Figure 3.6 show decay of IA (solid) at 650 nm signifying decay of $P_{Zn}^{\bullet+}$ with τ = 5.19 ns. The non-decaying IA (dot) at 700 nm is attributed to a $^3C_{60}$ species produced by ISC from $^1C_{60}$.[54, 57]

The mechanism of $^1C_{60}$ formation for **1c** in toluene was elucidated by monitoring the decay of $^1P_{Zn}$ by transient absorption spectroscopy (λ_{ex} = 590 nm). Global analysis of the data gave a good fit for the time constants obtained from the decay of $^1C_{60}$ emission and resulted in the three components DAS shown in Figure 3.7. The (solid) component with τ = 255 ps shows decay of SE at 600 and 650 nm arising from decay of $^1P_{Zn}$ and essentially simultaneous decay of ground state bleaching (GSB) at 550 and 600 nm signifying reformation of the ground state, P_{Zn}.

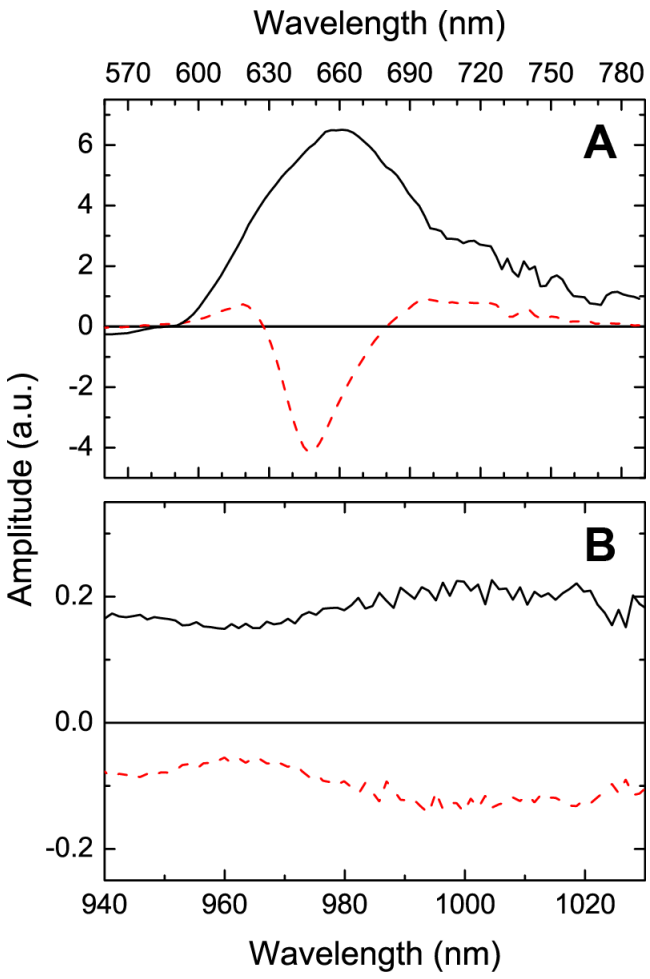

Figure 3.5 Decay associated spectra fit to transient absorption data collected from **1c** in CH_2Cl_2 (λ_{ex} = 550 nm). **A** The (dash) component represents decay of $^1P_{Zn}$ with τ = 190 p and the (solid) component arises from non-decaying $P_{Zn}^{\bullet+}$ species. **B** The (dash) component indicates formation of $C_{60}^{\bullet-}$ with τ = 190 ps that did not decay (solid) within the timescale of this experiment.

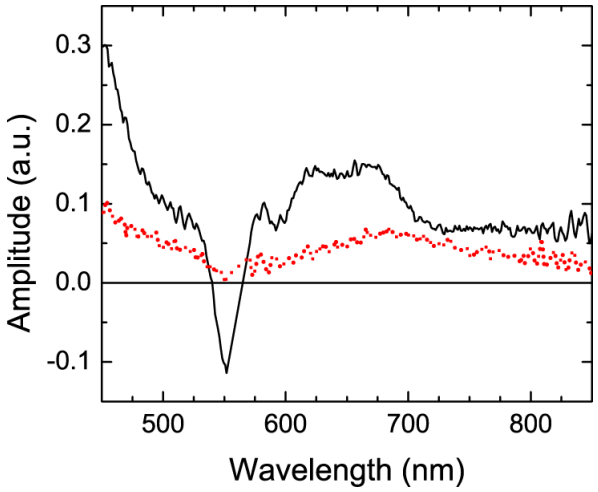

Figure 3.6 Decay associated spectra fit to transient absorption data collected from **1c** in deoxygenated CH_2Cl_2 (λ_{ex} = 560 nm). The (solid) component shows decay of $P_{Zn}^{\bullet+}$ with τ = 5.19 ns and the (dot) component arises from a non-decaying $^3C_{60}$.

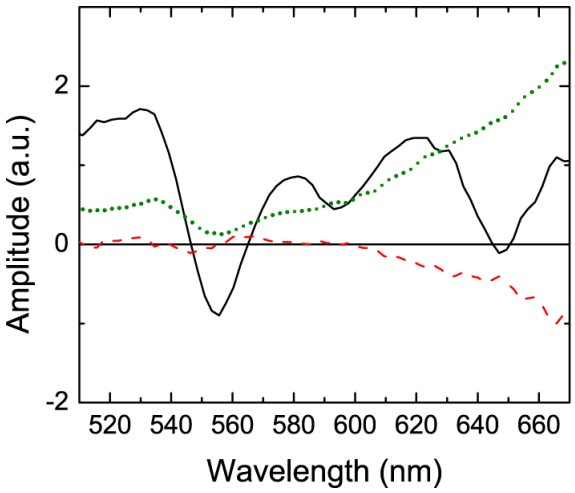

Figure 3.7 DAS fit to transient absorption data collected from **1c** in toluene (λ_{ex} = 590 nm). The (solid) component shows concerted decay of $^{1}P_{Zn}$ and reformation of its ground state with τ = 255 ps. The (dash) component represents formation of $^{3}C_{60}$ with τ = 1.34 ns that did not decay (dot) within the time scale of this experiment.

This concerted return to the ground state is indicative of an energy transfer mechanism, as formation of a transient charge separated state would show a delay in the decay of GSB.[54] The (dash) component represents decay of $^1C_{60}$ and formation of $^3C_{60}$ with a lifetime of 1.34 ns, which generated a non-decaying IA (dot) from the long-lived $^3C_{60}$.[57]

A CH_2Cl_2/AcOH solution comprised predominantly of **3o** was examined using transient absorption spectroscopy to determine the mechanism by which the singlet excited state of the open dye (^1D_O) decays. As no emission could be detected for this species by steady-state or time-resolved fluorescence measurements, it was expected to be an ultrafast process. The resulting DAS (λ_{ex} = 640 nm) shown in Figure 3.8 describe a three-component decay mechanism fit by time constants τ = 1.6 ps (solid), 2.9 ps (dash), and 12 ps (dot). The 1.6 ps component (solid) shows decay of SE at 700-770 nm signifying decay of ^1D_O and formation of GSB at 640 nm attributed to formation of a hot ground state, $^{hot}D_O$, with τ = 1.6 ps.[58] This ultrafast relaxation of ^1D_O likely occurs via intramolecular internal charge transfer (ICT).[58, 59] The other components show decay of GSB at 630 and 620 nm with τ = 2.9 ps and 12 ps, respectively. These decays are attributed to vibrational cooling of $^{hot}D_O$, typically the slowest components of relaxation, which yield the fully relaxed ground state, D_O.[58, 59] Alternatively, there could be an inverted kinetics case where the 2.9 ps component is assigned to relaxation of ^1D_O and the 1.6 ps component is assigned to cooling. The 12 ps component (dot) displays a slightly blue shifted GSB, indicative of a vibrational cooling process involving rearrangment of the solvent, and IA around 700 nm, characteristic of the non-equilibrated ground state where SE from ^1D_O decay is observed.[59] The most probable pathway for this relaxation process is illustrated in Figure 3.9.

Transient absorption measurements of **1o** and **2o** were collected to monitor energy transfer from $^1P_{Zn}$ to D_O. The DAS for **2o** in CH_2Cl_2 (λ_{ex} = 420 nm) shown in Figure 3.10A are composed of two components that describe decay of $^1P_{Zn}$ by energy transfer to D_O followed by ultrafast relaxation of ^{1}Do. The (dash) component shows decay of SE at 610 and 660 nm with τ = 19 ps signifying decay of $^1P_{Zn}$ concomitant with formation of ^1D_O. This time constant is consistent with the fluorescence decay lifetimes fit for **1o** and **2o**. Following energy transfer, the

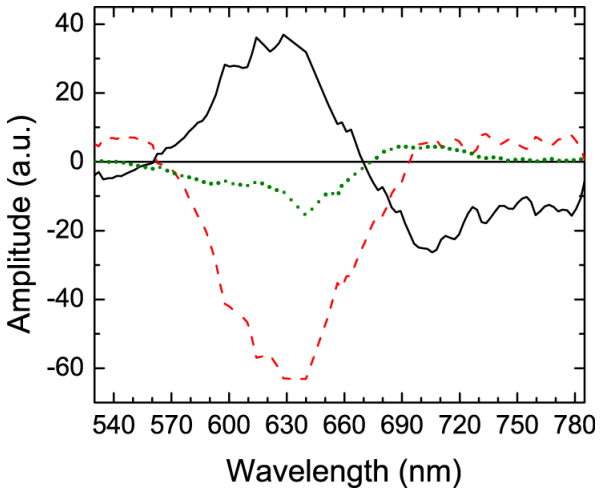

Figure 3.8 DAS fit to transient absorption data collected from **3o** in CH_2Cl_2 with an excess of AcOH (λ_{ex} = 640 nm). The solid component arises from decay of ^1D_O with τ = 1.6 ps. The remaining components arise from vibrational relaxation and cooling of the hot ground state, D_O^{hot}, with τ = 2.9 ps (dash) and 12 ps (dot).

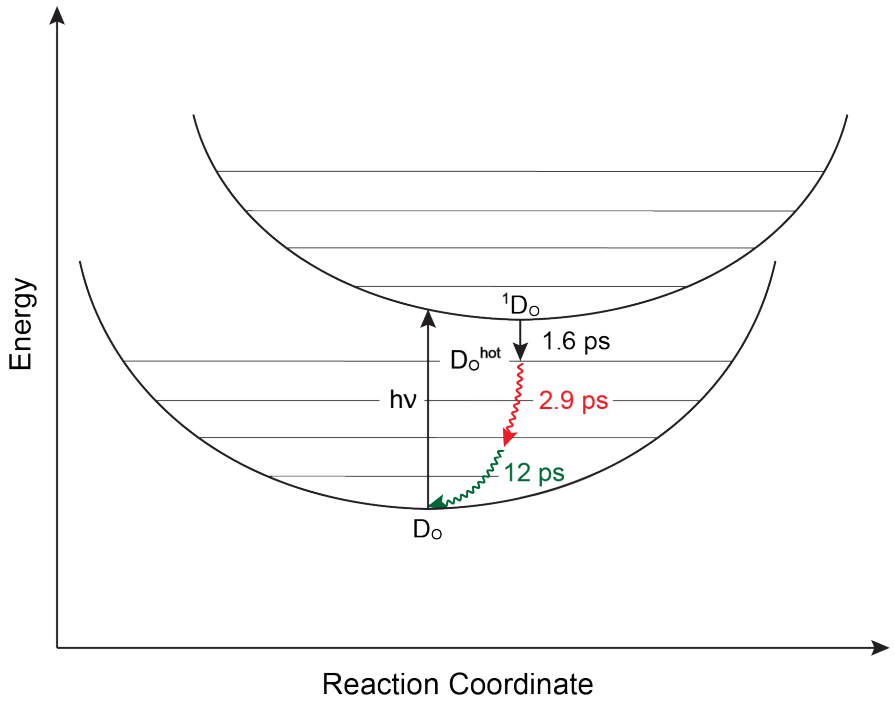

Figure 3.9 A schematic representation of the relaxation pathway of ^1D_O. The shapes and vertical positions of the energy wells, the placements and separations of vibrational energy levels, and the relative horizontal positions of the minima were chosen arbitrarily in order to illustrate the most probable relaxation pathway and its corresponding decay liftime assignments based on the transient absorption results for **3o**. The curvatures of the non-emissive transitions (shown in red and green) are meant to convey movement along a second reaction coordinate axis representing solvent reorganization.

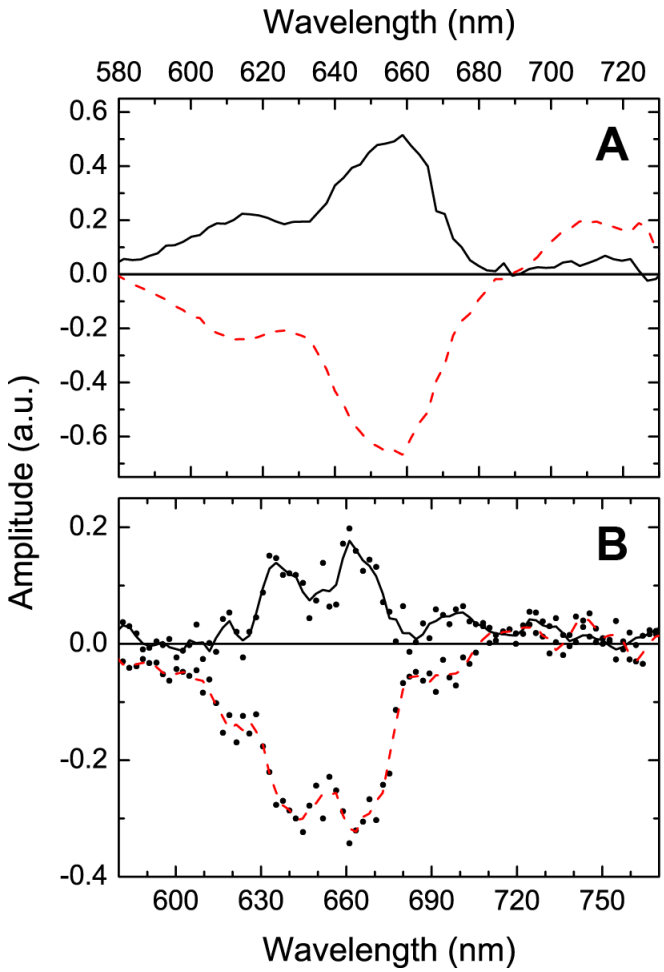

Figure 3.10 A DAS fit to transient absorption data collected from **2o** in CH_2Cl_2 with an excess of AcOH (λ_{ex} = 420 nm). The (dash) component arises from decay of $^1P_{Zn}$ with τ = 19 ps. The (solid) component is attributed to decay of ^1D_O with τ = 1.6 ps. **B** DAS fit to transient absorption data shown as (dot) were collected from **1o** in CH_2Cl_2 with an excess of AcOH (λ_{ex} = 420 nm) and could be fit by the same lifetimes as those for **2o**. Three-point smoothing of these data gave the (dash) and (solid) lines.

formation of IA at 610 and 660 nm for which the global analysis gave a good fit for τ = 1.6 ps (solid) suggests that this component can be ascribed to relaxation of ^1D_O as observed for **3o**. This component may also include relaxation from the P_{Zn} S_2 excited state, which has a lifetime of around 1.5 ps following excitation at the Soret.[60] These fitting results were obtained by fixing τ = 19 ps in order to obtain an acceptable fit with only the 19 ps and 1.6 ps components. Under identical experimental conditions, the data obtained from **1o** gave DAS with similar features to those of **2o** and were fit reasonably well using the same time constants (Figure 3.10B). For both sets of data, the 19 ps decay is mixed with the longer multi-component decay process associated with D_O as seen in **3o**.

Kinetics Analysis

For the calculations of rate constants that follow, the rates of IC, ISC and emission processes for $^1P_{Zn}$ are expressed as a sum total, k_0. The rate constants of the decay processes associated with $^1P_{Zn}$ for **1** are influenced significantly by whether or not energy transfer from $^1P_{Zn}$ to C_{60} occurs. Formation of the $^1C_{60}$ species, inferred from the time-resolved fluorescence and transient absorption experiments described, could likely occur by one of two mechanisms other than direct excitation of C_{60}. The photophysical analysis reported for a structurally analogous P_{Zn}-C_{60} dyad suggests that the mechanism could involve transient formation of a $P_{Zn}^{\bullet+}$-$C_{60}^{\bullet-}$ charge separated state, whose energy level in toluene lies between that of $^1P_{Zn}$ and $^1C_{60}$, followed by rapid recombination to form P_{Zn}-$^1C_{60}$.[54] However, the DAS for **1c** in toluene does not show evidence supporting the involvement of such an intermediate. Formation of a charge separated state would be characterized by formation of IA at around 660 nm from $P_{Zn}^{\bullet+}$ as seen in the spectra collected in for **1c** in CH_2Cl_2. There is, however, the possibility that the charge separated state is formed but decays too rapidly to produce any diagnostic transient signals above the instrument noise level.

The 255 ps time constant, τ_{Rise}, taken from fluorescence decay and transient absorption

measurements for **1c** in toluene is composed of decay kinetics for $^1P_{Zn}$. The 2.18 ns $^1P_{Zn}$ lifetime found in the fluorescence decay fitting for **1c** in toluene was used to determine k_0. The rate of energy transfer to C_{60} was determined to be $k_1 = 3.5 \times 10^9$ s^{-1} using Eq 3.4.

$$k_1 = \frac{1}{\tau_{Rise}} - k_0 \tag{3.4}$$

The rate of this proposed energy transfer process was also calculated using the Förster rate equation, Eq 3.3. The fluorescence quantum yield of $^1P_{Zn}$ was taken as 0.04.[61] The extinction coefficient of the functionalized C_{60} was measured as 2315 M^{-1} cm^{-1} for the anilinofullerene compound mentioned in the synthesis section. The structure of **1c** was minimized using the PM6 semiempirical method and the P_{Zn}-C_{60} center-to-center distance of 19 Å was taken as the interchromophore distance. Assuming a dipole-orientation factor of 2/3 (random orientation), the rate was determined to be $k_{FRET} = 2.8 \times 10^9$ s^{-1}. Comparing this to the experimentally determined rate in question and taking into consideration the assumption of random dipole orientation and that solvent was not included in the structure minimization, it is reasonable to assign the observed rise kinetics to through-space singlet-singlet energy transfer as implicated by the transient absorption dynamics. The rate of $^1C_{60}$ decay was determined from it's fluorescence lifetime as $k_2 = 7.5 \times 10^8$ s^{-1} which includes ISC to form $^3C_{60}$ and other typical relaxation processes.

The energy level diagram for **1** shown in Figure 3.11 provides a schematic view of the decay pathways from $^1P_{Zn}$ (2.09 eV) leading to the ground state, D-P_{Zn}-C_{60}, for which the remaining rate calculations are described herein. The charge separated state is estimated to lie 1.4 eV above the ground state based on that of a tetra-aryl zinc porphyrin-fullerene dyad in THF (1.42 eV).[53] The energy level for $^1C_{60}$ (1.75 eV) is an approximate value used for a range of organic solvents.[54] While $^3C_{60}$ is not included in this scheme, its energy level lies approximately 0.2-0.3 eV below that of $^1C_{60}$.[54] Based on the lowest energy absorption band of D_O (652 nm) and highest energy stimulated emission peak measured for ^1D_O (~700 nm), its first singlet excited

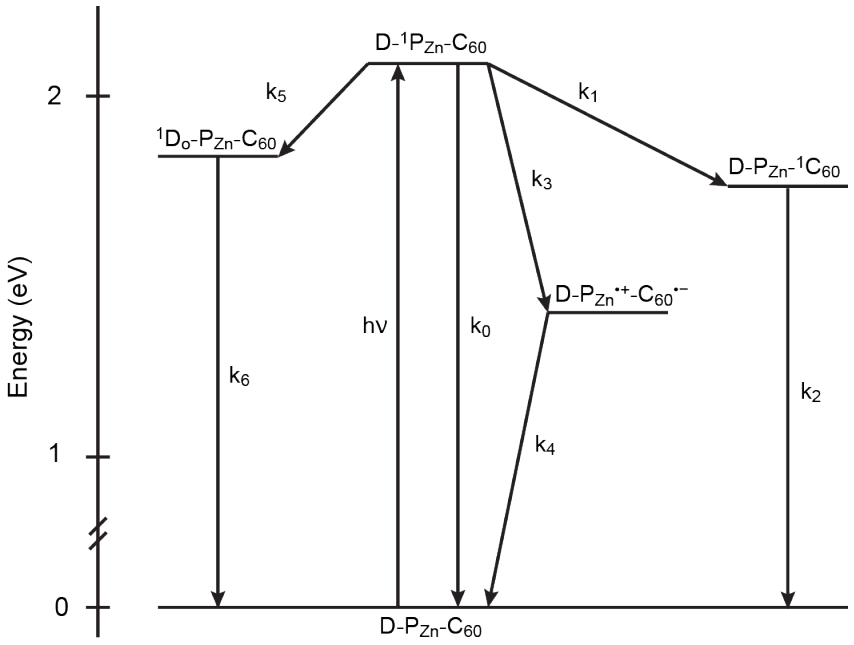

Figure 3.11 Energy level diagram showing the pathways of $^1P_{Zn}$ decay for **1** in CH_2Cl_2.

state is estimated to lie at 1.84 eV. Relaxation of ^1D_O is represented by a single, complex transition to the ground state as rate constants for the individual components of this process cannot be accurately determined from the experimental data. Kinetic treatment of ^1D_O relaxation is discussed vide infra.

The following calculations of rate constants are based off of the fitted fluorescence decay component lifetimes τ_1 and τ_2 found in Table 3.1. The lifetimes τ_1 = 182, 178, and 160 ps for **1c** include kinetics from charge separation, $^1P_{Zn}$ to C_{60} energy transfer, and intrachromophore relaxation of $^1P_{Zn}$. The 1.97 ns lifetime of **2c** in CH_2Cl_2 was used to determine k_0 for **1** in CH_2Cl_2. Thus, the rates of charge separation for **1** in CH_2Cl_2 with 0 M, 1.6 M, and 4.5 M AcOH were determined to be $k_3 = 1.5 \times 10^9$ s^{-1}, 1.7×10^9 s^{-1}, and 2.3×10^9 s^{-1}, respectively, using Eq 3.5.

$$k_3 = \frac{1}{\tau_1} - k_1 - k_0 \tag{3.5}$$

The rate of charge recombination was determined to be $k_4 = 1.9 \times 10^8$ s^{-1} from the $P_{Zn}^{\bullet+}$-$C_{60}^{\bullet-}$ lifetime measured by transient absorption. The shorter fluorescence decay components observed for **2** are significantly influenced by the rate of $^1P_{Zn}$ to D_O energy transfer, k_{EnT2}, occurring in the protonated species **2o.** Thus, the rate of energy transfer $k = 5.2 \times 10^{10}$ s^{-1} in both 1.6 M and 4.5 M AcOH/CH_2Cl_2 was determined using Eq 3.6.

$$k = \frac{1}{\tau_2} - k_0 \tag{3.6}$$

Similarly, the photophysical dynamics of **1o** are heavily influenced by rapid $^1P_{Zn}$ to D_O energy transfer as well as kinetics from ^1P to C_{60} energy and electron transfer. The rate constant for energy transfer to D_O for **1o** was determined to be $k_5 = 5.3 \times 10^{10}$ s^{-1} in both 1.6 M and 4.5 M AcOH/CH_2Cl_2 using Eq 3.7.

$$k_5 = \frac{1}{\tau_2} - k_1 - k_3 - k_0 \quad (3.7)$$

The transient absorption data for **3o** show a three component relaxation mechanism for ^1D_O of which the first step is ultrafast decay to a hot ground state with τ = 1.6 ps. While it is likely that this lifetime includes kinetic contributions from one or both of the subsequent cooling steps, the rate constant for ^1D_O relaxation to the ground state can be approximated as the inverse of this lifetime, which gives $k_6 = 6.3 \times 10^{11}$ s^{-1}.

For **1c**, the quantum yields of $^1P_{Zn}$ to C_{60} energy transfer (EnT1) and charge separation (CS) were determined using Eq 3.8 and 3.9 as follows: $\Phi_{EnT1} = 0.64$ and $\Phi_{CS} = 0.27$ (0 M AcOH), $\Phi_{EnT1} = 0.61$ and $\Phi_{CS} = 0.30$ (1.6 M AcOH), and $\Phi_{EnT1} = 0.55$ and $\Phi_{CS} = 0.36$ (4.5 M AcOH).

$$\Phi_{\mathrm{EnT1}} = \frac{k_1}{k_1+k_3+k_0} \quad (3.8)$$

$$\Phi_{\mathrm{CS}} = \frac{k_3}{k_1+k_3+k_0} \quad (3.9)$$

For **1o**, the quantum yields of $^1P_{Zn}$ to C_{60} energy transfer (EnT1), charge separation (CS) and $^1P_{Zn}$ to Do energy transfer (EnT2) were determined for **1o** using Eq 3.10, 3.11, and 3.12 as follows: $\Phi_{EnT1} = 0.060$, $\Phi_{CS} = 0.029$, $\Phi_{EnT2} = 0.90$ (1.6 M AcOH) and $\Phi_{EnT1} = 0.059$, $\Phi_{CS} = 0.039$, and $\Phi_{EnT2} = 0.89$ (4.5 M AcOH).

$$\Phi_{\mathrm{EnT1}} = \frac{k_1}{k_5+k_1+k_3+k_0} \quad (3.10)$$

$$\Phi_{\mathrm{CS}} = \frac{k_3}{k_5+k_1+k_3+k_0} \quad (3.11)$$

$$\Phi_{\mathrm{EnT2}} = \frac{k_5}{k_5+k_1+k_3+k_0} \quad (3.12)$$

For both open and closed forms, the yields of charge separation increase with increasing [AcOH] due to faster rates of charge separation (k_3) in more polar solutions. Relative to the yields of $^1P_{Zn}$

to C_{60} energy transfer and charge separation for **1c**, those of **1o** are observed to decrease by one order of magnitude due to $^1P_{Zn}$ to Do energy transfer accounting for roughly 90% of the decay kinetics.

In addition to the single-molecule kinetic descriptions above, these results can be viewed from the perspective of the net photophysical behavior of each sample by considering the total yields of $P_{Zn}^{\bullet+}$-$C_{60}^{\bullet-}$ and $^1C_{60}$ versus those of ^1D_O with respect to total $^1P_{Zn}$ (**1c** + **1o**) formed. In the absence of AcOH this is directly apparent from the quantum yields, which attribute decay of $^1P_{Zn}$ to 64% energy transfer to C_{60} and *27% charge separation*. In the presence of AcOH, the relative populations of **1c** and **1o** are reflected by the fluorescence decay component compositions shown in Table 1. With 1.6 M AcOH the sample was composed of 33% **1c** and 67% **1o**, which when multiplied by the quantum yields of their respective decay processes, gives the decay of total $^1P_{Zn}$ by 60% energy transfer to D_O, 24% energy transfer to C_{60}, and *12% charge separation*. Similarly, with 4.5 M AcOH the sample was composed of 15% **1c** and 85% **1o** for which the total $^1P_{Zn}$ decays by 76% energy transfer to D_O, 13% energy transfer to C_{60}, and *9% charge separation*. Thus, the formation of charge separated states from total $^1P_{Zn}$ is reduced by 56% in 1.6 M AcOH and by 67% in 4.5 M AcOH. Additionally, formation of $^1C_{60}$ from total $^1P_{Zn}$ is reduced by 63% in 1.6 M AcOH and by 80% in 4.5 M AcOH. The yield reductions for charge separation are lower than those for energy transfer because charge separation becomes more efficient with higher [AcOH] while the efficiency of energy transfer is assumed to be unaffected. Thus, the maximum degree of downregulation of charge separation is limited by the [AcOH] required to push the equilibrium further toward **1o** and the rate and relative efficiency of charge separation that result from the accompanying change in polarity. In a more practical sense, this is further limited by the maximum [AcOH] that **1** remains stable in; at some point irreversible loss of zinc from the porphyrin may occur, which would permanently compromise the total active population of **1**.

Concluding Remarks

Activation of NPQ in the photosynthetic apparatus of green plants has the effect of decreasing the emission intensities and fluorescence decay lifetimes of light harvesting antenna complexes, thereby inhibiting their ability to transfer excitation energy to photosynthetic reaction centers. This regulatory mechanism is activated in proportion to decreases in thylakoid lumen pH produced by increased photon flux. The efficiency of charge separation with respect to photons absorbed by the antennae is consequently reduced since much of the absorbed energy is diverted away from the reaction centers. Deactivation of NPQ follows increase of lumen pH at low-light levels as the surplus of absorbed energy is consumed. This research demonstrates analogous responsive, self-regulating reaction center functionality in **1**. The spectral analyses give evidence for i) reversible conversion between unquenched and quenched states that is dependent on acid concentration, ii) the capacity to form a long-lived charge separated state under neutral conditions, and iii) significant reduction of charge separation efficiency under acidic conditions.

Steady-state absorption and emission spectroscopy were used to monitor acidification and subsequent neutralization of a solution containing **1** to demonstrate reversible quenching of the zinc porphyrin excited state and dissipation of said energy by a vibrational process. These responsive and reversible changes indicate that the equilibrium between **1c** and **1o** is directly affected by acetic acid concentration. The significant reduction of porphyrin fluorescence concomitant with formation of **1o** is associated with energy transfer from the zinc porphyrin excited state to the open rhodamine dye via a Förster-type mechanism. This excitation energy is then rapidly dissipated as heat by a multi-step process. Transient absorption results indicate that the relaxation mechanism begins with ultrafast decay to a hot ground state followed by rapid cooling to its true ground state. Kinetics analysis of **1** indicates that the open dye effectively decreases the yield of charge separation by one order of magnitude on a per-molecule basis, and was shown to affect the overall population yield of charge separated states relative to zinc

porphyrin excited states formed by as much as 67%. Furthermore, the total yield of $^1C_{60}$ was observed to be reduced by as much as 80% in the presence of AcOH, which would therefore reduce formation of $^3C_{60}$ by intersystem crossing. Analogous to the photoproprotective functionality observed in NPQ, this may serve to prevent degradation of **1** by $^1O_2$. However, further experimentation is required to confirm that **1** exhibits photoprotective behavior under acidic conditions.

Together, these results demonstrate regulation of charge separation efficiency using acid concentration as a control signal, thus providing a functional analog to NPQ. The next logical step toward introducing additional biomimetic functionality would be to use a light-responsive proton source rather than titration with acetic acid so that the regulatory behavior could be controlled by photon flux. Reversible organic photoacids, typically phenolic compounds that behave as weak acids in the ground state and strong or super acids in the excited state, may be useful for achieving this goal. However, the rates of proton dissociation and recombination for such photoacids are generally characterized in aqueous solutions and have been found, by the author, to slow dramatically in all organic solvents and aqueous mixtures thereof. To circumvent this issue, forming water-soluble micelles containing triad **1** may allow for the desired proton transfer dynamics between **1** and a suitable photoacid to be achieved. Usage of micelles would also fill the auxiliary role of modeling the heterogeneous membrane environment in which photosynthesis occurs. Thus, the effects of surface charge, detergent rigidity, and micelle composition on the photophysical dynamics of **1** could also be investigated in such systems.

References

1. Stephanopoulos, N.; Solis, E.O.; and Stephanopoulos, G. Nanoscale Process Systems Engineering: Toward Molecular Factories, Synthetic Cells, and Adaptive Devices. *AIChE Journal*, **2005**, *51*, 1858-1869.

2. Gust, D.; Moore, T.A.; and Moore, A.L. Solar Fuels via Artificial Photosynthesis. *Accounts of Chemical Research*, **2009**, *42*, 1890-1898.

3. Gust, D.; Moore, T.A.; and Moore, A.L. Towards Molecular Logic and Artificial Photosynthesis. *From non-covalent assemblies to molecular machines*, **2010**, 321-353.

4. Gust, D.; Moore, T.A.; and Moore, A.L. Mimicking Photosynthetic Solar Energy Transduction. *Accounts of Chemical Research*, **2001**, *34*, 40-48.

5. Moore, T.A.; Moore, A.L.; and Gust, D. The design and synthesis of artificial photosynthetic antennas, reaction centres, and membranes. *Philosophical Transactions of the Royal Society B*, **2002**, *357*, 1481-1498.

6. Ruban, A.V.; Johnson, M.P.; and Duffy, C.D.P. The photoprotective molecular switch in the photosystem II antenna. *Biochimica et Biophysica Acta*, **2012**, *1817*, 167-181.

7. Horton, P.; Ruban, A.V.; and Walters, R.G. Regulation of light harvesting in green plants. *Plant Physiology*, **1994**, *106*, 415-420.

8. Telfer, A.; He, W.; and Barber, J. Spectral resolution of more than one chlorophyll electron donor in the isolated Photosystem II reaction center complex. *Biochimica et Biophysica Acta*, **1990**, *1017*, 143-151.

9. Barber, J. Molecular Basis of the Vulnerability of Photosystem II to Damage by Light. *Australian Journal of Plant Physiology*, **1994**, *22*, 201-208.

10. Nagy, L.; Balint, E.; Barber, J.; Ringler, A.; Cook, K.M.; and Maroti, P. Photoinhibition and Law of Reciprocity in Photosynthetic Reactions of Synechocystic sp. PCC 6803*. *Journal of Plant Physiology*, **1995**, *145*, 410-415.

11. Briantais, J.M.; Vernotte, C.; Picaud, M.; and Krause, G.H. *Biochimica et Biophysica Acta*, **1979**, *548*, 128-138.

12. Johnson, M.P.; and Ruban, A.V. Photoprotective energy dissipation in higher plants involves alteration of the excited state energy of the emitting chlorophyll(s) in the light harvesting antenna II (LHCII). *The Journal of Biological Chemistry*, **2009**, *284*, 23592-23601.

13. Millineaux, C.W.; Pascal, A.A.; Horton, P.; and Holzwarth, A.R. Excitation-energy quenching in aggregates of the LHC II chlorophyll-protein complex: a time-resolved fluorescence study. **1993**,

14. van Oort, B.; van Hoek, A.; Ruban, A.V.; and van Amerongen, H. Aggregation of light-harvesting complex II leads to formation of efficient excitation energy traps in monomeric and trimeric complexes. *FEBS Letters*, **2007**, *581*, 3528-3532.

15. Millineaux, C.W.; Ruban, A.V.; and Horton, P. Prompt heat release associated with ΔpH-dependent quenching in spinach thylakoid membranes. *Biochimica et biophysica acta. Bioenergetics*, **1994**, *1185*, 119-123.

16. Rees, D.; and Horton, P. The mechanisms of changes in photosystem II efficiency in spinach thylakoids. *Biochimica et Biophysica Acta*, **1990**, *1016*, 219-227.

17. Wraight, C.A.; and Crofts, A.R. Energy-Dependent Quenching of Chlorophyll a Fluorescence in Isolated Chloroplasts. *European Journal of Biochemistry*, **1970**, *17*, 319-327.

18. Horton, P.; Wentworth, M.; and Ruban, A. Control of the light harvesting function of chloroplast membranes: The LHCII-aggregation model for non-photochemical quenching. *FEBS Letters*, **2005**, 4201-4206.

19. Holzwarth, A.R.; Miloslavina, Y.; Nilkens, M.; and Jahns, P. Identification of two quenching sites active in the regulation of photosynthetic light-harvesting studied by time-resolved fluorescence. *Chemical Physics Letters*, **2009**, *483*, 262-267.

20. Rees, D.; Young, A.; Noctor, G.D.; Britton, G.; and Horton, P. Enhancement of the deltapH-dependent dissipation of excitation energy in spinach chloroplasts by light-activation; correlation with the synthesis of zeaxanthin. *FEBS Letters*, **1989**, *256*, 85-90.

21. Noctor, G.D.; Rees, D.; Young, A.; and Horton, P. The relationship between zeaxanthin, energy-dependent quenching of chlorophyll fluorescence and the transthylakoid pH-gradient in isolated chloroplasts. *Biochimica et Biophysica Acta*, **1991**, *1057*, 320-330.

22. Zia, A.; Johnson, M.P.; and Ruban, A. Acclimation- and mutation-induced enhancement of PsbS levels affects the kinetics of non-photochemical quenching in Arabidopsis thaliana. *Planta*, **2011**, *233*, 1253-1264.

23. Miloslavina, Y.; Wehner, A.; Lambrev, P.; Wientjes, E.; Reus, M.; Garab, G.; Croce, R.; and Holzwarth, A.R. Far-red fluorescence: A direct spectroscopic marker for LHCII oligomer formation in non-photochemical quenching. *FEBS Letters*, **2008**, *582*, 3625-3631.

24. Ma, Y.-Z.; Holt, N.E.; Li, X.; Niyogi, K.K.; and Fleming, G.R. Evidence for direct carotenoid involvement in the regulation of photosynthetic light harvesting. *Proceedings of the National Academy of Sciences*, **2003**, *100*, 4377-4382.

25. Liao, P.-N.; Holleboom, C.-P.; Wilk, L.; Kuehlbrandt, W.; and Walla, P.J. Correlation of Car S1 -> Chl with Chl -> Car S1 Energy Transfer Supports the Excitonic Model in Quenched Light Harvesting Complex II. *Journal of Physical Chemistry B*, **2010**, *114*,

26. Dreuw, A.; Fleming, G.R.; and Gordon-Head, M. Role of electron-transfer quenching of chlorophyll fluorescence by carotenoids in non-photochemical quenching of green plants. *Biochemical Society Transactions*, **2005**, *33*, 858-862.

27. Holt, N.E.; Zigmantas, D.; Valkunas, L.; Li, X.; Niyogi, K.K.; and Fleming, G.R. Carotenoid Cation Formation and the Regulation of Photosynthetic Light Harvesting. *Science*, **2005**, *307*, 433-436.

28. Ruban, A.V.; Berera, R.; Ilioaia, C.; van Stokkum, I.H.M.; Kennis, J.T.M.; Pascal, A.A.; van Amerongen, H.; Robert, B.; Horton, P.; and van Grongelle, R. Identification of a mechanism of photoprotective energy dissipation in higher plants. *Nature*, **2007**, *450*, 575-579.

29. Muller, M.G.; Lambrev, P.; Reus, M.; Wientjes, E.; Croce, R.; and Holzwarth, A.R. Singlet Energy Dissipation in the Photosystem II Light-Harvesting Complex Does Not Involve Energy Transfer to Carotenoids. *ChemPhysChem*, **2010**, *11*, 1289-1296.

30. Berera, R.; Herrero, C.; van Stokkum, I.H.M.; Vengris, M.; Kodis, G.; Palacios, R.E.; van Amerongen, H.; van Grondelle, R.; Gust, D.; Moore, T.A.; Moore, A.L.; and Kennis, J.T.M. A simple artificial light-harvesting dyad as a model for excess energy dissipation in oxygenic photosynthesis. *Proceedings of the National Academy of Sciences*, **2006**, *103*, 5343-5348.

31. Kodis, G.; Herrero, C.; Palacios, R.; Marino-Ochoa, E.; Gould, S.; de la Garza, L.; van Grondelle, R.; Gust, D.; Moore, T.A.; Moore, A.L.; and Kennis, J.T.M. Light Harvesting

and Photoprotective Functions of Carotenoids in Compact Artifical Photosynthetic Antenna Designs. *Journal of Physical Chemistry B*, **2004**, *108*, 414-425.

32. Straight, S.D.; Kodis, G.; Terazono, Y.; Hambourger, M.; Moore, T.A.; Moore, A.L.; and Gust, D. Self-regulation of photoinduced electron transfer by a molecule nonlinear transducer. *Nature Nanotechnology*, **2008**, *3*, 280-283.

33. Terazono, Y.; Kodis, G.; Bhushan, K.; Zaks, J.; Madden, C.; Moore, A.L.; Moore, T.A.; Fleming, G.R.; and Gust, D. Mimicking the Role of the Antenna in Photosynthetic Photoprotection. *Journal of the American Chemical Society*, **2011**, *133*, 2916-2922.

34. Marcus, R.A. On the Theory of Oxidation-Reduction Reactions Involving Electron Transfer. I. *The Journal of Chemical Physics*, **1956**, *24*, 966-978.

35. Forster, T. Energiewanderung und Fluoreszenz. *Naturwissenschaften*, **1946**, *33*, 166-175.

36. Forster, T. Zwischenmolekulare Energiewanderung und Fluoreszenz. *Annalen der Physik*, **1948**, *437*, 55-75.

37. Gust, D.; Moore, T.A.; and Moore, A.L. Molecular swithces controlled by light. *Chemical Communications*, **2006**, 1169-1178.

38. Woodroofe, C.C.; Lim, M.H.; Bu, W.; and Lippard, S.J. Synthesis of isomerically pure carboxylae- and sulfonate-substituted xanthene fluorophores. *Tetrahedron*, **2005**, *61*, 3097-3105.

39. Terazono, Y.; Liddell, P.A.; Garg, V.; Kodis, G.; Brune, A.; Hambourger, M.; Moore, A.L.; Moore, T.A.; and Gust, D. Artificial photosynthetic antenna-reaction center complexes based on a hexaphenylbenzene core. *Journal of Porphyrins and Phthalocyanines*, **2005**, *09*, 706-723.

40. Littler, B.J.; Ciringh, Y.; and Lindsey, J.S. Investigation of Conditions Giving Minimal Scrambling in the Synthesis of trans-Porphyrins from Dipyrromethanes and Aldehydes. *Journal of Organic Chemistry*, **1999**, *64*, 2864-2872.

41. Geier, G.R.; and Lindsey, J.S. Effects of aldehyde or dipyrromethane substituents on the reaction course leading to meso-substituted porphyrins. *Tetrahedron*, **2004**, *60*, 11435-11444.

42. Liddell, P.A.; Gervaldo, M.; Bridgewater, J.W.; Keirstead, A.E.; Lin, S.; Moore, T.A.; Moore, A.L.; and Gust, D. Porphyrin-Based Hole Conducting Electropolymer. *Chemistry of Materials*, **2008**, *20*, 135-142.

43. Gervaldo, M.; Liddell, P.A.; Kodis, G.; Brennan, B.J.; Johnson, C.R.; Bridgewater, J.W.; Moore, A.L.; Moore, T.A.; and Gust, D. A photo- and electrochemically-active porphyrin-fullerene dyad electropolymer. *Photochemical & Photobiological Sciences*, **2010**, *9*, 890-900.

44. Schmitz, R.A.; Liddell, P.A.; Kodis, G.; Kenney, M.J.; Brennan, B.J.; Oster, N.V.; Moore, T.A.; Moore, A.L.; and Gust, D. Synthesis and spectroscopic properties of a soluble semiconducting porphyrin electropolymer. *Physical Chemistry Chemical Physics*, **2014**, *16*, 17569-17579.

45. Ingold, K.U. Inhibition of the Autoxidation of Organic Substances in the Liquid Phase. *Chemical Reviews*, **1961**, *61*, 563-589.

46. Ingold, K.U.; and Pratt, D.A. Advances in Radical-Trapping Antioxidant Chemistry in the 21st Century: A Kinetics and Mechanisms Perspective. *Chemical Reviews*, **2014**, *114*, 9022-9046.

47. Wuts, P.G.M.; and Greene, T.W., *Protection for the Amino Group in Greene's Protective Groups in Organic Synthesis*. Fourth Edition ed. 2006, Hoboken, NJ, USA: John Wiley & Sons, Inc.

48. Battacharyya, S.; Kibel, A.; Kodis, G.; Liddell, P.A.; Gervaldo, M.; Gust, D.; and Lindsay, S. Optical Modulation of Molecular Conductance. *Nano Letters*, **2011**, *11*, 2709-2714.

49. Suzuki, A. Recent advances in the cross-coupling reactions of organoboron derivatives with organic electrophiles, 1995-1998. *Journal of Organometallic Chemistry*, **1999**, *576*, 147-168.

50. Imahori, H.; and Sakata, Y. Donor-Linked Fullerenes: Photoinduced Electron Transder and Its Potential Application. *Advanced Materials*, **1997**, *9*, 537-546.

51. Imahori, H.; and Sakata, Y. Fullerens as Novel Acceptors in Photosynthetic Electron Transfer. *European Journal of Organic Chemisry*, **1999**, 2445-2457.

52. Kuciauskas, D.; Lin, S.; Seely, G.R.; Moore, A.L.; Moore, T.A.; Gust, D.; Drovetskaya, T.; Reed, C.A.; and Boyd, P.D.W. Energy and Photoinduced Electron Transfer in Porphyrin-Fullerene Dyads. *Journal of Physical Chemistry*, **1996**, *100*, 15926-15932.

53. Imahori, H.; Hagiwara, K.; Aoki, M.; Akiyama, T.; Taniguchi, S.; Okada, T.; Shirakawa, M.; and Sakata, Y. Linkage and Solvent Dependence of Photoinduced Electron Transfer in Zincporphyrin-C60 Dyads. *Journal of the American Chemical Society*, **1996**, *118*, 11771-11782.

54. Imahori, H.; El-Khouly, M.E.; Fujitsuka, M.; Ito, O.; Sakata, Y.; and Fukuzumi, S. Solvent Dependence of Charge Separation and Charge Recombination Rates in Porphyrin-Fullerene Dyad. *Journal of Physical Chemistry A*, **2001**, *105*, 325-332.

55. Liddell, P.A.; Kodis, G.; Kuciauskas, D.; Andreasson, J.; Moore, A.L.; Moore, T.A.; and Gust, D. Photoinduced electron transfer in a symmetrical diporphyrin-fullerene triad. *Physical Chemistry Chemical Physics*, **2004**, *6*, 5509-5515.

56. Prato, M.; and Maggini, M. Fulleropyrrolidines: A Family of Full-Fledged Fullerene Derivatives. *Accounts of Chemical Research*, **1998**, *31*, 519-526.

57. Campidelli, S.; Vasquez, E.; Milic, D.; Prato, M.; Barbera, J.; Guldi, D.M.; Maracaccio, M.; Paolucci, D.; Paolucci, F.; and Deschenaux, R. Liquid-crystalline fullerene-ferrocene dyads. *Journal of Materials Chemistry*, **2004**, *14*, 1266-1272.

58. Kovalenko, S.A.; Schanz, R.; Farztinov, V.M.; Hennig, H.; and Ernsting, N.P. Femtosecond relaxation of photoexcited para-nitroaniline: solvation, charge transfer, internal conversion and cooling. *Chemical Physics Letters*, **2000**, *323*, 312-322.

59. Martin, M.M.; Plaza, P.; and Meyer, Y.H. Ultrafast intramolecular charge transfer in the merocyanine dye DCM. *Chemical Physics*, **1995**, *192*, 367-377.

60. Yu, H.-Z.; Baskin, S.; and Zewail, A.H. Ultrafast Dynamics of Porphyrins in the Condensed Phase: II. Zinc Tetraphenylporphyrin. *Journal of Physical Chemistry A*, **2002**, *106*, 9845-9854.

61. Hsiao, J.-S.; Krueger, B.P.; Wagner, R.W.; Johnson, T.E.; Delaney, J.K.; Mauzerall, D.C.; Fleming, G.R.; Lindsey, J.S.; Bocian, D.F.; and Donohoe, R.J. Soluble Synthetic Multiporphyrin Arrays. 2. Photodynamics of Energy-Transfer Processes. *Journal of the American Chemical Society*, **1996**, *118*, 11181-11193.

62. Rohand, T.; Dolusic, E.; Ngo, T.H.; Maes, W.; and Dehaen, W. Efficient synthesis of aryldipyrromethanes in water and their application in the synthesis of corroles and dipyrromethenes. *ARKIVOC*, **2007**, 307-324.

APPENDIX A

SYNTHETIC METHODS AND CHARACTERIZATION DATA

Materials

All commercially available reagents including 1-(4-methoxyphenyl)ethanol, 1-ethyl-3-(3-dimethylaminopropyl)carbodiimide hydrochloride (EDCI), 1,3,5-trimethoxybenzene, 2,4,6-trimethylbenzyl alcohol, 4-bromo-iodobenzene, 4-dimethylaminopyridine (DMAP), 4-*tert*-butylaniline, acetyl chloride, bis(pinacolato)diboron, boron trifluoride diethyl etherate (BF_3•OEt_2), cesium carbonate (Cs_2CO_3), copper(I) iodide (CuI), methyl 4-formylbenzoate, potassium acetate (KOAc), potassium hydroxide (KOH), pyridine, tetraphenylcyclopentadieneone, triethylamine (Et_3N), trifluoroacetic acid (TFA), trifluoroacetic anhydride, tripotassium phosphate (K_3PO_4), tri-*tert*-butylphosphine (P^tBu_3), and zinc acetate dihydrate [$Zn(OAc)_2$•$2H_2O$] were used as received. Palladium catalysts [1,1'-bis(diphenylphosphino)ferrocene]palladium(II) dichloride dichloromethane complex [Pd(dppf)Cl_2•CH_2Cl_2], bis(triphenylphosphine)palladium(II) dichloride [$PdCl_2(PPh_3)_2$], palladium(II) acetate [$Pd(OAc)_2$], and tetrakis(triphenylphospine)palladium(0) [$Pd(PPh_3)_4$] were purchased from Strem Chemicals, Inc. Dichloromethane (CH_2Cl_2) was distilled from calcium hydride when used as a reaction solvent or to prepare optical spectroscopy samples. Tetrahydrofuran (THF) and toluene were distilled from sodium/benzophenone for use in reactions. 1,4-Dioxane was distilled from lithium aluminum hydride. Other solvents including acetone, chloroform ($CHCl_3$), ethanol (EtOH), diethyl ether (Et_2O), diphenyl ether (Ph_2O), ethyl acetate (EtOAc), hexanes, and methanol (MeOH) were used as recieved. Column chromatography was performed using Silicycle SiliaFlash® F60 40-63 μm (230-400 mesh). Thin layer chromatography was performed using Analtech Silica Gel GHL/GHLF 250 μm plates.

Analytical Instrumentation and Methods

Nuclear magnetic resonance (NMR) spectra were collected using a Varian MR 400 MHz spectrometer equipped with a 5 mm liquids H-X broadband probe or a Varian VNMRS 500 MHz spectrometer equipped with a 5 mm liquids triple resonance ^{1}H-^{13}C-^{15}N probe. Samples were prepared in deuterochloroform ($CDCl_3$) (Cambridge Isotope Laboratories, Inc.) containing tetramethylsilane (TMS) (0.03% v/v) as an internal reference. Data was processed using ACD/NMR Processor Academic Edition. Chemical shifts were referenced to TMS. Mass spectra were obtained using an Applied Biosystems Voyager-DE STR matrix-assisted laser desorption/ionization time-of-flight mass spectrometer (MALDI-TOF-MS).

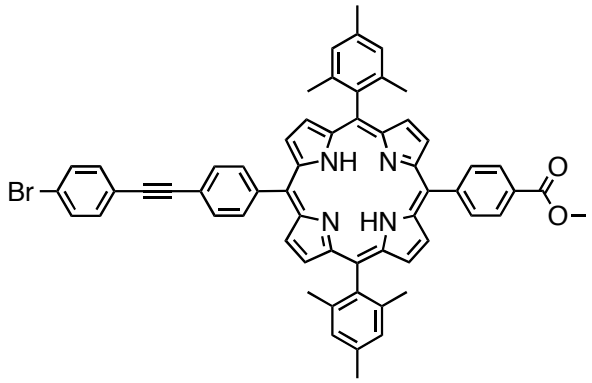

15-(4-(2-(4-bromophenyl)ethynyl)-phenyl)-5-(4-carbomethoxyphenyl)-10,20-bis(2,4,6-trimethylbenzene)porphyrin **5**. Condensations of 5-mesityldipyrromethane[62], 4-(4-bromophenylethynyl)benzaldehyde **4**, and methyl 4-formylbenzoate were carried out following general literature procedures.[40, 41] One method employed BF_3•OEt_2/EtOH as the acid catalyst in $CHCl_3$ and gave a 21% yield of **5** in one instance.[39] Alternatively, the reaction was catalyzed by TFA in CH_2Cl_2. However no final yields were calculated following this method, as the products were not of adequate purity to carry forward. ^{1}H NMR (400 MHz, $CDCl_3$, δ): -2.64 (br s, 2H, NH), 1.84 (s, 12H, CH_3), 2.63 (s, 6H, CH_3), 4.11 (s, 3H, OCH_3), 7.29 (s, 4H, ArH), 7.56 (m, 4H, ArH), 7.92 (d, *J* = 8 Hz, 2H, ArH), 8.21 (d, *J* = 8 Hz, 2H, ArH), 8.32 (d, *J* = 8.4 Hz, 2H, ArH), 8.43 (d, *J* = 8.4 Hz, 2H, ArH), 8.72 (m, 6H, βH), 8.80 (d, *J* = 5 Hz, 2H, βH). MALDI-TOF-MS *m/z*: calcd for $C_{60}H_{47}BrN_4O_2$ 936.29, obsd 936.60.

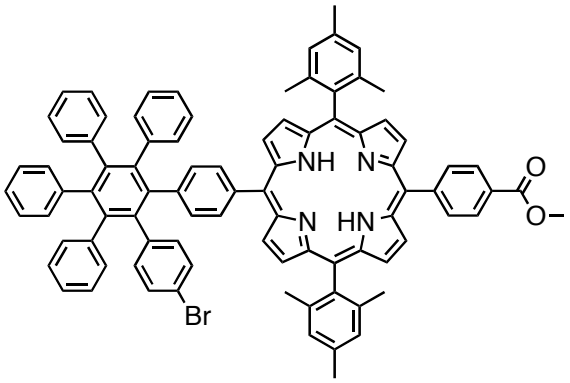

Porphyrin **6**. In a flask equipped with a magnetic stir bar, **5** (470 mg, 0.5 mmol) and tetraphenylcyclopentadieneone (3.5 g, 5 mmol) were dissolved in diphenyl ether (60 mL). The reaction was refluxed under Ar for 4 h. The solution was concentrated in vacuo and the residue was chromatographed (flash column, 3:2 CH_2Cl_2/hexanes). Recrystallization from CH_2Cl_2/MeOH gave 523 mg of **6** (81% yield). ^{1}H NMR (400 MHz, $CDCl_3$, δ): -2.74 (br s, 2H, NH), 1.80 (s, 12H, CH_3), 2.62 (s, 3H, CH_3), 2.63 (s, 3H, CH_3), 4.08 (s, 3H, OCH_3), 6.90-6.95 (m, 15H, ArH), 7.00 (d, *J* = 8 Hz, 2H, ArH), 7.08-7.16 (m, 7H, ArH), 7.26-7.29 (m, 6H, ArH), 7.72 (d, *J* = 8 Hz, 2H, ArH), 8.27 (d, *J* = 8 Hz, 2H, ArH), 8.33 (d, *J* = 5 Hz, 1H, βH), 8.41 (m, 3H, ArH and βH), 8.61 (d, *J* = 5 Hz, 1H, βH), 8.65-8.70 (m, 5H, βH). MALDI-TOF-MS *m/z*: calcd for $C_{88}H_{67}BrN_4O_2$ 1293.45, obsd 1292.94.

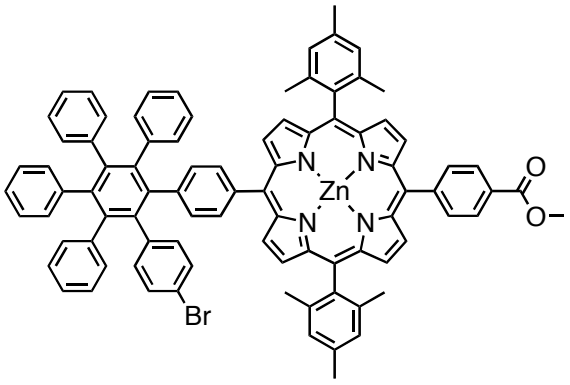

Porphyrin **7**. In a flask equipped with a magnetic stir bar, **6** (400 mg, 0.31 mmol) was dissolved in $CHCl_3$ (200 mL). To the solution was added $Zn(OAc)_2 \cdot 2H_2O$/MeOH (680 mg/25 mL) and the reaction was stirred under Ar overnight at room temperature. The solution was washed with water (x 2) and brine and then concentrated in vacuo. The residue was chromatographed (flash column, 2:1 CH_2Cl_2/hexanes to CH_2Cl_2) to obtain 418 mg of **7** (99% yield). ^{1}H NMR (400 MHz, $CDCl_3$, δ): 1.81 (s, 12H, CH_3), 2.63 (s, 3H, CH_3), 2.64 (s, 3H, CH_3), 4.09 (s, 3H, OCH_3), 6.92-6.97 (m, 15H, ArH), 7.02 (d, *J* = 8 Hz, 2H, ArH), 7.12-7.17 (m, 7H, ArH), 7.28-7.31 (m, 6H, ArH), 7.74 (d, *J* = 8 Hz, 2H, ArH), 8.30 (d, *J* = 8 Hz, 2H, ArH), 8.40 (d, *J* = 8 Hz, 2H, ArH), 8.45 (d, *J* = 4 Hz, 1H, βH), 8.53 (d, *J* = 5 Hz, 1H, βH) 8.71 (d, *J* = 5 Hz, 1H, βH), 8.75 (d, *J* = 4 Hz, 2H, βH), 8.78-8.80 (m, 3H, βH). MALDI-TOF-MS *m/z*: calcd for $C_{88}H_{65}BrN_4O_2Zn$ 1354.36, obsd 1354.98.

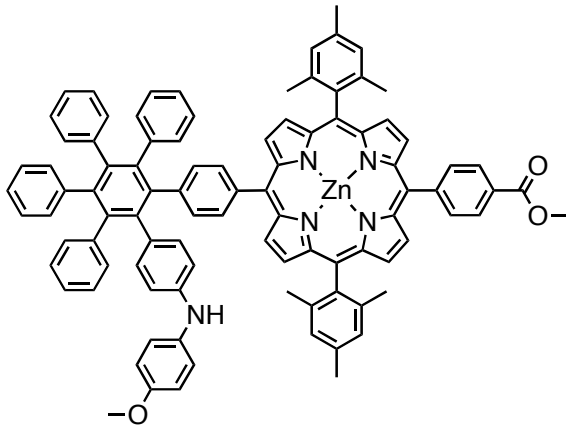

Porphyrin **8**. In a flask equipped with a magnetic stir bar, **7** (175 mg, 0.129 mmol), $Pd(OAc)_2$ (1.5 mg, 0.006 mmol), and Cs_2CO_3 (420 mg, 1.29 mmol), were dissolved in Ar bubbled toluene (20 mL). To the solution was added P^tBu_3 (12 uL, 1M in toluene). The reaction was refluxed under Ar overnight. The cooled reaction mixture was filtered through a short plug of silica gel and concentrated in vacuo. The residue was chromatographed (flash column, 9:1 CH_2Cl_2/hexanes to CH_2Cl_2) to obtain 157 mg of **8** (87% yield). ^{1}H NMR (400 MHz, $CDCl_3$, δ): 1.79 (s, 6H, CH_3), 1.81 (s, 6H, CH_3), 2.63 (s, 3H, CH_3), 2.64 (s, 3H, CH_3), 3.76 (s, 3H, OCH_3), 4.09 (s, 3H, OCH_3), 5.45 (br s, 1H, NH), 6.72 (d, *J* = 8 Hz, 2H, ArH), 6.75 (d, *J* = 9 Hz, 2H, ArH), 6.89-7.04 (m, 19H, ArH), 7.14 (m, 5H, ArH), 7.20 (d, *J* = 8 Hz, 2H, ArH), 7.27 (s, 2H, ArH), 7.29 (s, 2H, ArH), 7.74 (d, *J* = 8 Hz, 2H, ArH), 8.30 (d, *J* = 7.9 Hz, 2H, ArH), 8.40 (d, *J* = 7.9 Hz, 2H, ArH), 8.52 (d, *J* = 4 Hz, 1H, βH), 8.59 (d, *J* = 4 Hz, 1H, βH), 8.68 (d, *J* = 5 Hz, 1H, βH), 8.72 (d, *J* = 5 Hz, 1H, βH), 8.76 (d, *J* = 4 Hz, 2H, βH), 8.79 (d, *J* = 5 Hz, 2H, βH). MALDI-TOF-MS *m/z*: calcd for $C_{95}H_{73}N_5O_3Zn$ 1396.50, obsd 1398.08.

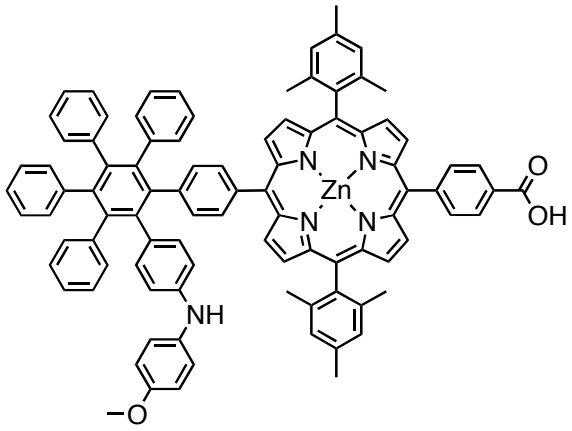

Porphyrin **9**. In a flask equipped with a magnetic stir bar, **8** (128 mg, 0.092 mmol) was dissolved in THF/MeOH (2/1, 180 mL). The solution was bubbled with Ar at 0 °C for 15 min followed by addition of aqueous KOH (10% w/v, 30 mL). The reaction was stirred under Ar overnight at room temperature. The solution was washed with water (2 x) and aqueous citric acid (0.1 M), and then concentrated in vacuo. The residue was chromatographed (flash column, 8% MeOH/CH_2Cl_2) to obtain 115 mg of **9** (91% yield). ^{1}H NMR (400 MHz, $CDCl_3$, δ): 1.81 (s, 6H, CH_3), 1.82 (s, 6H, CH_3), 2.64 (s, 3H, CH_3), 2.65 (s, 3H, CH_3), 3.77 (s, 3H, OCH_3), 6.73 (d, *J* = 8 Hz, 2H, ArH), 6.76 (d, *J* = 9 Hz, 2H, ArH), 6.88-7.05 (m, 19H, ArH), 7.14 (m, 5H, ArH), 7.21 (d, *J* = 8 Hz, 2H, ArH), 7.28 (s, 2H, ArH), 7.30 (s, 2H, ArH), 7.75 (d, *J* = 8 Hz, 2H, ArH), 8.36 (d, *J* = 7.9 Hz, 2H, ArH), 8.50 (d, *J* = 7.9 Hz, 2H, ArH), 8.53 (d, *J* = 5 Hz, 1H, βH), 8.60 (d, *J* = 4 Hz, 1H, βH), 8.69 (d, *J* = 4.4 Hz, 1H, βH), 8.73 (d, *J* = 4.4 Hz, 1H, βH), 8.78 (d, *J* = 5 Hz, 2H, βH), 8.82 (d, *J* = 4 Hz, 2H, βH). MALDI-TOF-MS *m/z*: calcd for $C_{94}H_{71}N_5O_3Zn$ 1382.49, obsd 1383.93.

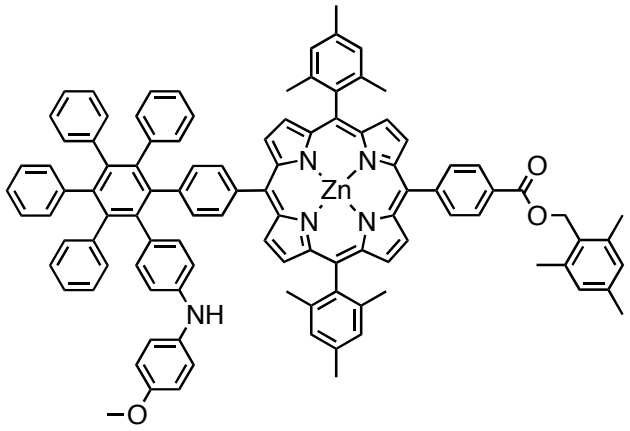

Porphyrin **10**. In a flask equipped with a magnetic stir bar, **9** (115 mg, 0.083 mmol), 2,4,6-trimethylbenzyl alcohol (14 mg, 0.116 mmol), DMAP (20 mg, 0.166 mmol), and EDCI (32 mg, 0.166 mmol) were dissolved in CH_2Cl_2 (18 mL). The reaction was cooled to 0 °C and bubbled with Ar for 15 min. Stirring was continued for 10 min at 0 °C before the reaction was brought to room temperature and stirred for an additional 24 h. The solution was diluted with CH_2Cl_2, washed with water, and concentrated in vacuo. The residue was chromatographed (flash column, 3:1 CH_2Cl_2/hexanes to CH_2Cl_2) to obtain 87 mg of **10** (69% yield). ^{1}H NMR (400 MHz, $CDCl_3$, δ): 1.79 (s, 6H, CH_3), 1.80 (s, 6H, CH_3), 2.32 (s, 3H, CH_3), 2.54 (s, 6H, CH_3), 2.63 (s, 3H, CH_3), 2.64 (s, 3H, CH_3), 3.74 (s, 3H, OCH_3), 5.43 (br s, 1H, NH), 5.55 (s, 2H, CH_2), 6.71 (d, *J* = 8 Hz, 2H, ArH), 6.74 (d, *J* = 9 Hz, 2H, ArH), 6.88-7.03 (m, 21H, ArH), 7.14 (m, 5H, ArH), 7.20 (d, *J* = 8 Hz, 2H, ArH), 7.27 (s, 2H, ArH), 7.28 (s, 2H, ArH), 7.74 (d, *J* = 8 Hz, 2H, ArH), 8.25 (d, *J* = 8 Hz, 2H, ArH), 8.35 (d, *J* = 8 Hz, 2H, ArH), 8.52 (d, *J* = 4.9 Hz, 1H, βH), 8.59 (d, *J* = 4.4 Hz, 1H, βH), 8.68 (d, *J* = 4.4 Hz, 1H, βH), 8.72 (d, *J* = 4.9 Hz, 1H, βH), 8.75 (d, *J* = 4.4 Hz, 2H, βH), 8.77 (d, *J* = 4.4 Hz, 2H, βH).

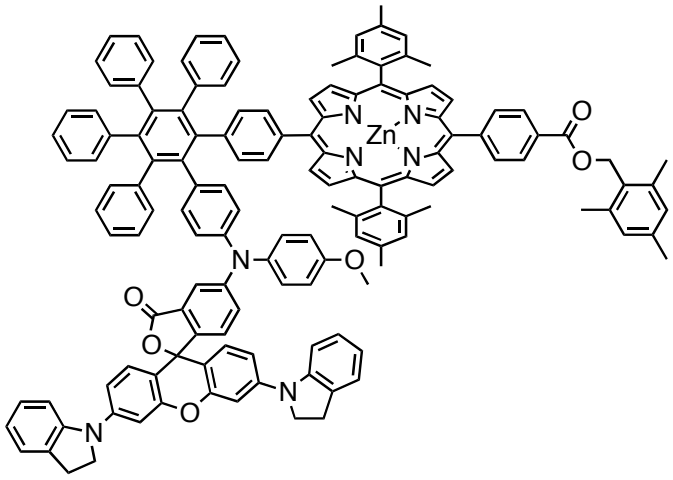

Dyad **12**. In a flask equipped with a magnetic stir bar, **10** (133 mg. 0.088 mmol), rhodamine **11** (72 mg, 0.117 mmol), $Pd(OAc)_2$ (15 mg, 0.066 mmol), and Cs_2CO_3 (238 mg, 0.730 mmol), were dissolved in toluene (10 mL). The solution was cooled to 0 °C and bubbled with Ar for 15 min. To the solution was added P^tBu_3 (135 uL, 1M in toluene). The reaction was refluxed under Ar overnight. The cooled reaction mixture was diluted with CH_2Cl_2, washed water, and then concentrated in vacuo. The residue was chromatographed twice (flash column, 3% MeOH/CH_2Cl_2 then 6% acetone/CH_2Cl_2) to obtain 99 mg of **12** (55% yield). ^{1}H NMR (400 MHz, $CDCl_3$, δ): 1.69 (s, 6H, CH_3), 1.80 (s, 6H, CH_3), 2.33 (s, 3H, CH_3), 2.48 (s, 3H, CH_3), 2.55 (s, 6H, CH_3), 2.64 (s, 3H, CH_3), 3.09 (t, *J* = 9 Hz, 4H, CH_2), 3.50 (s, 3H, OCH_3), 3.92 (m, 4H, CH_2), 5.58 (s, 2H, CH_2), 6.60 (d, *J* = 9 Hz, 2H, ArH), 6.74-7.23 (m, 48H, ArH), 7.28 (s, 2H, ArH), 7.50 (d, *J* = 2 Hz, 1H, ArH), 7.76 (d, *J* = 8 Hz, 2H, ArH), 8.24 (d, *J* = 8.4 Hz, 2H, ArH), 8.36 (d, *J* = 8.4 Hz, 2H, ArH), 8.53 (d, *J* = 5 Hz, 1H, βH), 8.65 (d, *J* = 5 Hz, 1H, βH), 8.68-8.77 (m, 6H, βH). MALDI-TOF-MS *m/z*: calcd for $C_{140}H_{107}N_7O_6Zn$ 2046.76, obsd 2048.21.

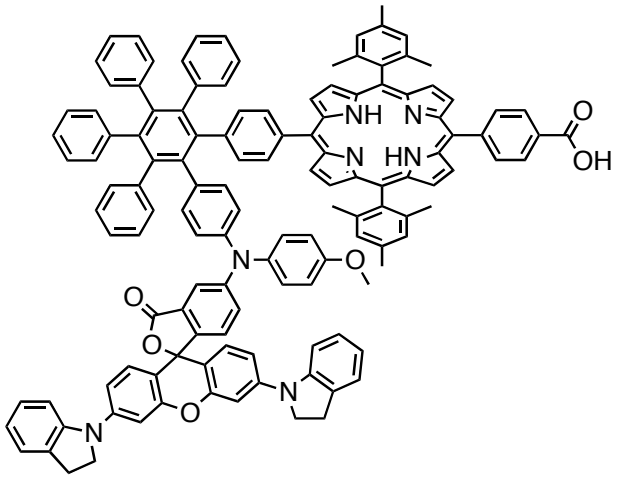

Dyad **13**. In a flask equipped with a magnetic stir bar, **12** (70 mg, 0.034 mmol) was dissolved in 10 mL of an Ar bubbled 1:1 mixture of TFA and CH_2Cl_2. The reaction was stirred under argon for 1.5 h. The reaction mixture was diluted to 100 mL with CH_2Cl_2, washed with water, saturated aqueous $NaHCO_3$ (x 2), aqueous citric acid (0.5 M), and brine, and then concentrated in vacuo. The residue was chromatographed multiple times to give 53 mg of a mixture containing **13**. MALDI-TOF-MS *m/z*: calcd for $C_{130}H_{97}N_7O_6$ 1852.75, obsd 1853.13 (100%), 1985.27 (86%), 2118.40 (23%).

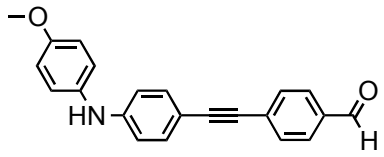

4-(4-formylphenylethynyl)-N-(4-methoxyphenyl)aniline **17.** In a flask equipped with a magnetic stir bar, 4-ethynyl-*N*-(4-methoxyphenyl)aniline **16**[33] (1.00 g, 4.50 mmol), 4-iodobenzaldehyde (1.07 g, 4.60 mmol), and CuI (48 mg, 0.23 mmol) were dissolved in THF/Et_3N (12 mL/1.5 mL). The solution was bubbled with Ar at 0 °C for 30 min, $PdCl_2(PPh_3)_2$ (80 mg, 0.11 mmol) was added, and bubbling continued for 15 min. The reaction was stirred overnight under Ar at room temperature. The solution was diluted to 100 mL with CH_2Cl_2, filtered through a pad of Celite rinsing with CH_2Cl_2, and concentrated in vacuo. The residue was chromatographed twice (flash column, 7:3 then 9:1 CH_2Cl_2/hexanes) and recrystallized from CH_2Cl_2/hexanes to obtain 345 mg of **17** (23% yield). ^{1}H NMR (400 MHz, $CDCl_3$, δ): 3.82 (s, 3H, OCH_3), 5.70 (br s, 1H, NH), 6.83 (d, *J* = 8.6 Hz, 2H, ArH), 6.90 (d, *J* = 9 Hz, 2H, ArH), 7.12 (d, *J* = 8.6 Hz, 2H, ArH), 7.39 (d, *J* = 9 Hz, 4H, ArH), 7.63 (d, *J* = 8 Hz, 2H, ArH), 7.84 (d, *J* = 8 Hz, 2H, ArH), 10.00 (s, 1H, CH).

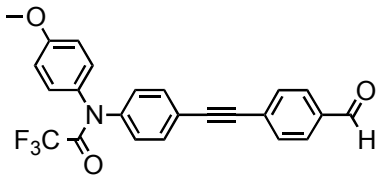

N-(4-(4-formylphenyl)ethynylphenyl)-N-(4-methoxyphenyl)trifluoroacetamide **18.** In a flask equipped with a magnetic stir bar, **17** (100 mg, 0.31 mmol) and pyridine (98 µL, 1.22 mmol) were dissolved in CH_2Cl_2 (31 mL) and placed under Ar. Trifluoroacetic anhydride (420 µL, 1M in CH_2Cl_2) was added at 0 °C and the reaction was brought to room temperature. Additional pyridine (98 µL, 1.22 mmol) and trifluoroacetic anhydride/CH_2Cl_2 (420 µL) were added after 2 h and stirring continued for 10 min. The solution was diluted to 50 mL with CH_2Cl_2, washed with saturated aqueous $NaHCO_3$ (2 x), and then concentrated in vacuo. The residue was and chromatographed (flash column, 1:1 Et_2O/hexanes) to obtain 120 mg of **18** (93% yield). ^{1}H NMR (400 MHz, $CDCl_3$, δ): 3.83 (s, 3H, OCH_3), 6.94 (d, *J* = 9 Hz, 2H, ArH), 7.24 (d, *J* = 8 Hz, 2H, ArH), 7.30 (d, *J* = 8 Hz, 4H, ArH), 7.56 (d, *J* = 8 Hz, 2H, ArH), 7.66 (d, *J* = 8.2 Hz, 2H, ArH), 7.87 (d, *J* = 8.2 Hz, 2H, ArH), 10.02 (s, 1H, CH).

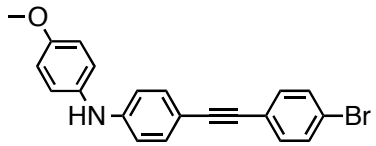

4-(4-bromophenylethynyl)-N-(4-methoxyphenyl)aniline **23.** In a flask equipped with a magnetic stir bar, 4-ethynyl-*N*-(4-methoxyphenyl)aniline **16**[33] (446 mg, 2.00 mmol), 4-bromo-iodobenzene (566 mg, 2.00 mmol), and CuI (19 mg, 0.10 mmol) were dissolved in THF/Et_3N (9.5 mL/0.5 mL). The solution was bubbled with Ar at 0 °C for 15 min, $PdCl_2(PPh_3)_2$ (35 mg, 0.050 mmol) was added, and bubbling continued for 15 min. The reaction was stirred overnight under Ar at room temperature. The solution was diluted with CH_2Cl_2 (50 mL), filtered through a pad of Celite rinsing with CH_2Cl_2, and then concentrated in vacuo. The residue was chromatographed (flash column, 2:1 CH_2Cl_2/hexanes) and recrystallized from CH_2Cl_2/hexanes to obtain 475 mg of **23** (63% yield). ^{1}H NMR (400 MHz, $CDCl_3$, δ): 3.81 (s, 3H, OCH_3), 5.64 (br s, 1H, NH), 6.82 (d, *J* = 9 Hz, 2H, ArH), 6.89 (d, *J* = 8.6 Hz, 2H, ArH), 7.10 (d, *J* = 9 Hz, 2H, ArH), 7.35 (dd, *J* = 8.6, 2.3 Hz, 4H, ArH), 7.45 (d, *J* = 8.6 Hz, 2H, ArH).

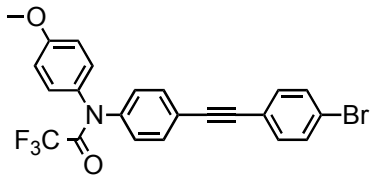

N-(4-(4-bromophenylethynyl)phenyl)-N-(4-methoxyphenyl)trifluoroacetamide **24.** In a flask equipped with a magnetic stir bar, **23** (40 mg, 0.11 mmol) and pyridine (68 µL, 0.85 mmol) were dissolved in CH_2Cl_2 (20 mL) and placed under Ar. Trifluoroacetic anhydride (420 µL, 1M in CH_2Cl_2) was added at 0 °C and the reaction was stirred for 10 min before being brought to room temperature. The solution was concentrated to 10 mL in vacuo and chromatographed (gravity column, CH_2Cl_2) to obtain 50 mg of **24** (quantitative). ^{1}H NMR (400 MHz, $CDCl_3$, δ): 3.83 (s, 3H, OCH_3), 6.92 (d, *J* = 9 Hz, 2H, ArH), 7.22-7.28 (m, 4H, ArH), 7.37 (d, *J* = 8 Hz, 4H, ArH), 7.47-7.53 (m, 4H, ArH).

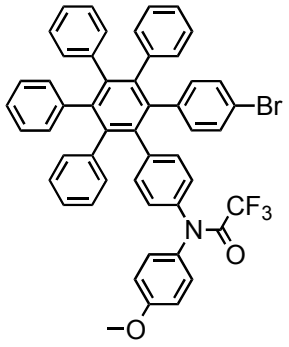

N-(4''-bromo-3',4',5',6'-tetraphenyl-[1,1':2',1''-terphenyl]-4-yl)-N-(4-methoxyphenyl)trifluoroacetamide **25**. In a flask equipped with a magnetic stir bar, **24** (20 mg, 0.042 mmol) and tetraphenylcyclopentadieneone (81 mg, 0.21 mmol) were dissolved in Ph_2O (2 mL). The reaction was refluxed under Ar for 6 h. Additional tetraphenylcyclopentadieneone (78 mg, 0.20 mmol) was added and reflux continued for 3 h. The reaction mixture was concentrated in vacuo and the residue was chromatographed (flash column, CH_2Cl_2/hexanes: 3/2 to 9/1) to isolate a single band that yielded 26 mg of material. The mass spectrum indicated that **25** was present in the material however, the ^{1}H NMR was nondescript indicating the presence of substantial impurities.

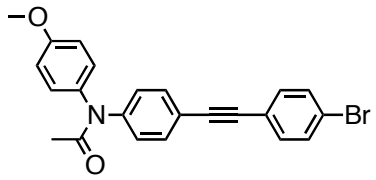

N-(4-(4-bromophenylethynyl)phenyl)-N-(4-methoxyphenyl)acetamide **26.** In a flask equipped with a magnetic stir bar, **23** (333 mg, 0.881 mmol) and pyridine (0.71 mL, 8.8 mmol) were dissolved in CH_2Cl_2 (65 mL) and placed under Ar. Acetyl chloride (125 µL, 1.75 mmol) was added in two equal portions 15 min apart at 0 °C. The reaction was stirred for 45 min. The solution was washed with saturated aqueous $NaHCO_3$ (x 2), dried over Na_2SO_4, and then concentrated in vacuo. The residue was chromatographed (flash column, 8% EtOAc/CH_2Cl_2) to obtain 368 mg of **26** (99% yield). ^{1}H NMR (400 MHz, $CDCl_3$, δ): 2.06 (s, 3H, CH_3), 3.82 (s, 3H, OCH_3), 6.92 (d, *J* = 9 Hz, 2H, ArH), 7.18 (d, *J* = 9 Hz, 2H, ArH), 7.24 (d, *J* = 8.5 Hz, 2H, ArH), 7.36 (d, *J* = 8.5 Hz, 2H, ArH), 7.47 (d, *J* = 8.5 Hz, 4H, ArH).

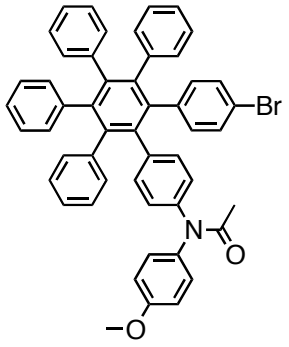

N-(4''-bromo-3',4',5',6'-tetraphenyl-[1,1':2',1''-terphenyl]-4-yl)-N-(4-methoxyphenyl)acetamide **27.** In a flask equipped with a magnetic stir bar and an air condenser, **26** (355 mg, 0.845 mmol) and tetraphenylcyclopentadieneone (3.25 g, 8.46 mmol) were dissolved in Ph_2O (40 mL) and the reaction was refluxed under Ar for 19 h. The solution was concentrated in vacuo and the residue was chromatographed (flash column, 1:4 EtOAc/toluene). The material was recrystallized from refluxing toluene (x 2) to obtain 494 mg of **27** as a 1:1 complex with toluene (67% yield). ^{1}H NMR (400 MHz, $CDCl_3$, δ): 1.82 (br s, 3H, CH_3), 2.35 (s, 3H, toluene-CH_3), 3.78 (s, 3H, OCH_3), 6.68 (d, *J* = 7.3 Hz, 2H, ArH), 6.76-6.98 (m, 32H, ArH), 7.14-7.18 (m, 3H, toluene-ArH), 7.24-7.27 (m, 2H, toluene-ArH). MALDI-TOF-MS *m/z*: calcd for $C_{51}H_{38}BrNO_2$ 775.21, obsd 777.48.

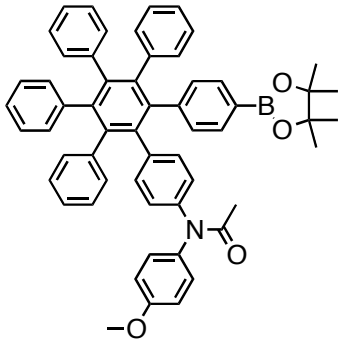

Boronate Ester **28.** In a heavy-walled tube equipped with a magnetic stir bar, **27** (389 mg, 0.448 mmol), bis(pinacolato)diboron (152 mg, 0.600 mmol) and KOAc (245 mg, 2.50 mmol) were dissolved in 1,4-dioxane (10 mL). The solution was bubbled with Ar at 0 °C for 10 min, then $Pd(dppf)Cl_2•CH_2Cl_2$ (18 mg, 0.025 mmol) was added, and bubbling continued for 10 min. The tube was sealed with a PTFE screw plug and the reaction was held at 100 °C for 36 h. The solution was suspended in water, extracted with CH_2Cl_2 (x 3), and the combined extracts were washed with brine and then concentrated in vacuo. The residue was chromatographed (flash column, 1:3 EtOAc/toluene) to obtain 261 mg of **28** (71% yield). ^{1}H NMR (400 MHz, $CDCl_3$, δ): 1.27 (s, 12H, CH_3), 1.76 (br s, 3H, CH_3), 3.76 (s, 3H, OCH_3), 6.70-6.95 (m, 32H, ArH). MALDI-TOF-MS *m/z*: calcd for $C_{57}H_{50}BNO_4$ 823.38, obsd 823.62.

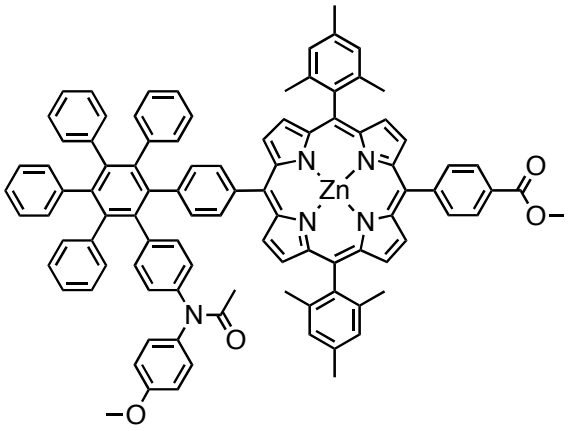

Porphyrin **31.** In a heavy-walled tube equipped with a magnetic stir bar, **28** (124 mg, 0.15 mmol), (5-bromo-15-(4-carbomethoxyphenyl)-10,20-bis(2,4,6-trimethylphenyl)porphyrinato)zinc(II)[48] **30** (124 mg, 0.150 mmol), and K_3PO_4 (636 mg, 3.00 mmol) were dissolved in toluene (30 mL). The solution was bubbled with Ar at 0 °C for 20 min, then $Pd(PPh_3)_4$ (17 mg, 0.015 mmol) was added, and bubbling was continued for 15 min. The tube was sealed with a PTFE screw plug and the reaction was refluxed for 3 d. The solution was filtered through Celite rinsing with 10% methanol/CH_2Cl_2 and then concentrated in vacuo. The residue was chromatographed (flash column, 5% EtOAc/CH_2Cl_2) to obtain 160 mg of **31** (74% yield). ^{1}H NMR (400 MHz, $CDCl_3$, δ): 1.80 (s, 6H, CH_3), 1.81 (s, 6H, CH_3), 1.92 (s, 3H, OCH_3), 2.61 (br s, 3H, CH_3), 2.65 (s, 3H, CH_3), 3.23 (br s, 3H, CH_3), 4.09 (s, 3H, OCH_3), 6.42-7.29 (m, 36H, ArH), 7.71 (d, *J* = 7 Hz, 2H, ArH), 8.3 (d, *J* = 8 Hz, 2H, ArH), 8.39-8.44 (m, 3H, βH and ArH), 8.59 (d, *J* = 4 Hz, 1H, βH), 8.72 (d, *J* = 4 Hz, 2H, βH), 8.75-8.80 (m, 4H, βH). MALDI-TOF-MS *m/z*: calcd for $C_{97}H_{75}N_5O_4Zn$ 1437.41, obsd 1439.81. UV-Vis (CH_2Cl_2): λ_{max}, nm 422, 549, 589.

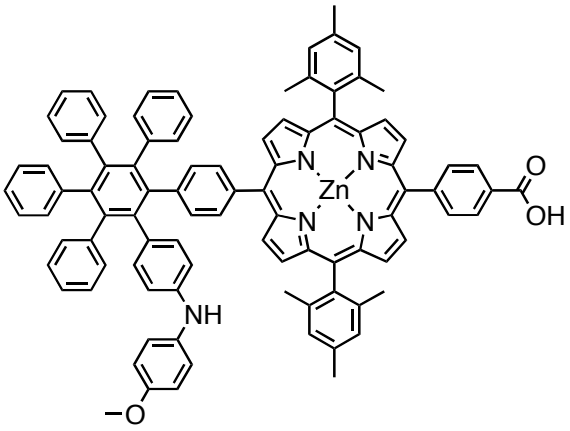

Porphyrin **9.** In a heavy walled pressure vessel equipped with a magnetic stir bar, **31** (75 mg, 0.052 mmol) was dissolved in THF (5 mL) followed by addition of KOH/MeOH (2 M, 15 mL). The solution was bubbled with Ar at 0 °C for 30 min, brought to room temperature, and the vessel was flame-sealed under low vacuum. The reaction was heated at 75 °C for 14 d. The solution was diluted with CH_2Cl_2 (50 mL) and washed with brine. The aqueous layer was extracted with CH_2Cl_2 (50 mL) and the combined organic layers were washed with aqueous citric acid (0.2 M, 150 mL) then concentrated in vacuo. The residue was loaded onto a pad of silica gel, flushed with (x 5) with CH_2Cl_2, and eluted with 10% MeOH/CH_2Cl_2 to obtain 71 mg of **9** (99% yield). ^{1}H NMR (400 MHz, $CDCl_3$, δ): 1.81 (s, 6H, CH_3), 1.82 (s, 6H, CH_3), 2.64 (s, 3H, CH_3), 2.65 (s, 3H, CH_3), 3.76 (s, 3H, OCH_3), 6.71 (d, *J* = 9 Hz, 2H, ArH), 6.78 (d, *J* = 9 Hz, 2H, ArH), 6.87-7.04 (m, 19H, ArH), 7.14 (m, 5H, ArH), 7.21 (d, *J* = 8 Hz, 2H, ArH), 7.28 (s, 2H, ArH), 7.30 (s, 2H, ArH), 7.75 (d, *J* = 8 Hz, 2H, ArH), 8.36 (d, *J* = 8.2 Hz, 2H, ArH), 8.50 (d, *J* = 8.2 Hz, 2H, ArH), 8.53 (d, *J* = 4.4 Hz, 1H, βH), 8.60 (d, *J* = 4.8 Hz, 1H, βH), 8.69 (d, *J* = 4.4 Hz, 1H, βH), 8.73 (d, *J* = 4.8 Hz, 1H, βH), 8.78 (d, *J* = 4.8 Hz, 2H, βH), 8.82 (d, *J* = 4.8 Hz, 2H, βH). MALDI-TOF-MS *m/z*: calcd for $C_{94}H_{71}N_5O_3Zn$ 1381.48, obsd 1383.74. UV-Vis (CH_2Cl_2): λ_{max}, nm 422, 549, 589.

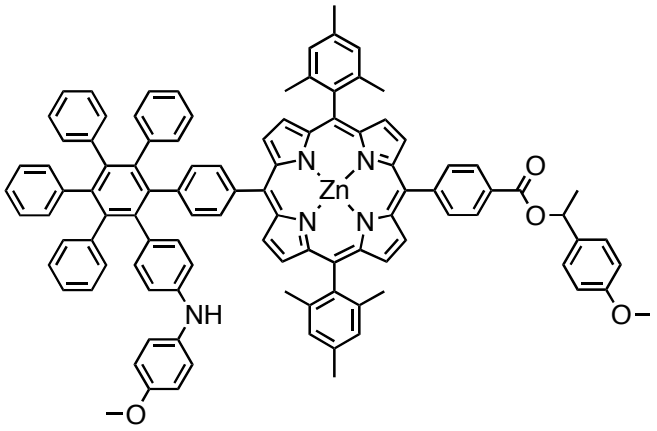

Porphyrin **32.** In a flask equipped with a magnetic stir bar, **9** (63 mg, 0.046 mmol), 1-(4-methoxyphenyl)ethanol (128 µL, 0.909 mmol), DMAP (56 mg, 0.46 mmol), and (41 mg, 0.23 mmol) were dissolved in CH_2Cl_2 (20 mL). The reaction was stirred overnight at room temperature. The solution was diluted with CH_2Cl_2, washed with saturated aqueous $NaHCO_3$, and then concentrated in vacuo. The residue was chromatographed (x 2) (gravity column, 4:1 CH_2Cl_2/hexanes) to obtain 40 mg of **32** (58% yield). ^{1}H NMR (400 MHz, $CDCl_3$, δ): 1.8 (m, 15H, CH_3), 2.63 (s, 3H, CH_3), 2.64 (s, 3H, CH_3), 3.76 (s, 3H, OCH_3), 3.84 (s, 3H, OCH_3), 5.44 (br s, 1H, NH), 6.27 (q, *J* = 7 Hz, 1H, CH), 6.72 (d, *J* = 8 Hz, 2H, ArH), 6.76 (d, *J* = 9 Hz, 2H, ArH), 6.81-7.04 (m, 21H, ArH), 7.14 (m, 5H, ArH), 7.20 (d, *J* = 8 Hz, 2H, ArH), 7.27 (s, 2H, ArH), 7.29 (s, 2H, ArH), 7.53 (d, *J* = 8 Hz, 2H, ArH), 7.74 (d, *J* = 8 Hz, 2H, ArH), 8.28 (s, *J* = 8.1 Hz, 2H, ArH), 8.40 (d, *J* = 8.1 Hz, 2H, ArH), 8.52 (d, *J* = 4.8 Hz, 1H, βH), 8.59 (d, *J* = 4.8 Hz, 1H, βH), 8.68 (d, *J* = 4.8 Hz, 1H, βH), 8.72 (d, *J* = 4.8 Hz, 1H, βH), 8.75 (d, *J* = 4 Hz, 2H, βH), 8.78 (d, *J* = 4 Hz, 2H, βH). MALDI-TOF-MS *m/z*: calcd for $C_{103}H_{81}N_5O_4Zn$ 1515.56, obsd 1517.63. UV-Vis (CH_2Cl_2): λ_{max}, nm 422, 549, 588.

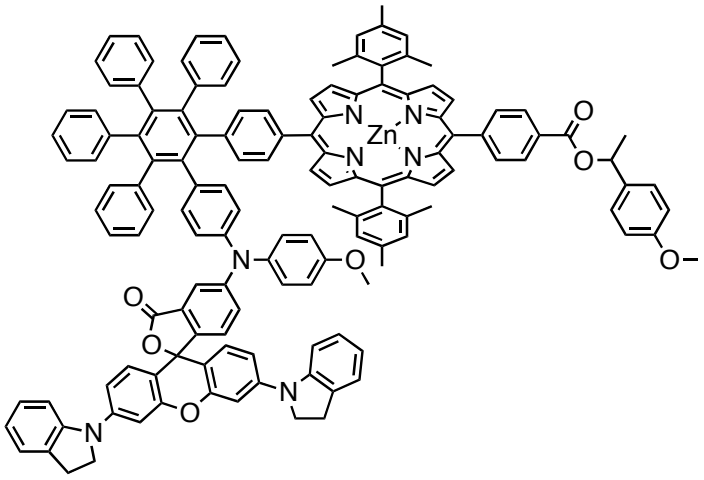

Dyad **33.** In a flask equipped with a magnetic stir bar, **10** (39 mg, 0.026 mmol), rhodamine **11** (24 mg, 0.039 mmol), $Pd(OAc)_2$ (2.9 mg, 0.013 mmol), and Cs_2CO_3 (84 mg, 0.26 mmol) were dissolved in toluene (3 mL). The solution was bubbled with Ar at 0 °C for 20 min, an Ar balloon was attached, and P^tBu_3 (26 µL, 1 M in toluene) was added. The reaction was slowly brought to reflux and stirred overnight. The solution was poured over a pad of silica gel, eluted with 10% MeOH/CH_2Cl_2, and concentrated in vacuo. The residue was chromatographed (flash column, 3-5% acetone/CH_2Cl_2) to obtain 42 mg of **33** (79% yield).

^{1}H NMR (400 MHz, $CDCl_3$, δ): 1.69 (s, 6H, CH_3), 1.80 (m, 9H, CH_3), 2.48 (s, 3H, CH_3), 2.64 (s, 3H, CH_3), 3.09 (t, *J* = 8 Hz, 4H, CH_2), 3.50 (s, 3H, OCH_3), 3.84 (s, 3H, OCH_3), 3.86-3.96 (m, 4H, CH_2), 6.27 (q, *J* = 7 Hz, 1H, CH), 6.60 (d, *J* = 9 Hz, 2H, ArH), 6.74-7.21 (m, 48H, ArH), 7.28 (s, 2H, ArH), 7.5 (d, *J* = 2 Hz, 1H, ArH), 7.53 (d, *J* = 9 Hz, 2H, ArH), 7.76 (d, *J* = 8 Hz, 2H, ArH), 8.26 (d, *J* = 8.4 Hz, 2H, ArH), 8.40 (d, *J* = 8.4 Hz, 2H, ArH), 8.53 (d, *J* = 5 Hz, 1H, βH), 8.65 (d, *J* = 5 Hz, 1H, βH), 8.68-8.79 (comp, 6H, βH).

MALDI-TOF-MS *m/z*: calcd for $C_{139}H_{105}N_7O_7Zn$ 2047.74.74, obsd 2050.23.

UV-Vis (CH_2Cl_2): λ_{max}, nm 336, 422, 549, 588.

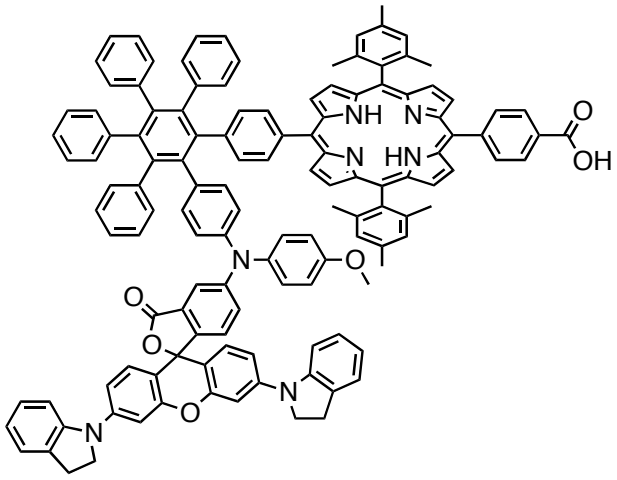

Dyad **13.** In a flask equipped with a magnetic stir bar, **33** (42 mg, 0.02 mmol) and 1,3,5-trimethoxybenzene (1 g, 6 mmol) were dissolved in CH_2Cl_2 (10 mL). TFA/CH_2Cl_2 (2% v/v, 10 mL) was added and the reaction was stirred for 5 h at room temperature. TFA (200 µL) was added and stirring continued for 5 h. The solution was washed with saturated aqueous $NaHCO_3$ (x 2) and concentrated in vacuo. The residue was loaded onto a short pad of silica gel and flushed with CH_2Cl_2 (1.5 L) then 0.5% MeOH/CH_2Cl_2 (300 mL) and eluted with 10% MeOH/CH_2Cl_2 to obtain 34 mg of **13** (89% yield). ^{1}H NMR (400 MHz, $CDCl_3$, δ):
-2.70 (br s, 2H, NH), 1.70 (s, 6H, CH_3), 1.82 (s, 6H, CH_3), 2.47 (s, 3H, CH_3), 2.64 (s, 3H, CH_3),
3.10 (t, *J* = 8 Hz, 4H, CH_2), 3.57 (s, 3H, OCH_3), 3.86-3.97 (m, 4H, CH_2),
6.67 (d, *J* = 9 Hz, 2H, ArH), 6.75-7.22 (m, 48H, ArH), 7.29 (s, 2H, ArH),
7.54 (d, *J* = 2 Hz, 1H, ArH), 7.75 (d, *J* = 8 Hz, 2H, ArH), 8.33 (d, *J* = 8 Hz, 2H, ArH),
8.45 (d, *J* = 5 Hz, 1H, βH), 8.51 (d, *J* = 9 Hz, 2H, ArH), 8.57 (d, *J* = 4 Hz, 1H, βH),
8.62-8.73 (comp, 6H, βH). MALDI-TOF-MS *m/z*: calcd for $C_{130}H_{97}N_7O_6$ 1851.75, obsd 1852.80.
UV-Vis (CH_2Cl_2): λ_{max}, nm 420, 515, 549, 591, 647.

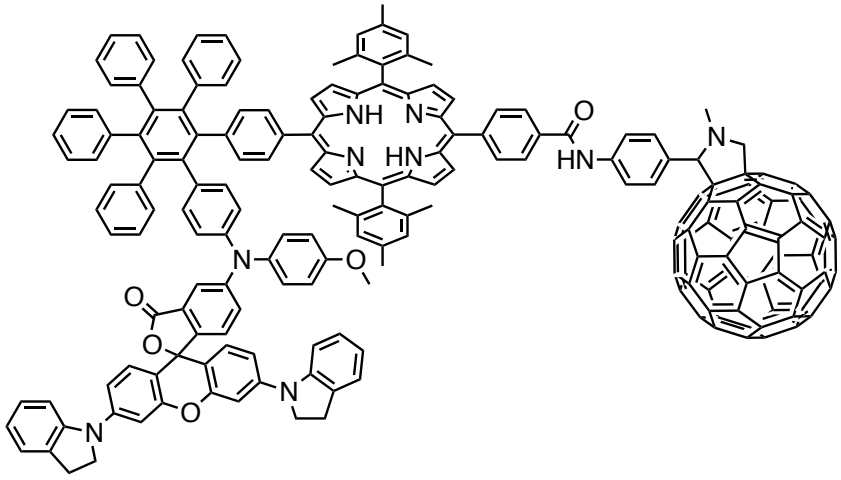

Triad **15.** In a flask equipped with a magnetic stir bar, **13** (34 mg, 0.018 mmol), anilinofullerene **14**[39] (20 mg, 0.023 mmol), DMAP (9 mg, 0.07 mmol), and EDCI (7 mg, 0.04 mmol) were dissolved in CH_2Cl_2 (4 mL). The reaction was stirred under Ar for 24 h at room temperature. The solution was diluted with CH_2Cl_2 (50 mL), washed with aqueous citric acid (0.5 M) and saturated aqueous $NaHCO_3$, and then concentrated in vacuo. The residue was chromatographed (thin layer, 5% EtOAc/CH_2Cl_2) to obtain 20 mg of **14** (40% yield). ^{1}H NMR (400 MHz, $CDCl_3$, δ): -2.71 (br s, 2H, NH), 1.69 (s, 6H, CH_3), 1.81 (s, 6H, CH_3), 2.46 (s, 3H, CH_3), 2.63 (s, 3H, CH_3), 2.82 (s, 3H, NCH_3), 3.08 (t, *J* = 9 Hz, 4H, CH_2), 3.57 (s, 3H, OCH_3), 3.85-3.95 (m, 4H, CH_2), 4.23 (d, *J* = 9 Hz, 1H, CH), 4.93-4.98 (m, 2H, CH_2), 6.67 (d, *J* = 9 Hz, 2H, ArH), 6.74-7.22 (comp, 45H, ArH), 7.28 (s, 2H, ArH), 7.53 (d, *J* = 2 Hz, 1H, ArH), 7.53 (d, *J* = 9.3 Hz, 2H, ArH), 7.75 (d, *J* = 8 Hz, 2H, ArH), 7.88 (br s, 3H, ArH), 8.20-8.23 (m, 3H, ArH and NH), 8.28 (d, *J* = 8 Hz, 2H, ArH), 8.44 (d, *J* = 4 Hz, 1H, βH), 8.56 (d, *J* = 5 Hz, 1H, βH), 8.61-8.70 (m, 6H, βH). MALDI-TOF-MS *m/z*: calcd for $C_{199}H_{107}N_9O_5$ 2701.84, obsd 2704.31. UV-Vis (CH_2Cl_2): λ_{max}, nm 308, 332, 420, 515, 549, 591, 646.

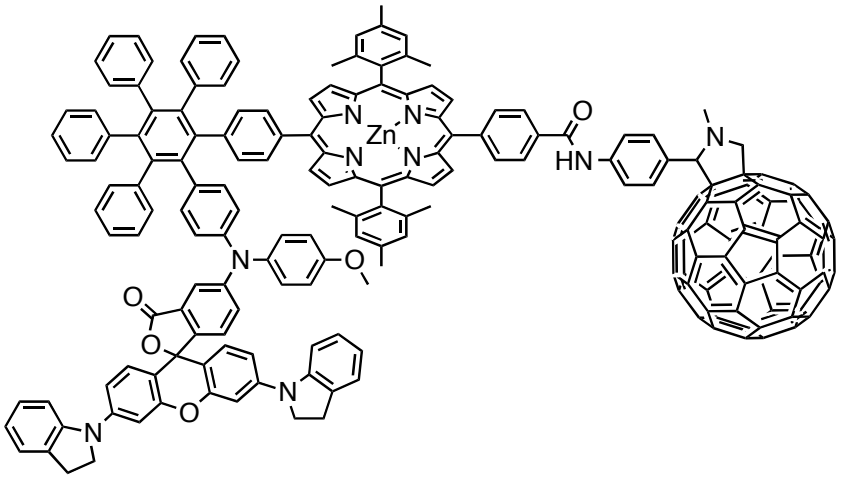

Triad **1.** In a flask equipped with a magnetic stir bar, **15** (19 mg, 0.0070 mmol) was dissolved in CH_2Cl_2 (4 mL). $ZnOAc_2$•$2H_2O$/MeOH (50 mg/mL, 300 μL) was added and the reaction was stirred under Ar for 24 h at room temperature. The solution was diluted with CH_2Cl_2, washed with water and saturated $NaHCO_3$, and concentrated in vacuo. The residue was loaded onto a short plug of silica gel, flushed with CH_2Cl_2 (300 mL), and eluted with 10% MeOH/CH_2Cl_2 to obtain 20 mg of **1** (quantitative). ^{1}H NMR (400 MHz, $CDCl_3$, δ): 1.67 (s, 6H, CH_3), 1.78 (s, 6H, CH_3), 2.48 (s, 3H, CH_3), 2.61 (s, 3H, CH_3), 2.72 (s, 3H, NCH_3), 3.05 (t, *J* = 8 Hz, 4H, CH_2), 3.54 (s, 3H, OCH_3), 3.82-3.92 (m, 4H, CH_2), 4.08 (d, *J* = 10 Hz, 1H, CH), 4.77-4.83 (m, 2H, CH_2), 6.64 (d, *J* = 9 Hz, 2H, ArH), 6.70-7.25 (m, 50H, ArH), 7.48 (d, *J* = 2 Hz, 1H, ArH), 7.74-7.83 (m, 4H, ArH), 8.09-8.19 (m, 4H, ArH), 8.37 (br s, 1H, NH), 8.53 (d, *J* = 5 Hz, 1H, βH), 8.64 (d, *J* = 5 Hz, 1H, βH), 8.67 (d, *J* = 4 Hz, 1H, βH), 8.70-8.75 (m, 5H, βH). MALDI-TOF-MS *m/z*: calcd for $C_{199}H_{105}N_9O_5Zn$ 2763.75, obsd 2767.08. UV-Vis (CH_2Cl_2): λ_{max}, nm 311, 330, 422, 549, 589.

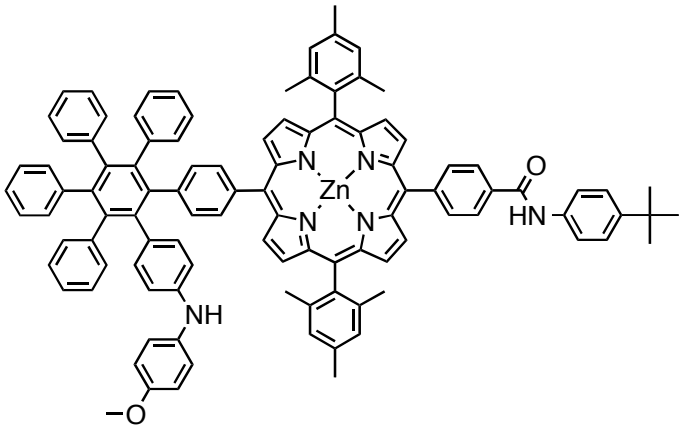

Porphyrin **34.** In a flask equipped with a magnetic stir bar, **9** (30 mg, 0.022 mmol), 4-*tert*-butylaniline, DMAP (12 mg, 0.098 mmol), and EDCI (8 mg, 0.044 mmol) were dissolved in CH_2Cl_2 (10 mL). The reaction was stirred under Ar for 24 h at room temperature. The solution was applied directly to a short column of silica gel, eluted with CH_2Cl_2 to 10% MeOH/CH_2Cl_2, and concentrated in vacuo. The residue was chromatographed (gravity column, 1% EtOAc/CH_2Cl_2) to obtain 29 mg of **34** (87% yield). ^{1}H NMR (400 MHz, $CDCl_3$, δ): 1.37 (s, 9H, CH_3), 1.80 (s, 6H, CH_3), 1.81 (s, 6H, CH_3), 2.63 (s, 3H, CH_3), 2.64 (s, 3H, CH_3), 3.76 (s, 3H, OCH_3), 5.44 (s, 1H, NH), 6.71 (d, *J* = 9 Hz, 2H, ArH), 6.76 (d, *J* = 9 Hz, 2H, ArH), 6.88-7.04 (m, 19H, ArH), 7.14 (m, 5H, ArH), 7.20 (d, *J* = 8 Hz, 2H, ArH), 7.28 (s, 2H, ArH), 7.29 (s, 2H, ArH), 7.47 (d, *J* = 9 Hz, 2H, ArH), 7.66 (d, *J* = 9 Hz, 2H, ArH), 7.75 (d, *J* = 8 Hz, 2H, ArH), 8.05 (s, 1H, NH), 8.17 (d, *J* = 8.2 Hz, 2H, ArH), 8.33 (d, *J* = 8.2 Hz, 2H, ArH), 8.52 (d, *J* = 4.8 Hz, 1H, βH), 8.59 (d, *J* = 4.4 Hz, 1H, βH), 8.68 (d, *J* = 4.4 Hz, 1H, βH), 8.72 (d, *J* = 4.8 Hz, 1H, βH), 8.77 (d, *J* = 5 Hz, 2H, βH), 8.81 (d, *J* = 4 Hz, 2H, βH). MALDI-TOF-MS *m/z*: calcd for $C_{104}H_{84}N_6O_2Zn$ 1513.60, obsd 1514.61. UV-Vis (CH_2Cl_2): λ_{max}, nm 421, 549, 586.

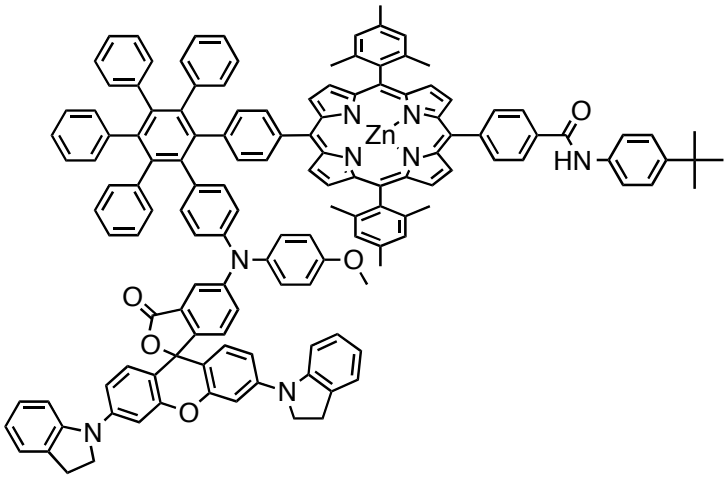

Dyad **2.** In pressure tube equipped with a magnetic stir bar, **34** (28 mg, 0.018 mmol), rhodamine **11** (17 mg, 0.028 mmol), $Pd(OAc)_2$ (2 mg, 0.009 mmol), and Cs_2CO_3 (59 mg, 0.18 mmol) were dissolved in toluene (2 mL). The solution was bubbled with Ar at 0 °C for 15 min, P^tBu_3 (18 µL, 1 M in toluene) was added and bubbling continued for an additional 15 min. The tube was sealed with a PTFE screw plug, heated slowly to 115 °C, and stirred for 36 h. The solution was applied directly to a pad of silica gel, eluted with 10% MeOH/CH_2Cl_2, and then concentrated in vacuo. The residue was chromatographed (gravity column, 5-7.5% EtOAc/CH_2Cl_2) to obtain 10 mg of **2** (27% yield). ^{1}H NMR (400 MHz, $CDCl_3$, δ): 1.38 (s, 9H, CH_3), 1.70 (s, 6H, CH_3), 1.81 (s, 6H, CH_3), 2.48 (s, 3H, CH_3), 2.64 (s, 3H, CH_3), 3.08 (t, *J* = 8 Hz, 4H, CH_2), 3.50 (s, 3H, OCH_3), 3.86-3.95 (m, 4H, CH_2), 6.60 (d, *J* = 9 Hz, 2H, ArH), 6.73-7.21 (m, 46H, ArH), 7.29 (s, 2H, ArH), 7.47-7.50 (m, 3H, ArH), 7.69 (d, *J* = 8 Hz, 2H, ArH), 7.76 (d, *J* = 8 Hz, 2H, ArH), 8.07 (s, 1H, NH), 8.18 (d, *J* = 7.9 Hz, 2H, ArH), 8.32 (d, *J* = 7.9 Hz, 2H, ArH), 8.54 (d, *J* = 5 Hz, 1H, βH), 8.66 (d, *J* = 4 Hz, 1H, βH), 8.70-8.81 (m, 6 H, βH). MALDI-TOF-MS *m/z*: calcd for $C_{140}H_{108}N_8O_5Zn$ 2045.78, obsd 2046.82. UV-Vis (CH_2Cl_2): λ_{max}, nm 308, 334, 421, 511, 549.

APPENDIX B

METHODS FOR OPTICAL SPECTROSCOPY

Optical spectroscopy samples were prepared using CH_2Cl_2 distilled from CaH_2. Sample concentrations for steady-state absorption, emission and time-resolved fluorescence were ca. 10^{-6} M. Transient absorption samples were ca. 10^{-4} M. Glacial acetic acid was used to produce the open, protonated forms of **1**, **2**, and **3**.

Steady-State Spectroscopy

Absorption spectra were measured on Shimadzu UV2100U UV-vis and UV-3101PC UV-Vis-NIR spectrometers. Fluorescence spectra were measured using a Photon Technology International MP-1 spectrometer and corrected for detection system response. Excitation was provided by a 75 W xenon-arc lamp and single grating monochromator. Fluorescence was detected 90^{o} to the excitation beam via a single grating monochromator and an R928 photomultiplier tube having S 20 spectral response and operating in the single photon counting mode.

Time-Resolved Fluorescence

Fluorescence decay measurements were performed by the time-correlated single-photon-counting method. The excitation source was a fiber supercontinuum laser based on a passive mode-locked fiber laser and a high-nonlinearity photonic crystal fiber supercontinuum generator (Fianium SC450). The laser provides 6-ps pulses at a repetition rate variable from 0.1-40 MHz. The laser output was sent through an Acousto-Optical Tunable Filer (Fianium AOTF) to obtain excitation pulses at desired wavelength of ca. 450-900 nm. Fluorescence emission was detected at the magic angle (54.7°) using a double grating monochromator (Jobin Yvon Gemini-180) and a microchannel plate photomultiplier tube (Hamamatsu R3809U-50). The instrument response function was 35-55 ps. The spectrometer was controlled by software based on the LabView

programming language and data acquisition was done using a single photon counting card (Becker-Hickl, SPC-830).

Transient Absorption

The femtosecond transient absorption apparatus consisted of a kHz pulsed laser source and a pump-probe optical setup. Laser pulses of 100 fs at 800 nm were generated from an amplified, mode-locked Titanium Sapphire kHz laser system (Millennia/Tsunami/Spitfire, Spectra Physics). Part of the laser pulse energy was sent through an optical delay line and focused on a 3 mm sapphire plate to generate a white light continuum for the probe beam. The remainder of the pulse energy was used to pump an optical parametric amplifier (Spectra Physics) to generate excitation pulses, which were selected using a mechanical chopper. The white light generated was compressed by prism pairs (CVI) before passing through the sample. The polarization of the pump beam was set to the magic angle relative to the probe beam and its intensity adjusted using a continuously variable neutral density filter. The white light probe was dispersed by a spectrograph (300 line grating) onto a charge-coupled device (CCD) camera (DU420, Andor Tech.). The final spectral resolution was about 2.3 nm over a 300 nm spectral region. Instrument response function was ca. 150 fs. Nanosecond time scale measurements were collected using an EOS spectrometer from Ultrafast Systems (IRF ~800 ps); excitation was from the same optical parametric amplifier as descibed above.

Data analysis was carried out using locally written software (ASUFIT) developed in MATLAB (Mathworks Inc.). Decay-associated spectra were obtained by fitting the transient absorption or fluorescence change curves over a selected wavelength region simultaneously as described by the parallel kinetic model:

$$\Delta A(\lambda, t) = \sum_{i=1}^{n} A_i(\lambda) \exp(-t/\tau_i) \quad (1)$$

where $\Delta A(\lambda,t)$ is the observed absorption (or fluorescence) change at a given wavelength at time delay t and n is the number of kinetic components used in the fitting. A plot of $A_i(\lambda)$ vs. wavelength is called a decay-associated spectrum (DAS), and represents the amplitude spectrum of the i^{th} kinetic component, which has a lifetime of τ_i. Random errors associated with the reported lifetimes obtained from fluorescence and transient absorption measurements were typically ≤ 5%.